/
Article / Book Information

( )	
Title(English)	Ion desorption from H2O chemisorbed on Si(100) by O 1s electron excitation
( )	
Author(English)	Tetsuhiro Sekiguchi
( )	: ( ), : , : 3059 , :1995 5 31 , : , :
Citation(English)	Degree:Doctor (Science), Conferring organization: Tokyo Institute of Technology, Report number: 3059 , Conferred date:1995/5/31, Degree Type:Course doctor, Examiner:
( )	
Type(English)	Doctoral Thesis

Ion Desorption from H2O Chemisorbed

on Si(100) by O 1s Electron Excitation

by

Tetsuhiro Sekiguchi

Thesis submitted to Tokyo Institute of Technology

for the Degree of Doctor of Science

January 1995

ACKNOWLEDGMENTS

CONTENTS

LIST OF TABLES

LIST OF FIGURES

vii

Chapter 1

INTRODUCTION

The photon stimulated ion desorption (PSID) of H^+ and O^+ from monolayer H_2O adsorbed on the Si(100) using pulsed synchrotron radiation is presented in this thesis. Ions were detected and mass analyzed by means of time-of-flight spectroscopy. Results were interpreted by assuming that ion desorption was enhanced by multiple ionization and was strongly affected by decay processes with the surface. In order to clarify the mechanism of the PSID, the technique of photoion-photoion-coincidence (PIPICO) was also applied.

In this chapter, the significance and the historical background of present investigation are described. The up-to-date studies related to the present work are reviewed.

1.1 Significance of the present work

Photochemical reactions of adsorbed molecules on solid surfaces have received much attention due to the following points: 1) they play important roles in reaction dynamics as well as in application to the fabrication of microelectronics devices[1], 2) the coupling of adsorbed molecules with the substrate influences the excitation and deexcitation processes, and 3) they often show some interesting surface-specificities. Among a number of photochemical surface processes, photon stimulated desorption (PSD) is a relatively simple process to investigate reaction dynamics of adsorbed molecules both theoretically and experimentally[2]. PSD has been extensively studied for more than 15 years, since it offers the information concerning the property of the local electronic structure and bonding aspects of the chemically adsorbed molecules[3]. A solid surface sometimes provides extra pathways for deexcitation, which do not exist in the gas phase. Since ions can be detected with high efficiency and sensitivity, ion desorption has been extensively investigated more than neutral desorption. Photon stimulated ion desorption (PSID) becomes an important process in core excitations due to its very high efficiency[4-6], and extensive data on photoionization of gaseous molecules provide useful information to understand PSID[7].

1.2 History of study on structure and properties of H_2O - chemisorbed on Si(100)-2×1

The oxidation of Si with water is known as a technologically useful process in semiconductor device preparation (e.g., wet-oxidation). In the past, therefore, the interaction of H_2O molecules with the Si surface has been extensively studied both experimentally and theoretically. The surface structure of this system has been well studied.

There is, however, an unresolved question whether H_2O dissociatively adsorbs or molecularly? Studies have been focused on the reaction of H_2O with Si surface. First, Thiel et al. estimated the thermodynamic feasibility of water dissociation on Si[8]. The heat for dissociative adsorption has a larger negative value (-700 to -892 kJ/mol) than that for molecular adsorption (-50 kJ/mol), and hence, they concluded that dissociation was strongly favored over molecular adsorption on Si surfaces. In 1971, Meyer first studied adsorption of water on Si(111) and Si(100) at room temperature using ellipsometry[9] and concluded that complete dissociation to O_a and H_a occurred. In 1975, Fujiwara and Nishijima used electron energy loss spectroscopy (EELS) for H_2O on Si(111) at 300 K and interpreted their (electronic excitation) spectra by a mechanism that water did not dissociate[10]. In 1981, Fujiwara used ultraviolet photoemission spectroscopy (UPS) and proposed that the observed spectra corresponded to those of molecular H_2O[11]. In 1983-85's papers[12], Schmeisser et al. extensively studied the same system using UPS and described as follows: (1) adsorption on the reconstructed Si(111)-(7×7) and Si(110) surfaces at room temperature (RT) resulted in dissociation to OH_a and H_a, and also possibly O_a; (2) adsorption on the reconstructed Si(100)-(2×1) face at RT

yields molecularly adsorbed H_2O; (3) adsorption of H_2O at 100 K on any Si plane, followed by heating to RT, yields undissociative H_2O_a.

The first work using vibrational analysis in this area is that published by Ibach, Wagner, and Bruchmann in 1982[13]. These authors use the technique of high resolution electron energy loss spectroscopy (HREELS). They were followed by Kobayashi, Kubota, Onchi, and Nishijima in 1983[14]. Since then, many reports have appeared, including those by Chabal and Christman using infrared spectroscopy[15], Lapeyre and colleagues using HREELS[16], and Nishijima *et al.* also using HREELS[17]. The spectra have been consistently interpreted to support dissociative adsorption of water, i.e., formation of OH_a and H_a on Si(100)-(2×1), Si(111)-(7×7), and Si(111)-(2×1) surfaces at temperatures between 80 and 400 K[13-17].

Figure 1-1 schematically illustrates the dissociative adsorption layer of H_2O on Si(100)-(2×1) surface. According to recent studies, it appeared that HREELS[18], surface IR spectroscopy[19], UPS[20], ESDIAD[21], ARUPS[22], STM[23], and theoretical studies[24] were all consistent with dissociative adsorption (SiH + SiOH) of water on Si(100)-(2×1) surface at room temperature. The (2×1) symmetry is maintained up to a saturation exposure of 1 Langmuir (1×10^{-6} Torr·sec; 0.5 monolayer H_2O), which indicates that each surface dimer forms a Si(H)-Si(OH) complex without disturbing the substrate geometry[19].

Well-defined surfaces are suitable for clarifying the mechanism of an ion desorption process. In this thesis, therefore , the Si (100) face is used as a sample substrate to study PSID from the H_2O on the Si surface, because the reconstruction of the Si(100) is simpler than that of the Si(111). It is well-known that the Si(100) surface is reconstructed to a stable (2x1) structure by

hv (VUV, SX)

Si(100)
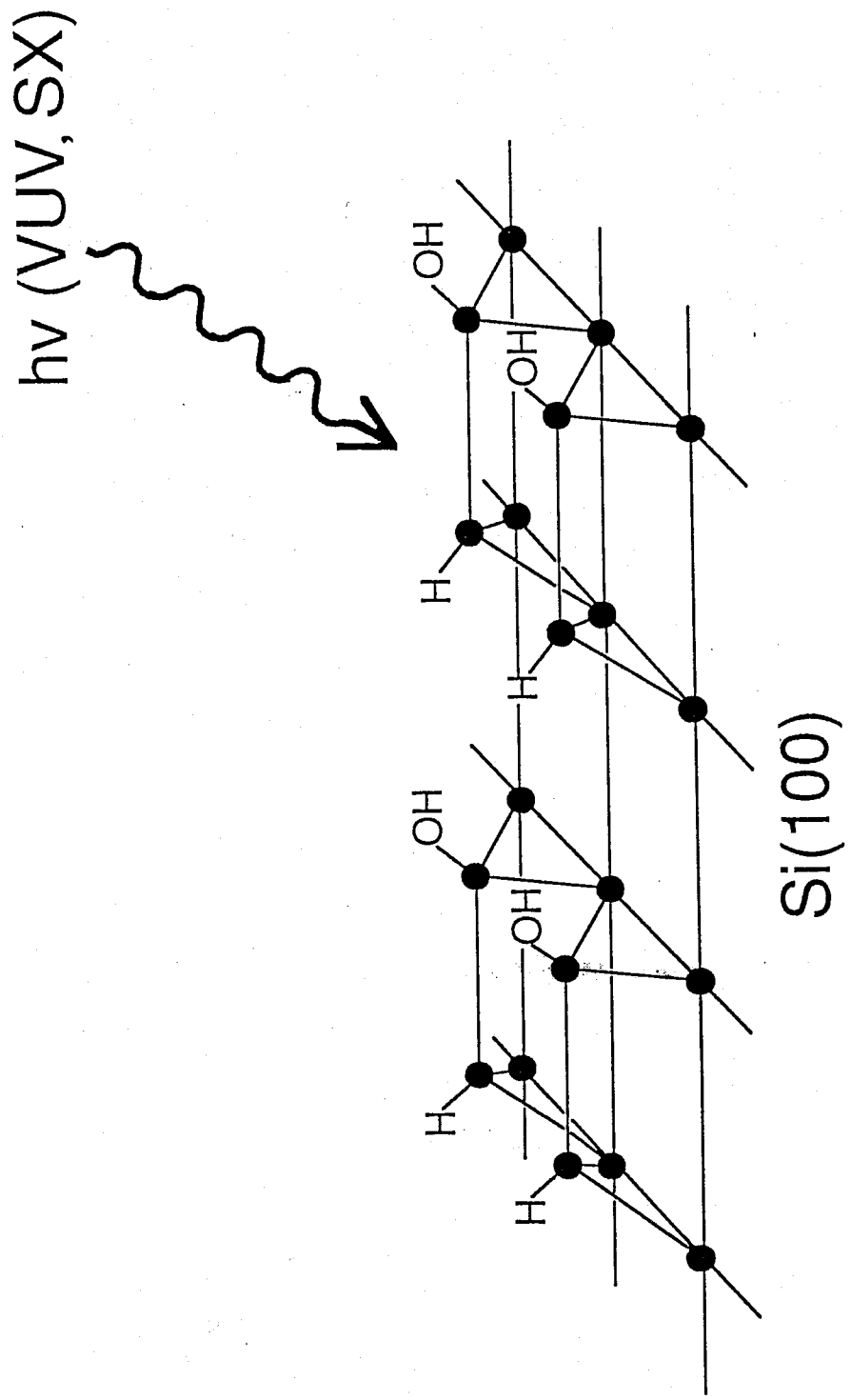
Figure 1-1   The adsorption sites for H and OH on the Si-Si symmetric dimer.

annealing after cleaning sample. In contrast, the Si(111) surface can be reconstructed either to a stable (7×7) structure or to a (2×1) structure, depending on the condition of the sample preparation of Si(111) substrate. Therefore, the Si(100) is thought to be a suitable plane for the study of mechanism in PSID.

As described above, the conclusions on adsorbed structures based on UPS studies were not consistent with each other. This may be due to influences of surface contaminants[12], difficulties in assignment of the UPS spectra, and diversity of experimental conditions (especially a temperature in adsorption of water)[8]. On the other hand, the conclusions based on the vibrational analysis were all consistent with that H_2O adsorbs dissociatively on Si(100)-(2×1) at room temperature. The vibrational techniques are seem to be more suitable for the investigation of surface chemical bonding, than the UPS studies. In the present thesis, therefore, the author adopts the conclusion based on the vibrational studies[13-17] which are also consistent with other recent studies of ESDIAD[21], ARUPS[22], and STM[23]; H_2O dissociates on Si(100)-(2×1) surface. Figure 1-1 schematically illustrates the dissociative adsorption layer of H_2O on Si(100)-(2×1) surface. It is assumed that H_a and OH_a on the Si-Si symmetric dimer are produced by adsorbing H_2O on the surface at room temperature. In the whole thesis, the author discusses the mechanism of the PSID on the basis of this surface structure.

1.3 Mechanisms of photon stimulated ion desorption

In PSID, monochromatic light interacts with a surface complex and causes an ion to desorb. The resulting mass spectrum of the desorbed ions yields information on what species are originally bound to the surface, and the photon-energy dependence of the various ion yields is specific to the surface site. Therefore, photon stimulated desorption (PSD) of ions and neutrals from various surfaces have been shown to be very useful probes for studying surface atom-atom and adsorbate-substrate interactions. The discovery of PSID in 1979 by Knotek, Jones, and Rehn[25] stimulated a great deal of experimental and theoretical effort[2]. At that time, several models were proposed to explain the ESD and PSD of ions and neutrals.

The Menzel-Gomer-Redhead (MGR) model

One of the earliest models to explain ESD from surfaces was independently developed by Menzel and Gomer[26] and Redhead[27] in 1964 (MGR model). This general model incorporates adiabatic approximations and a semiclassical description of possible excitations in an adsorbate (A) - substrate (M) system, which is schematically shown in Figure 1-2. The MGR model is based on an assumption that the system is initially in a ground state configuration (M + A) with respect to some reaction coordinate (z), which is often taken as distance above the surface. Interaction with an incident photon
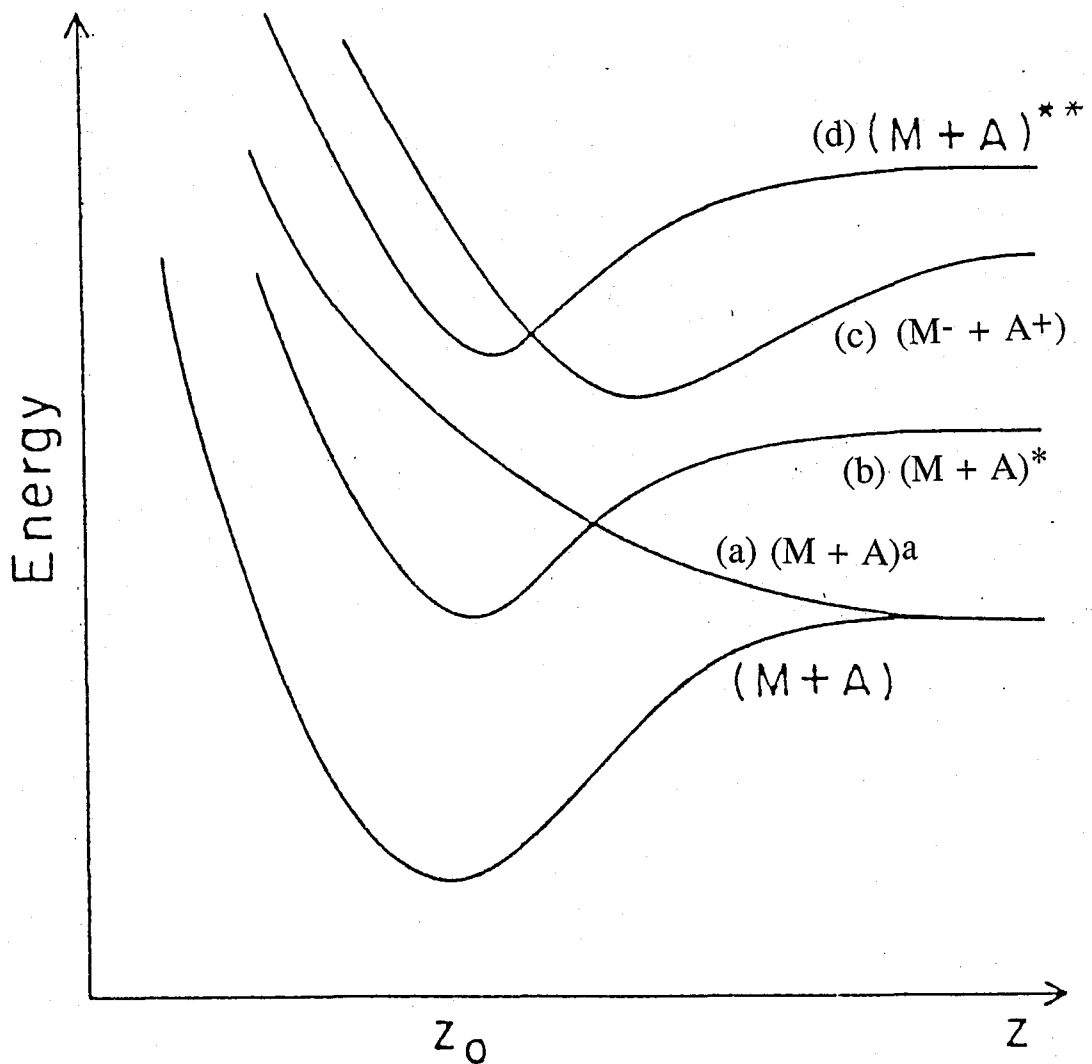
Figure 1-2   Possible potential energy curves within the MGR framework. (M + A) represents the ground state configuration. (a) (M + A)^a antibonding, (b) and (d) (M + A)* metastable and (c) (M$^-$ + A$^+$) ionic states. Figure illustrates possible curve crossings during nuclear motion of desorbing species in the MGR picture.
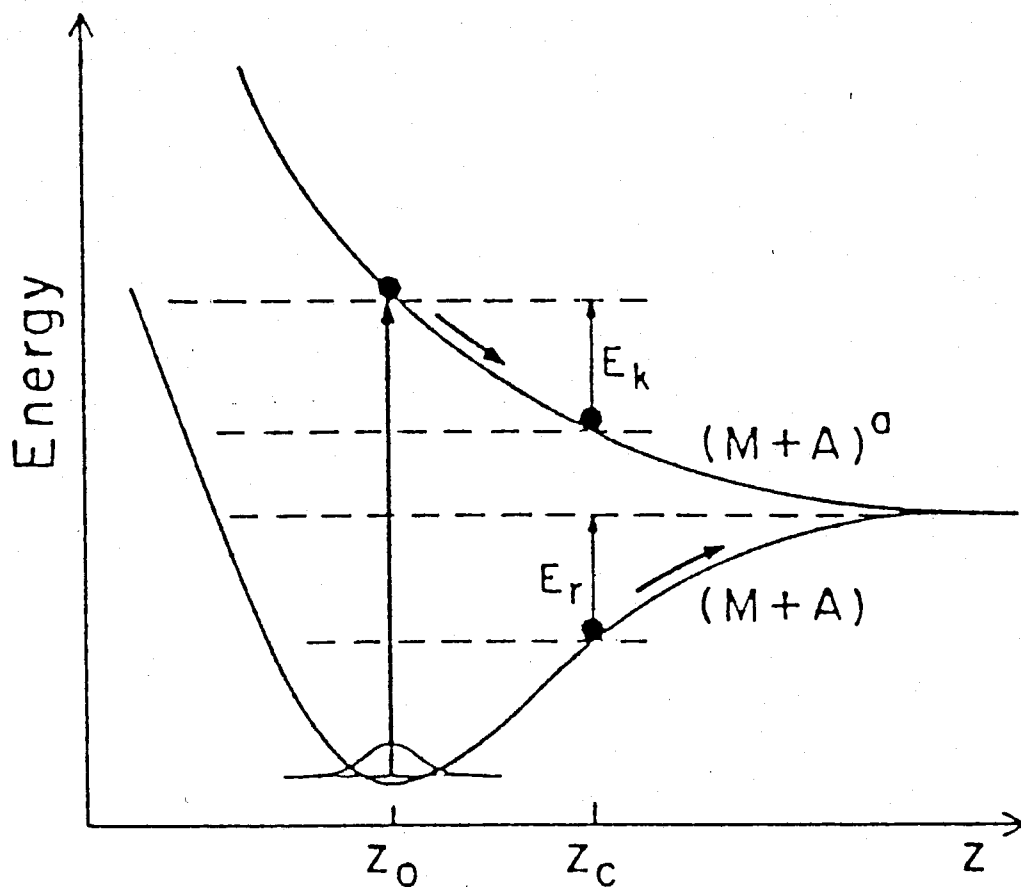
Figure 1-3   Schematic energy diagram illustrating the critical distance z_C in the MGR model. For deexcitation occurring at $z>z_C$, the kinetic energy (E_k) of the desorbing particle is greater than the barrier for recapture (E_r), allowing the particle to asymptotically escape along the (M + A) curve. Deexcitation at $z<z_C$ results in recapture of the adparticle into the ground state.

(or electron) induces a Franck-Condon (FC) transition from the (M + A) state to an excited state, possibly (a) antibonding $(M + A)^a$, (b) metastable atomic $(M + A)^*$ or (c) ionic $(M^- + A^+)$ state in nature. These excited states normally involve only valence-level excitations in the MGR model. The FC principle is equivalent to saying that the transition is vertical with respect to z, or in other words that the excitation is purely electronic and occurs so swiftly that nuclear motion is negligible during the excitation time ($\sim 10^{-15}$ sec.). Starting from the ground state configuration at an equilibrium position (z_0), a FC transition promotes the system to one of these possible higher energy states. After excitation, nuclear motion may occur over a time scale of $\sim 10^{-13}$ sec., converting potential energy of newly sampled potential surface into kinetic energy. Figure 1-2 represents the possibility of curve crossings during subsequent nuclear motion. For instance, the possibility of curve crossing of the $(M + A)^a$ to the $(M + A)^*$ exists, and if the dissociation limit of this curve lies above the initial excitation energy, then the desorption will be prevented; but if its dissociation limit lies below the initial energy, then the adsorbate will have sufficient kinetic energy to desorb as a neutral.

In the MGR model, the total PSD (or ESD) cross section is given as a product between the probabilities of the primary excitation in the (M + A) system and the total escape. Figure 1-3 illustrates the meaning of critical distance, z_c for the case of photoabsorption to a repulsive state. Asymptotically, desorption will proceed along the ground state curve for deexcitation occurring in $z > z_c$, where the kinetic energy (E_k) of the desorbing particle becomes high enough to permit escape. For transition where $z < z_c$, the desorbing particle is recaptured into the (M + A) state since it cannot overcome the recapture barrier (E_r). Similar pictures can be drawn for other values of z_c along other possible excited state curves. MGR model could explain various

properties of desorbing particle obtained experimentally, which contain the desorption cross section, the desorption threshold energy, the isotope effect of desorption, and the kinetic energy distribution of ions and neutrals.

Knotek and Feibelman (KF) model

Another model which has received widespread application in describing PSD (or ESD) phenomena was proposed in 1978 by Knotek and Feibelman[28]. Originally the model was formulated to explain experimental results concerning ESD from highly ionic maximal valency oxide surface, such as TiO_2, V_2O_5, and WO_3, in which all metal valence electrons were formally donated to the lattice. Very small total desorption yields were obtained for incident electron energies below about 20 eV, where the MGR picture would predict bonding-antibonding transition leading to significant neutral desorption. However, O^+ desorption yields increased dramatically when the bombarding electron energy reached 25-35 eV, corresponding to ionization energies of metal core levels of the metal oxide substrate. Another feature of ESD in these systems was that since oxygen resided in a charge configuration O^- or O^{2-}, the observation of desorbing O^+ implied that charge transfer (>2 electrons) was taking place during the desorption sequence. Figure 1-4 illustrates the KF mechanism for TiO_2 proposed to explain the above observations. An incident electron ionizes an electron in the highest (in energy) lying metal atom core level ($Ti3p$), which would be swiftly filled by an intra-atomic Auger process from a higher lying Ti level under normal circumstances. However, the maximal valence

11
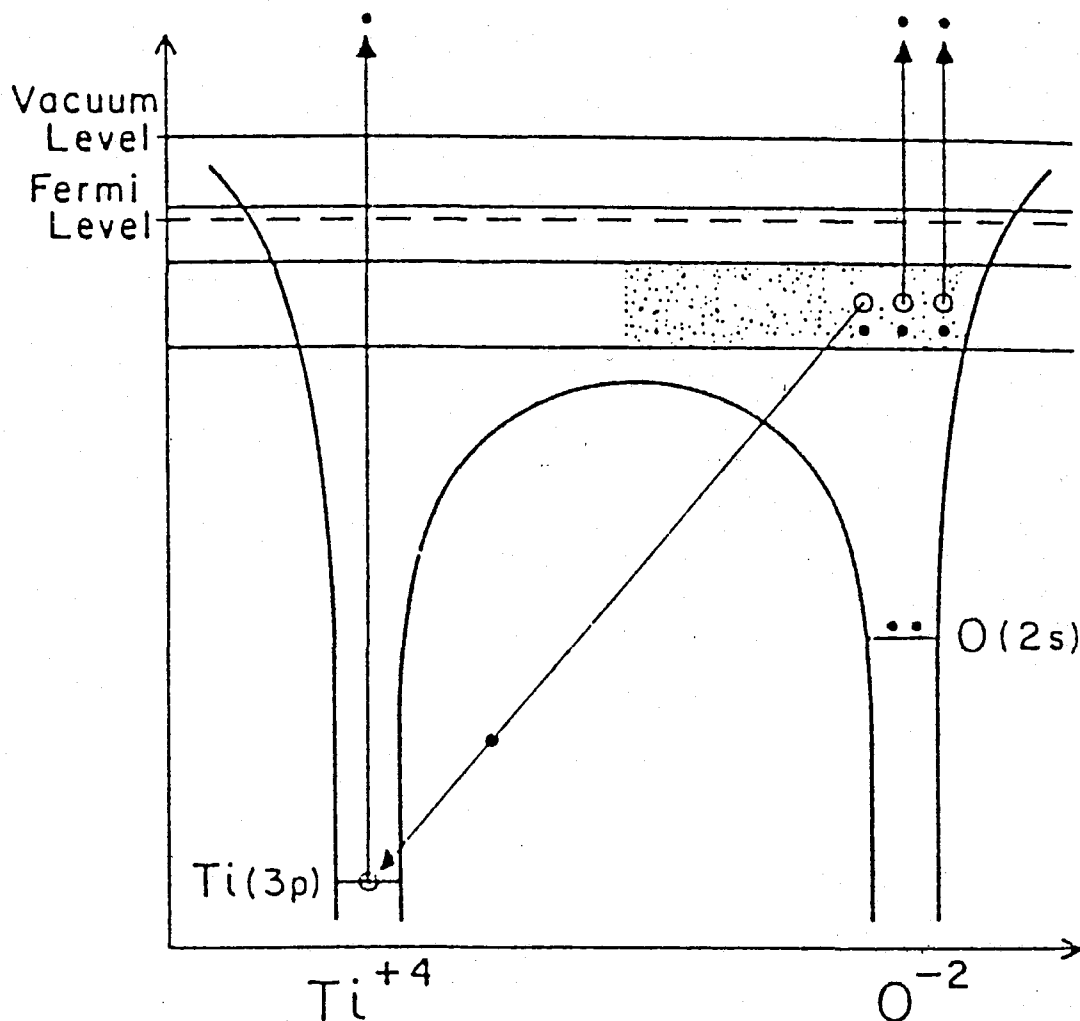
Figure 1-4   Energy diagram of the TiO$_2$ maximal valency configuration and schematic illustration of the KF desorption mechanism. A hole created in the Ti($3p$) level is filled via inter-atomic Auger decay from a neighboring oxygen site. This makes the oxygen moiety positively charged, causing it to be Coulombically repelled from its lattice site. Filled circles (●) signify electrons and open circles (O) represent holes.

configuration means that the Ti atoms are fully stripped (Ti^{4+}) of valence electrons, against the quenching process. Thus, an inter-atomic Auger mechanism is proposed, where the metallic core hole is filled via an Auger process with a neighboring O^{2-} ion. The oxygen moiety suddenly finds itself in a state O^+ where it experiences a repulsive Madelung potential, and the O^+ ion is violently ejected from the surface by a mechanism resembling a Coulomb explosion process common in gas-phase molecular dissociation[29].

Extending this mechanism to an adsorbate-substrate system, the inner-shell hole on a substrate or adsorbate surface atom is filled by an inter-atomic Auger process; this results in at least two holes in the valence levels of the adsorbate, and the breaking of the bond of the adsorbate complex. The adsorbate is desorbed as a positively charged ion due to Coulomb repulsion.

Auger stimulated desorption (ASD) model

Ramaker[30], Cini[31], Madden[32], and Feibelman[33] independently emphasized the role of hole-hole localization in the desorption process and proposed the Auger-stimulated desorption (ASD) model. This idea has received significant attention in a number of literature. The ASD model assumes that the desorption occurs due to an unmasked nuclear-nuclear Coulomb repulsion resulting from essentially two holes in a bond and is applied to covalently bonding chemisorption systems.

Figure 1-5 illustrates the ASD picture, where symbols are a surface
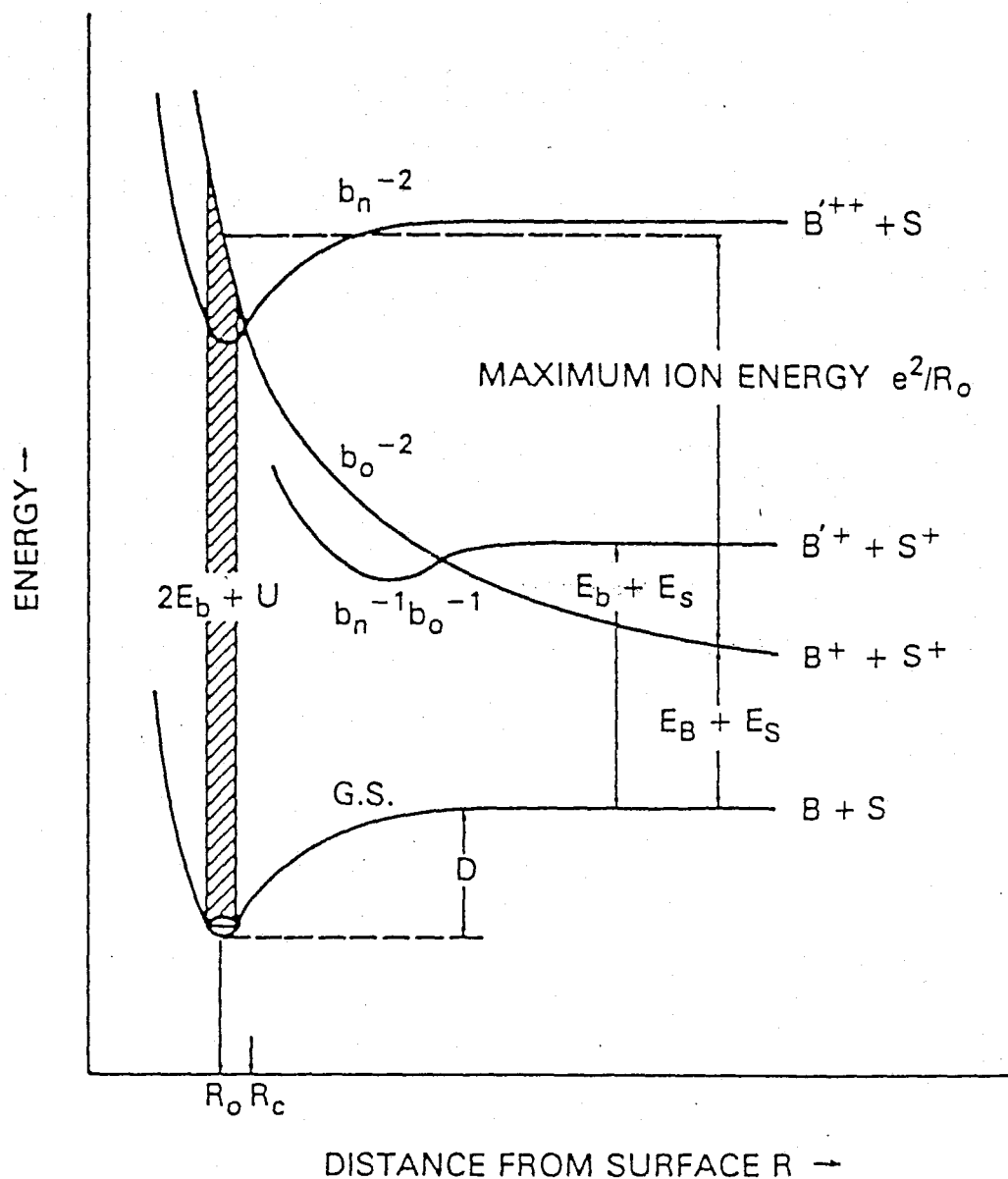
Figure 1-5   Schematic potential energy curves for interaction between a bulk atom, B, and surface atom, S, before (the ground state curve) and after the Auger process. Curves are labeled by the bond orbital states and by the separated states of the atoms. B' denotes bulk atoms not bonded to S.

atom, S, covalently bonded via bonding orbital b_O to a single bulk atom, B, with bond energy D. The Auger process resulting from a core hole in S or B initially leaves the system in the repulsive state b_O^{-2}, with excitation energy $2 \times E_b + U$, where E_b is the one-electron binding energy of b_O and U is the Coulomb interaction energy resulting from two holes in b_O. The atom S is pushed off the surface initially in state b_O^{-2}. If the holes decay before a critical distance, R_c, S is recaptured; otherwise S gains sufficient kinetic energy to be desorbed. Beyond Rc, S is neutralized leading to the desorption of neutrals (escape along b_n^{-2} where b_n is a bulk bond orbital). The maximum kinetic energy of the outgoing ions is e^2/R_0 (for escape along b_O^{-2}).

This model describes two key points on the PSD and ESD processes in view of dynamic nuclear motion and hole hopping. The first is about the localization of two holes (b_O^{-2}) on a bonding orbital, which is a necessary condition to provide the Coulomb repulsion for expulsion of the ion. General criteria of localization have been recently proposed in the context of Auger spectroscopy. According to Cini-Sawatzky (CS) theory[34,35] or configuration interaction (CI) theory[30,36], localization of the valence holes occurs only if the effective hole-hole repulsion U^{eff} is greater than some appropriate covalent interaction or bandwidth V (i.e., $U^{eff} > V$). Core-valence-valence (CVV) Auger line shape provided direct experimental evidence for localization or delocalization of the valence holes[30].

Second, this model explains the drastic reduction in the ion desorption cross section due to hole-hopping into the bulk (b_O^{-2} to $b_O^{-1} b_n^{-1}$ or b_n^{-2}), while the KF model does not take account of hole-hopping. The lifetime of a multiple hole state is determined by the one or two hole hopping rates, which is closely related to V and U^{eff}. As one- and two-hole hopping rates are given as,

$$R_1 \propto V, \qquad\qquad\qquad \text{Equation (1-1)}$$

$$R_2 \propto (V / U) \times R_1, \qquad\qquad\qquad \text{Equation (1-2)}$$

respectively, two-hole states remain in localized states long enough, which results in increase PSD or ESD probability. In covalent bond systems, the Auger process creates two holes localized in a bonding orbital if $U^{eff} > V$. In addition, if the holes are localized for sufficient long time in the bonding orbital between the atom and the surface, the expulsion of a positively charged ion takes place as a result of the unshielded nuclear-nuclear repulsion (called hole-hole repulsion).

Relation between primary core excitations and final states through Auger processes

PSID is strongly influenced by many-body effects in the primary excitation, fast electronic relaxation, Auger decay, and bond breaking processes. Among them, Auger induced bond-rapture was described above.

How the primary excitations affect both to quantum yields of ion desorption and to internal energy distribution of desorbed species? Below the

author describes the relation between the primary excitation and Auger final states with holes. Final states distribution (in energy) after core excitations makes the PSID process more complicated. However, the molecule's memory of the primary excitation process surely exists (i.e., Memory Effect), and this effect will be actually demonstrated in this thesis with respect to the excitation energy dependence in kinetic energy distributions of ions and ion desorption probability.

Concerning the primary core-excitation, four categories of core-excited states are concerned with PSID, 1) neutral core-excited states ($1s \rightarrow v^*$), 2) ionic core-excited states ($1s \rightarrow c$), 3) core-excited states generated via shake-up ionization ($1s, v \rightarrow c, v^*$) and 4) core-excited states generated via shake-off ionization ($1s, v \rightarrow c, c'$) in the order of the excitation energy, where v, v^*, and c denote, respectively, an occupied and unoccupied valence level, and ionized continuum. The relation between the primary excitation and final states with holes is summarized in Figures 1-6 (a-d).

Near a core ionization threshold [Figure 1-6 (a)], core-resonant excitation ($1s \rightarrow v^*$) occurs and primarily produces core-hole excited states with one-electron in an originally unoccupied orbital. Two types of electronic decay of this state are expected depending on whether the excited electron participates in it or remains in the originally unoccupied orbital. This core-excited state decays to two-valence hole one-electron (2h-1e) final states via spectator Auger process or one-valence hole (1h) states via participant Auger process, where h and e stand for a valence hole and an excited electron, respectively. In addition, two-valence hole (2h) states are formed if the excited electron is ejected via autoionization or delocalizes before Auger process. So-called multiply excited two hole one electron (2h-1e) state is fundamental in initiating dissociation. In the 2h-1e state, the expulsion of the ion usually results from the
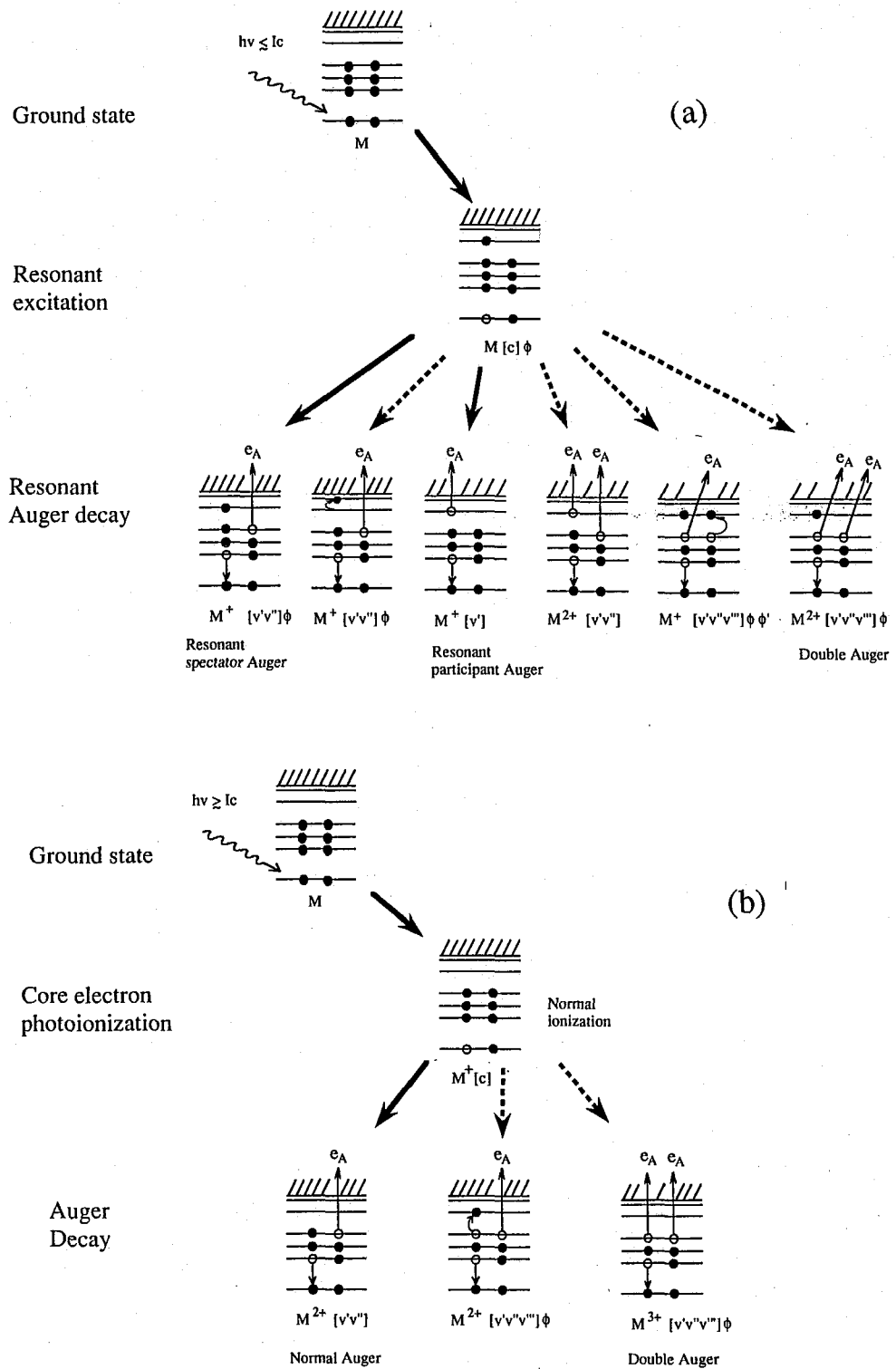
Figure 1-6   Schematic diagram of photoionization and following Auger decay processes using photon energies (a) below (and just on) the resonant excitation, (b) just above,(c) above, and (d) much above the core electron ionization threshold.

Figure 1-6 (continued) — Schematic diagram of photoionization and following Auger decay processes using photon energies (a) below (and just on) the resonant excitation, (b) just above,(c) above, and (d) much above the core electron ionization threshold.

evacuation of a bonding orbital (2h) together with the occupation of a strongly antibonding orbital (1e). The 2h-1e final states were reported to be much effective for the ion desorption as compared with 2h final states[7,30,37]. In the metal-adsorbate system, however, an electron promoted from an inner-shell orbital experiences Auger decay or transfers to substrate depending on the strength of coupling between admolecules and substrate[38,39]. If coupling is strong, the latter process dominates and PSID is suppressed.

Ionic core-excited states ($1s \rightarrow c$) [Figure 1-6 (b)] are primarily formed above a core ionization threshold energy, which mainly yield 2h final states through a normal-Auger (K-VV) process. From the ionic core-excited states, outer-valence three-hole (3h) final states are also formed through a double-Auger (K-VVV) process, which has quite small probability as compared with normal-Auger process[40,41].

At a core ionization threshold energy plus some excess energies, the shake-up ionization process [Figure 1-6 (c)], which is core ionization associated with one-electron excitation ($1s, v \rightarrow c, v^*$) occurs. On the analogy of the core-resonant excitation, these excited states are expected to yield 2h, 3h and 3h-1e final states through Auger process.

At much excess energies from a core ionization threshold, the shake-off ionization process [Figure 1-6 (d)], which is core ionization associated with one-electron ejection ($1s, v \rightarrow c, c'$), occurs. The excited states generated via shake-off ionization mainly yield 3h final states through normal-Auger process and slightly 4h through double-Auger process. The overall production probability of these multiple hole states results in quite small as compared with that of 2-hole by normal K-shell ionization and following normal Auger. Nevertheless, these multiple-holes states have extremely strong Coulomb

interaction and show high localization and repulsiveness. On the surfaces, strongly repulsive and highly localized final states survive without strong influence of screening and quenching by charge transfer and effectively bring about the ion desorption[42,43]. In addition, according to ASD model the reneutralization probability of doubly ionized surface species was shown to be 10^{-1} - 10^{-2} times smaller than that of a singly ionized one, due to hole localization effect or orbital shrinkage effect[33]. Extending this relation to the situation for four-hole (4h) states versus one-hole states, neutralization of the 4h states is much less probable than that of single hole states, which is due to much more localized and shrinkage 4h states.

1.4 History of study on desorption induced by core excitation on the well-defined surface

PSID from a wide variety of surface systems has been demonstrated utilizing specific core excitations by synchrotron radiation. Core excitation is of special interest because drastic changes in the desorption yield have been observed in this region.

Menzel *et al.* have intensively investigated PSID in the adsorption system of CO[4,43], NO[42], C_6D_6[44], and D_2O/H_2O[45] on well-defined single crystal surfaces of transition metals, Ru(001), Cu(100), and Ni(111). They have utilized the polarization of synchrotron radiation and determined the symmetry of primary excitation in PSID. In the covalent system (e.g., CO on Ru(001)), they observed the several fragment ions such as C^+, O^+, O^{2+}, and

CO+ at the C and O K-edge excitation. For two diatomic adsorbate systems (CO and NO), they found following similarities of the energy dependence in PSID: (1) no fragment ion was observed by core excitation of C-atom or N-atom which are directly bonded to substrate atoms; (2) singly and doubly charged fragment ions were much observed by core excitation of O-atom which was not directly bonded to substrate. However, C^+ and O^{2+} ion yield spectra showed a delayed threshold at excess energies of more than 30 eV; (3) the ion yield spectra seem to consist of two components in each fragment ion. One is a relatively small component having polarization-dependent and resonant excitation features. The other is a relatively large component, having overall polarization-independent, and non-resonant excitation features. Latter component gradually increases with an increase in a high excitation region. They concluded the following PSID mechanisms in terms of primary excitation: the former component corresponds to several doubly or triply excitation involving core ionization, and the latter to the shake-off ionization. By comparing the PSID yield spectra with fragment ion yield spectra of the free molecules, they concluded that higher excited states (3h-ne or 4h-ne, n = 0 - 3) survive the quenching with substrate and desorb as ions. The delayed threshold was understood in terms of the influence of tight coupling of the C-atom (or N-atom) of adsorbate CO (or NO) to the substrate, as well as consequent transfer of energy and charge.

In a hydrogen-containing system, other aspects of the desorption mechanism have recently been found[45]. In the gas phase, it has been shown that a light particle, such as hydrogen atom, moves so fast that dissociation occurs during the lifetime of the core ionized states[46]; this is called ultrafast dissociation or rapid dissociation. For a gaseous HBr in the core-to-bound excited state, for example, the rapid dissociation competing with autoionization

has been demonstrated using photoelectron spectroscopy[46]. This was explained in terms of the repulsive nature of Br $3d$ core-hole excited state occupying an antibonding $4p$ /σ^*(H–Br) MO. For PSID, this phenomenon becomes remarkable because only strongly repulsive states can survive quenchings.

Coulman et al.[45] studied the PSID of mono-, bi-, and multi-layers of water on Ru(001) in the O $1s$ excitation region. They observed a strong and sharp peak in the H+ ion yield spectrum and suggested that this was caused by ultra-fast dissociation due to a transition of an O $1s$ electron into the $4a_1$ /σ^*(O–H) strongly antibonding unoccupied orbital localized on the O-H bond sticking out of the surface. Several PSID studies concerning the valence excitation of the adsorbate or core excitation of the substrate[25,47-49]. However, the PSID of hydrogen-containing molecules adsorbed on a semiconductor concerning the core excitation of the adsorbate has scarcely been studied as compared with that on a metal. If the surface $4a_1$ /σ^*(O–H) orbital has strong antibonding character, the ultra-fast dissociation would occur even on the semiconductor surfaces.

Rosenberg et al.[50] studied PSID from D_2O on clean Si(111) surfaces by O $1s$ excitation region. However, they discussed mainly on the surface structures from the PSID results and did not discuss on the desorption mechanisms. They observed only D+ ions in the PSID mass spectrum. By comparison of the D+ desorption yield spectrum from a D_2O-dosed clean Si surface with the total electron yield from an acid-etched (oxide) Si surface by O $1s$ excitation, core-level shift of -2.6 eV from oxide Si was found, which was thought to be caused by the dissociative adsorption of water (Si_3-Si-OH). The D+ PSID yield spectrum has been observed in the O $1s$ excitation region, however, no heavy ions, such as O+ and OH+, were observed. These heavy

ions were barely observed less than a factor of 1/500 relative to the H+ ion in the ice water on Ru(001)[45]. The author believes that yield spectra of ions such as OH+ or O+, which directly bonded to substrate atoms, will provide information on the ion desorption mechanism in the water/semiconductor adsorption system.

1.5 Significance of ion kinetic energy released distribution (KERD) measurement

It has been suggested that resonant excitation from a core level to a σ^*-type antibonding molecular orbital (MO) can give rise to a state-specific desorption occurring in several adsorbates[44,45]. This will enable us to obtain detailed information on the elementary processes of photochemical surface reactions, the electronic property of adsorbate, as well as surface adsorbate-substrate interactions. Recently, therefore, the photon stimulated ion desorption (PSID) regarding the resonant excitation near the core ionization threshold has been extensively studied using a synchrotron radiation with high energy resolution and high photon flux.

The ion desorption is drastically quenched by delocalization of the excitation and/or neutralization of the charged species. Thus, the strongly repulsive states, which are induced by the σ^*-type resonant excitation, can survive these quenching and desorb as ions. As described in Section 1.2, the author has chosen an H_2O-adsorbed Si(100) surface to study the σ^*-resonant enhanced ion-desorption, because this surface has a well-defined dissociative

adsorption structure (SiH + SiOH)[3]. The author briefly describes the properties of O $1s$ core excited states of H_2O adsorbate in the resonant excitation region. With respect to the PSID of the adsorbed H_2O, Coulman *et al.* studied H_2O on Ru(001) in the O $1s$ excitation region[45] (see Section 1.4). The $4a_1/\sigma^*(O-H)$ core excited state, observed by Coulman *et al.*, will be comparable with the state revealed by the ion kinetic energy released distributions (KERDs); see Section 3.5. Moreover, in the K-shell photoabsorption spectrum of gas phase H_2O, five fine structures have been observed and assigned to $4a_1$(534.0 eV), $2b_2$(535.9 eV), and Rydberg states(537.0, 537.8, and 538.4 eV)[53]. The peak corresponding to the $1a_1(O_{1s}) \rightarrow 4a_1/\sigma^*(O-H)$ core-excited state showed relatively large width as well as the absence of resolved vibrational structure. These facts indicate that the $4a_1$ MO has a strongly antibonding nature. The core-excited state can partly decay to two-hole one-electron (2h1e, 1e = $4a_1/\sigma^*(O-H)$) ionic states through spectator Auger processes[7]. In isolated H_2O, most of the 2h1e states occupying the $4a_1/\sigma^*(O-H)$ orbital have the steep repulsive-potential curve along the R_{O-H} coordinate in which the states lead to protons at the asymptotic dissociation limit[7,54,55].

For the rapid dissociation via strongly repulsive states, fragments with high kinetic energies are expected to be released. In other words, kinetic energy released distribution (KERD) will provide information on the mechanism or the potential energy surface of repulsive states in the desorption or dissociation process. For the rapid dissociation of HBr[46] (see Section 1.4), for example, the excitation of $3d$ level to $4p/\sigma^*(H-Br)$ is believed to induce rapid elongation of an H-Br bond (from the equilibrium internuclear distance R_e=1.41 Å) to about 3 Å during the core decay. From this picture, the excited HBr possesses the excess energy corresponding to the difference between

photon energy and dissociation limit; 3.0 eV was estimated. This energy entirely transfers to the hydrogen atom kinetic energy because of the high Br/H mass ratio of 80.

For an electron stimulated desorption (ESD) process, Takano *et al.* studied the KERD of O^+ ions from CO-covered Ni(110) surface in the C $1s$ and O $1s$ excitation regions. They assumed that the KERD comprises three component Gaussian distributions with distinct appearance potentials[56]. From the appearance potentials, these components were assigned to three types of desorption mechanisms, those are valence level ionization, C $1s$ ionization, and shake-off involving O $1s$ ionization. One can, hence, expect that the KERD of ions through photon impact also provides the useful information on the mechanism of the PSID[57,58]. For example, KERDs of O^+ ions photodesorbed from molecularly adsorbed O_2 on Si(111)-(7x7) have been reported[58]. After 46 eV photon absorption and subsequent formation of one electron hole in the O_2/Si(111) inner valence orbital $(2\sigma_g^{-1})$, the KERD consists in a peak centered around 2.5 eV. After Si $2p \rightarrow O_2 3\sigma_u^*(O-O)$ core excitation at 108 eV, on the other hand, the KERD is dominated by a high kinetic energy distribution which has a maximum around 9 eV and extends up to around 13 eV. The 2.5 eV peak of the KERD was believed to result from the removing of two valence electrons from the π and 3σ orbitals. The PSID process producing high energetic O^+ ions was believed most probably to result from the removing more than two valence electrons. These results demonstrate the state-selectivity of the photofragmentation of chemisorbed molecules. From author's view, however, this report is thought to leave ambiguity in the excitation energy dependence of KERD; this report does not describe the results other than the two KERD mentioned above. The KERDs obtained just below and above the ionization thresholds as well as the KERDs obtained enough high

energy region to ionize Si L-shell level should be reported and taken into account for the mechanism of PSID.

The kinetic energy released distribution (KERD) of the desorbed ions induced by the σ^*-type resonant excitation has not yet been investigated in detail. Therefore, in order to investigate the σ^*-resonant excitation in the ion-desorption of the $H_2O/Si(100)$ surface, we planned to measure the KERD of desorbed H^+ ions, using a time-of-flight (TOF) technique with a pulsed synchrotron radiation. The excitation region (500-750 eV) in the present study covers the three types of primary excitations: an Si L-shell ionization ($Si\,2p$ or $2s \to \infty$, 99 eV $<$ hv)[59], O K-shell ionization (O $1s \to \infty$, ca. 537 eV $<$ hv)[16,61], and the lowest shake-off ionization threshold (O $1s, 1b_1 \to \infty, \infty$ or O $1s, 3a_1 \to \infty, \infty$ ca. 570 eV $<$ hv)[62]. Therefore, it will be demonstrated that the observed KERDs are decomposed by three components. By means of measurements and analysis of KERD, it will be clarified that the occupation to a strongly antibonding $\sigma^*(O-H)$ orbital plays an important role in the ion-desorption process. The author notes that this is the first demonstration of the state-specific or bond-selective desorption of core-excited adsorbates.

1.6   About this thesis

The author has investigated an ion desorption mechanisms in the H_2O/Si(100) adsorption system by O $1s$ excitation[51]. This adsorption system contains the several interesting aspects described above. In this thesis, an experimental detail and a mechanism in the PSID is reported. In order to elucidate the mechanism of ion desorption, desorbing ions were efficiently detected by using a time-of-flight mass analysis with the pulsed synchrotron-radiation light, which became a powerful tool for investigating the desorption process[25]. In addition, to obtain the photo-physical information concerning the adsorption layer, an O(KVV) Auger electron yield (AEY) spectrum was measured which corresponded to the inner-shell photoabsorption spectrum of the adsorbate OH species at the surface. The primary excitation processes for the features seen in the relative ion yield spectra are assigned by comparing the experimental results with the theoretical calculations and the previous EELS of isolated H_2O. To examine the role of multiply ionized states in the ion-desorption process, relative ion-desorption yield spectra were compared with those of multiply charged fragments from isolated H_2O. Ion-desorption is enhanced by multiply ionized states formed by shake-off. To assess this mechanism, the photoion-photoion coincidence[52] (PIPICO) was measured. This kind of experiment has never been performed on surfaces, because reneutralization and recapture occur readily. Here, we describe an attempt to measure coincident events between the two kinds of ions which are desorbed by either multiple ionization or excitation. In order to clarify the mechanism on the ion-desorption for the σ^*-resonant excitation, the author has planned to measure the KERD of desorbed ions.

1.7 References

[1] T.J. Chuang, Surf. Sci. Rep., **3**, 1 (1983).

[2] *"Desorption Induced by Electronic Transitions, DIET I"*, edited by N.H. Tolk, M.M. Traum, J.C. Tully, and T.E. Madey, (Springer, Berlin, 1982).

[3] R.D. Ramsier and J.T. Yates, Jr., Surf. Sci. Rep., **12**, 243 (1991) and references therein.

[4] R. Treichler, W. Riedl, W. Wurth, P. Feulner, and D. Menzel, Phys. Rev. Lett., **54**, 462 (1985); in *"Desorption Induced by Electronic Transition, DIET II"*, edited by W. Brenig and D. Menzel, (Springer, Berlin, 1984), p. 68.

[5] R. Jaeger, R. Treichler, and J. Stöh Surf. Sci., **117**, 533 (1982).

[6] R. Jaeger, R. Treichler, and K. Baberschke, Phys. Rev. Lett., **47**, 1300 (1981).

[7] D. E. Ramaker, Chem. Phys., **80**, 183 (1983); J. Chem. Phys., **78**, 2998 (1983).

[8] P.A. Thiel and T.E. Madey, Surf. Sci. Rep., **7**, 211 (1987) and references therein.

[9] F. Meyer, Surf. Sci., **27**, 107 (1971).

[10] K. Fujiwara and M. Nishijima, Phys. Lett., **A55**, 211 (1975).

[11] K. Fujiwara, Surf. Sci., **108**, 124 (1981); J. Chem. Phys., **75**, 5172 (1981).

[12] D. Schmeisser, F. J. Himpsel, and G. Hollinger, Phys. Rev., **B27**, 7813 (1983); D. Schmeisser, Surf. Sci., **137**, 197 (1984); W. Ranke and D. Schmeisser, Surf. Sci., **149**, 485 (1984); W. Ranke, D. Schmeisser, and Y.R. Xing, Surf. Sci., **152/153**, 1103 (1985).

[13] H. Ibach, H. Wagner, and D. Bruchmann, Solid State Commun., **42**, 457

(1982).

[14] H. Kobayashi, T. Kubota, M. Onchi, and M. Nishijima, Phys. Lett., **A95**, 345 (1983).

[15] Y.J. Chabal, Phys. Rev., **B29**, 3677 (1984); Y.J. Chabal and S.B. Christman, Phys. Rev., **B29**, 6974 (1984); Y.J. Chabal, J. Vac. Sci. Technol., **A3**, 1448 (1985).

[16] J.A. Schaefer, J. Anderson, and G. J. Lapeyre, J. Vac. Sci. Technol., **A3**, 1443 (1985); F. Stucki, J. Anderson, G. J. Lapeyre, and H.H. Farrell, Surf. Sci., **143**, 84 (1984); J.A. Schaefer, F. Stucki, D.J. Frankel, W. Goepel, and G.J. Lapeyre, J. Vac. Sci. Technol., **B2**, 359 (1984).

[17] M. Nishijima, K. Edamoto, Y. Kubota, S. Tanaka, and M. Onchi, J. Chem. Phys., **84**, 6458 (1986).

[18] H. Ibach, H. Wagner, and D. Bruchmann, Solid State Commun., **42**, 457 (1982); F. Stucki, J. Anderson, G. J. Lapeyre and H.H. Farrell, Surf. Sci., **142**, 84 (1984).

[19] Y.J. Chabal and S.B. Christman, Phys. Rev., **B29**, 2974 (1984); Y.J. Chabal, J. Vac. Sci. Technol., **A3**, 1448 (1985); Y.J. Chabal and S.B. Christman, Phys. Rev., **B29**, 6974 (1984); Y.J. Chabal, J. Vac. Sci. Technol., **A3**, 1448 (1985).

[20] E.M. Oellig, R. Butz, H. Wagner, and H. Ibach, Solid State Commun., **51**, 7 (1984).

[21] C.U.S. Larsson, A.L. Johnson, A. Frodström and T.E. Madey, J. Vac. Sci. Technol., **A5**, 842 (1987).

[22] K. Fives, R. McGrath, C. Stephens, I.T. McGovern, R. Cimino, D.S-.L. Law, A.L. Johnson, and G. Thornton, J. Phys.: Condens. Matter **1**, SB105 (1989).

[23] L. Andersohn and U. Köhler, Surf. Sci., **284**, 77 (1993) M. Chander, Y.Z. Li, J.C. Patrin, and J.H. Weaver, Phys. Rev., **B48**, 2493 (1993).

[24] S. Katircioglu, Surf. Sci., **187**, 569 (1987).

[25] M.L. Knotek, V.O. Jones, and V. Rehn, Phys. Rev. Lett, **43**, 300 (1979).

[26] D. Menzel and R. Gomer, J. Chem. Phys., **41**, 3311 (1964).

[27] P.A. Redhead, Can. J. Phys., **42**, 886 (1964).

[28] M.L. Knotek and P.J. Feibelman, Phys. Rev. Lett., **40**, 964(1978); Surf. Sci., **90**, 78 (1979); Phys. Rev., **B18**, 6531(1978); P.J. Feibelman, Surf. Sci.,**102**, L51 (1981).

[29] T.A. Carlson, DIET I, p. 169.

[30] D.E. Ramaker, C.T. White, and J.S. Murday, Phys. Lett., **89A**, 211 (1982); D.E. Ramaker, J. Vac. Sci. Technol., **A1**, 1137 (1983); D.E. Ramaker, Phys. Rev. **B21**, 4608 (1980); B.I. Dunlap, F.L. Hutson, and D.E. Ramaker, J. Vac. Sci. Technol., **18**, 556 (1981).

[31] M. Cini, Phys. Rev., **B32**, 1945 (1985).

[32] H.H. Madden, D.R. Jennison, M.M. Traum, G. Margaritondo, and N.G. Stoffel, Phys. Rev., **B26**, 896 (1982).

[33] P.J. Feibelman, Surf, Sci., **102**, L51 (1981).

[34] M. Cini, Phys. Rev., **B17**, 2788 (1978); Surf. Sci., **87**, 483 (1979).

[35] G.A. Sawatsky, Phys. Rev. Lett., **39**, 504 (1977); G.A. Sawatsky and A. Lenselink, Phys. Rev., **B21**, 1790 (1980).

[36] R. Arneberg, J. Müller, and R. Manne Chem. Phys., **64**, 249 (1982).

[37] T.E. Madey, D.E. Ramaker, R. Stockbauer, Ann. Rev. Phys. Chem., **35**, 215 (1984).

[38] W. Wurth, C. Schneider, R. Treichler, E. Umbach, and D. Menzel, Phys. Rev., **B35**, 7741 (1987); W.Wurth, P. Feulner, and D. Menzel, Physica Scripta, **T41**,213(1992).

[39] O. Björneholm, A. Sandell, A. Nilsson, N. Mårtensso J.N. Andersen, Physica. Scripta., **T41**, 217 (1992).

[40] T.A. Carlson, *"Photoelectron and Auger spectroscopy"* chapter 6, and

references therein.

[41] *"Advances in Chemical Physics Vol. LXXVII"* edited by I. Prigogine and S.A Rice (John Wiley and Sons, Inc., 1990) and references therein.

[42] R. Treichler, W. Riedl, P. Feulner, and D. Menzel, Surf. Sci., **243**, 239 (1991).

[43] R. Treichler, W. Wurth, W. Riedl, P. Feulner, and D. Menzel, Chem. Phys., **153**, 259 (1991).

[44] D. Menzel, G. Rocker, H.-P. Steinrück, D. Coulman P.A. Heimann, W. Huber, P. Zebisch, and D.R. Lloyd, J. Chem. Phys., **96**, 1724 (1992); D. Menzel, AIP Conference Proceedings No. 258, *"Synchrotron Radiation and Dynamic Phenomena"*, edited by. A.Beswick (Amer. Inst. Phys., 1992).

[45] D. Menzel, G. Rocker, D. Coulman, P. Feulner, and W. Wurth, Physica Scripta, **41**, 588 (1990); D. Coulman, A. Puschmann, W. Wurth, H.-P. Steinrück and D. Menzel, Chem. Phys. Lett., **148**, 371(1988); D. Coulman, A. Puschmann, U. Höfer, H.-P. Steinrück W. Wurth, P. Feulner, and D. Menzel, J. Chem. Phys., **93**, 58 (1990).

[46] P. Morin and I. Nenner, Phys. Rev. Lett., **56**, 1913 (1986).

[47] G. Thornton, R.A. Rosenberg, V. Rehn, A.K. Green, and C.C. Parks, Solid State Commun., **40**, 131 (1981); R.A. Rosenberg, and C.-R. Wen, J. Vac. Sci. Technol., **A6**, 827 (1988).

[48] M. Niwano, Y. Takakuwa, H. Katakura, N. Miyamoto, J. Vac. Sci. Technol., **A9**, 212 (1991).

[49] R. McGrath, I.T. McGovern, D.R. Waburton, G. Thornton, and D. Norman, Surf. Sci., **178**, 101 (1986); R. McGrath, I.T. McGovern, D.R. Waburton, D. Purdie, C.A. Muryn, N.S. Prakash, P.L. Wincott, G. Thornton, D.S-L. Law, and D. Norman, Phys. Rev., **B45**, 9327 (1992).

[50] R.A. Rosenberg, P.J. Love, V. Rehn, I. Owen, G. Thornton, J. Vac. Sci. Technol., **A4**, 1451 (1986); R.A. Rosenberg, C.R-. Wen, and D.C. Mancini, in *"Desorption Induced by Electronic Transition, DIET III"*,

edited by R.H. Stulen and M.L. Knotek, (Springer, Berlin, 1987), p.220.

[51] T. Sekiguchi, H. Ikeura, K. Tanaka, K. Obi, N. Ueno, and K. Honma, J. Chem. Phys., **102**, 1422(1995); K. Tanaka, H. Ikeura, N. Ueno, Y. Kobayashi, K. Obi, T. Sekiguchi, and K. Honma, AIP Conference Proceedings No. 258, "*Synchrotron Radiation and Dynamic Phenomena*", edited by A. Beswick (Amer. Inst. Phys., 1992); H. Ikeura, T. Sekiguchi, K. Tanaka, K. Obi, N. Ueno, and K. Honma, Jpn. J. Appl. Phys., **32**, **Suppl. 32-2**, 246 (1993).

[52] G. Dujardin, S. Leach, O. Dutuit, P-.M. Guyon, and M. Richard-Viard, Chem. Phys., **88**, 339 (1984).

[53] J. Schirmer, A.B. Trofimov, K.J. Randall, J. Feldhaus, A.M. Bradshaw, Y. Ma, C.T. Chen, and F. Sette, Phys. Rev., **A47**, 1136 (1993).

[54] J.O. Noell, C.F. Melius, and R.H. Stulen, Surf. Sci., **157**, 119(1985).

[55] J.C. Leclerc, J.A. Horsely, and J.C. Lorquet, Chem. Phys., **4**, 337(1974).

[56] A. Takano and K. Ueda, Appl. Surf. Sci., **60/61**, 693 (1992).

[57] G. Dujardin, L. Hellner, L. Philippe, M-J. Besnard-Ramage, and P. Cirkel, Phys. Rev., **B48**, 14529 (1993).

[58] G. Dujardin, G. Comlet, L. Hellner, T. Hirayama, M. Rose, L. Philippe, and M.J. Besnard-Ramage, Phys. Rev. Lett., **73**, 1727 (1994).

[59] "*Handbook of X-Ray Photoelectron Spectroscopy*", p. 53, edited by C.D. Wagner, W.M. Riggs, L.E. Davis, J.F. Moulder, and G.E. Muilenberg, (Perkin-Elmer Corp., Minnesota, 1979).

[60] V.S. Fomenko, Handbook of Thermionic Properties (Plenum, New York, 1966).

[61] The author approximately estimates the O K-edge threshold energy by summing the binding energy (E_b^F = 532 eV) for O $1s$ level in the H_2O/Si(100) [Ref. 16] and the work function (~4.8 eV) of Si [Ref. 60].

[62] H. Ågren and V. Carravetta, J. Chem. Phys., **87**, 370(1987).

Chapter 2

EXPERIMENTAL

2.1 Experimental apparatus

The experiments were performed at the grasshopper monochromator beam line (BL 11A[1]) of the Photon Factory (PF) at the National Laboratory for High Energy Physics. The photon energy range of this beam line is 90-1000 eV, which covers the K-shell excitation of carbon, nitrogen, oxygen and fluorine atoms. A schematic diagram of an experimental apparatus is shown in Figure 2-1. A double-pass cylindrical mirror electron energy analyzer (CMA [Perkin Elmer 15-255G]) was equipped for photoelectron spectroscopy (XPS), Auger electron spectroscopy (AES), and Auger NEXAFS, i.e., Auger electron yield (AEY) spectra, at a fixed angle of 75° with respect to the light beam. A quadrupole mass spectrometer (QMS [ULVAC MSQ-400]) was equipped for background gas analysis in a chamber. Sputter cleaning of the sample was carried out with an ion gun. [Varian 981-2046] A time-of-flight mass spectrometer (TOF-MS) was also equipped for the detection of desorbing ions. The TOF-MS was fixed at an angle of 75° with respect to the light beam. The TOF-MS for the PSID experiments, which was specially designed and made for this experiments, is schematically shown in Figure 2-2. It comprised an accelerating plate (Pacc), a field-free drift tube (DT) of 9 cm length and a microchannel plate detector (MCP [Hamamatsu F1094-21]). The accelerating plate was located at the normal direction and 3 cm away from the sample surface. In the detection of electrons and ions, the angles between the

CMA

Ion gun

Sample

Au mesh

SR

Q-mass

TOF-MCP

0   100   200   300   400   500 mm
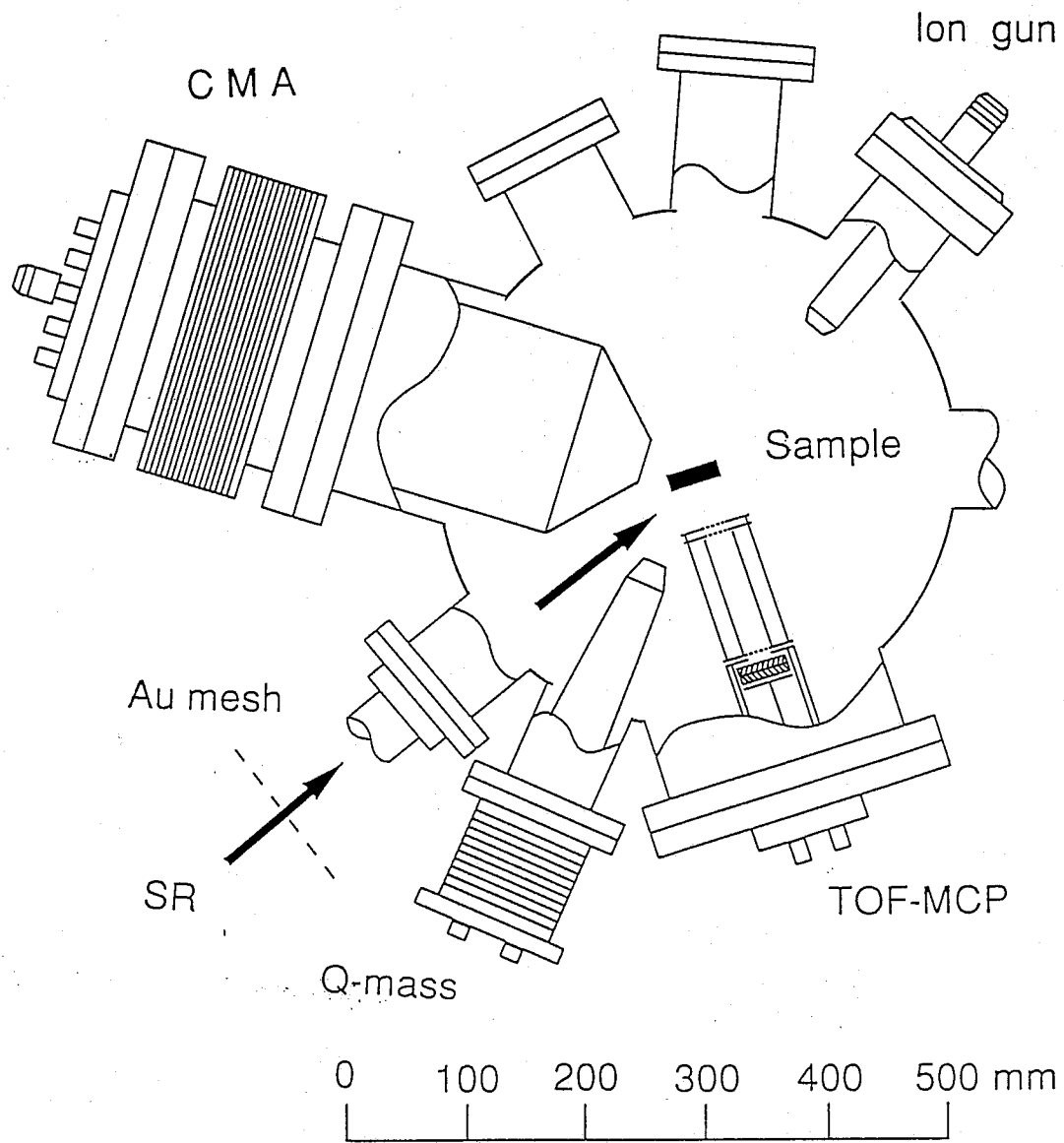
Figure 2-1   Top view of ultrahigh vacuum apparatus for PSID experiments.

MCP

DT

P_ACC

0 1 2 3 4 5cm
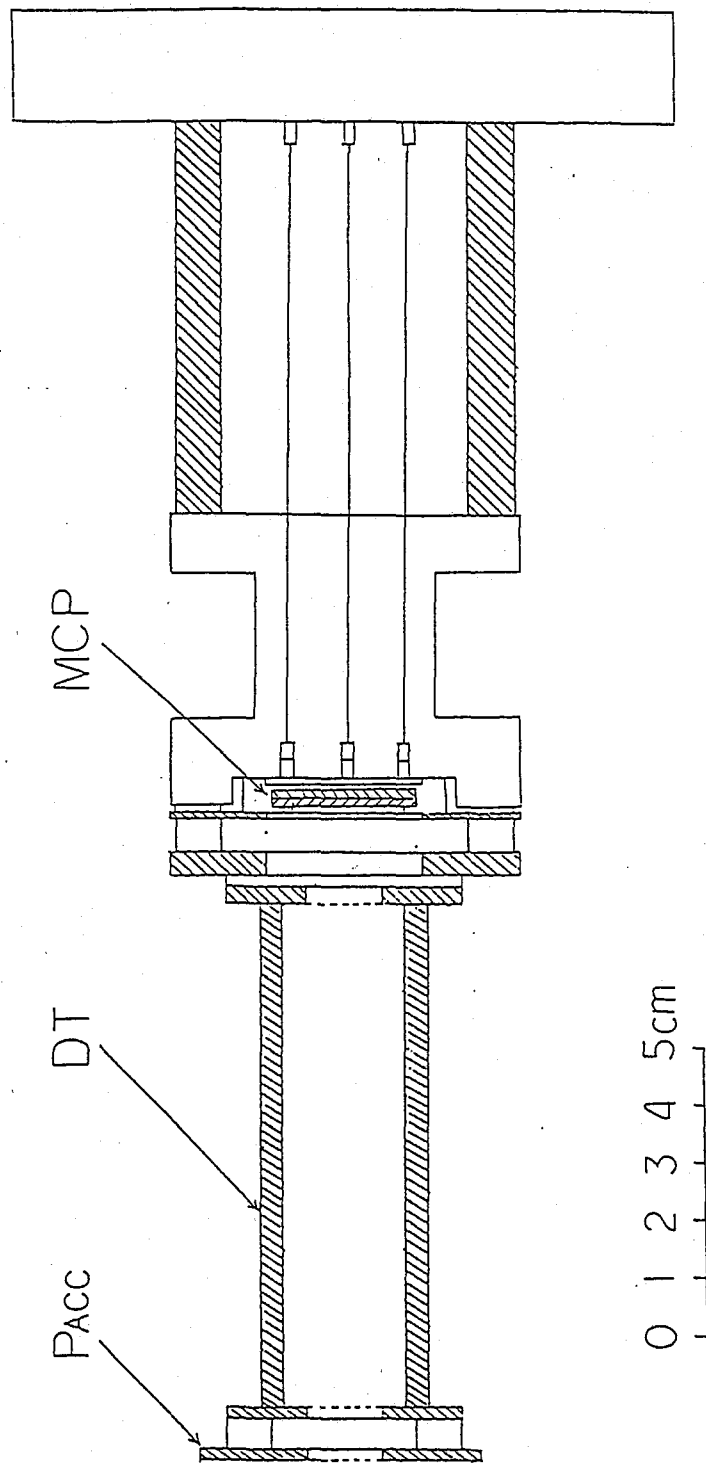
Figure 2-2   A schematic diagram of TOF-MS for PSID measurements.

polarization vector of light (**E**) and the crystal surface normal were both fixed at 15°.

All equipments were set up in an ultra-high vacuum (UHV) chamber, which was evacuated with 400 l/s and 50 l/s tandem turbomolecular pumps and a titanium cryo-sublimation pump. After being baked out, the base pressure was typically 2×10^{-8} Pa. The pressure during measurements was 9×10^{-8} Pa. The sample crystal was mounted on a precision manipulator which allowed it to rotate for either ion or electron detection. The sample could be heated up to 1200 K indirectly by passing current through a tantalum foil located close behind the sample, the temperature of which was monitored with a chromel-alumel thermocouple attached to the sample holder. All of the measurements were made at room temperature.

2.2 Principle of measurements of the ion time-of-flight (TOF) spectra

Desorbing ions were detected using the TOF-MS with pulsed synchrotron radiation. A schematic diagram of the experimental arrangement for the ion TOF measurement is shown in Figure 2-3. The PF ring was operated at 2.5 GeV with a maximum current of approximately 60 mA in the single-bunch mode. Soft X-ray pulses with a 624 ns interval and 100 ps width were incident on the sample at an angle of 15° from the surface. Desorbing ions generated with the pulsed synchrotron radiation were efficiently mass

Figure 2-3   Schematic diagram of experimental arrangement for ion TOF measurements. The abbreviations used are as follows: Au, gold-coated tungsten grid; A, amperemeter; AMP, amplifier; CFD, constant-fraction discriminator; DELAY, delay circuit. See text for other abbreviations.

analyzed with the TOF-MS tube.

Ion TOF spectra were obtained using a time-to-amplitude converter (TAC [ORTEC 567]) and a pulse-height analyzer (PHA [CANBERRA model 3502]), where an ion signal was fed into the start-input and a radio-frequency (RF) timing signal into the stop-input of the TAC. This start and stop order on the TAC can minimize the dead time of the TAC more than the reverse order, and the use of the RF timing signal instead of a light trigger signal can collect the signal more efficiently. In a typical ion TOF measurement, the following voltages were applied to the TOF-MS detector, achieving the time resolution of about 2 ns: E_{SAM} = 400 V, E_{ACC} = -2000 V, E_{TOF} = -2000 V and E_{MCP} = -2200 V (see Figure 2-3). A reference in the time scale was determined with a prompt peak corresponding to the scattered light from the sample surface. The TOF of each desorbing ion was obtained from the difference in time between the prompt peak and the observed peak.

Figure 2-4 shows a typical ion TOF spectrum obtained from 10L H_2O/Si(100) at 700 eV photon energy. The H^+ ion was found to be the dominant product. O^+ and O^{2+} ions can easily be identified from their TOF's by using a linear relation between the TOF and $(m/q)^{1/2}$ value. The calculated mass scale is given in Figure 2-4. Since the time reproducibility of the SR pulses is extremely good, heavy ions whose flight times were longer than 624 ns could also be observed. The TOF of the heavy ions is given by its position in the spectrum plus an integer multiple of the SR pulse interval (624 ns). Therefore, all of the ions are superimposed on the TOF spectrum with a fixed time range of 624 ns.
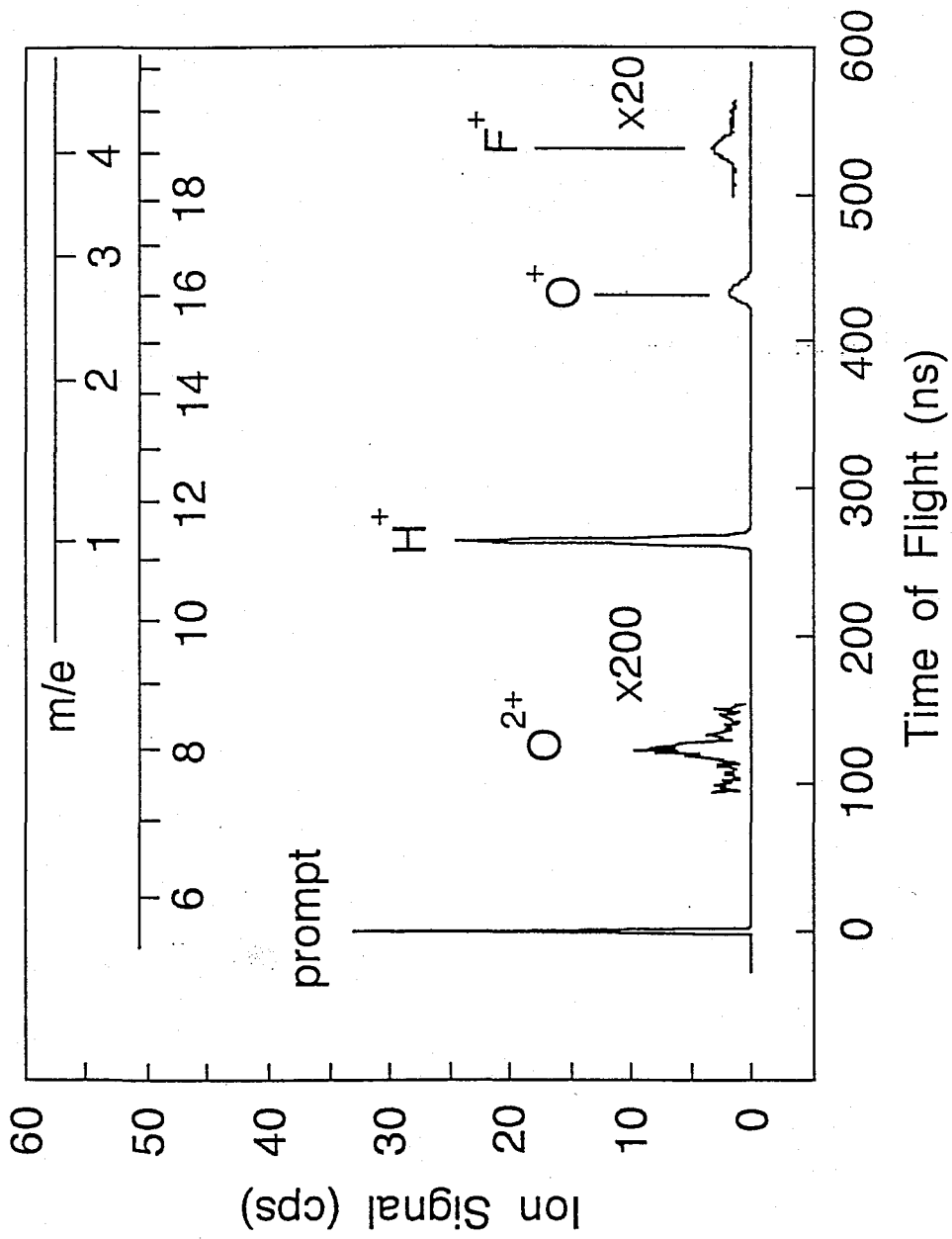
Figure 2-4   Typical ion TOF spectrum obtained in H2O/Si(100) at 700
eV photon energy.

2.3 Principle of measurements of the photoion photoion coincidence (PIPICO) spectra

Photoion photoion coincidence (PIPICO) measurements were performed with a synchrotron radiation under multi-bunch-mode operation. In this mode, the synchrotron radiation is used as continuous light source, in fact, which is pulse light with 2 ns interval and 100 ps width. A schematic diagram of the experimental arrangement for the PIPICO measurement is shown in Figure 2-5. The PIPICO spectra were obtained using modified TOF-MS techniques, in which the TAC was started and stopped by signals from the same ion detector; the start signal was delayed for ca. 60 ns in order to diminish electrical ringing noises. In the PIPICO measurements, the same potentials as TOF measurements were applied to the TOF-MS detector (see the preceding section). PIPICO signals were obtained and accumulated at the TOF difference between two ions produced simultaneously by one photon excitation.

Because a probability of coincident events for two ion desorption is very low, signal rate was greatly small, which was order of $\sim 10^{-2}$ cps with the conditions of photon flux of ca. 10^{12} photon/sec and the photon energy of 700 eV. This is much lower as compared with that ($\sim 10^4$ cps) of PIPICO measurement in the gas phase. In addition, a noise rate was about $2\text{-}3 \times 10^{-2}$ cps. Therefore, it took for about 3 hours to obtain one typical PIPICO spectrum.
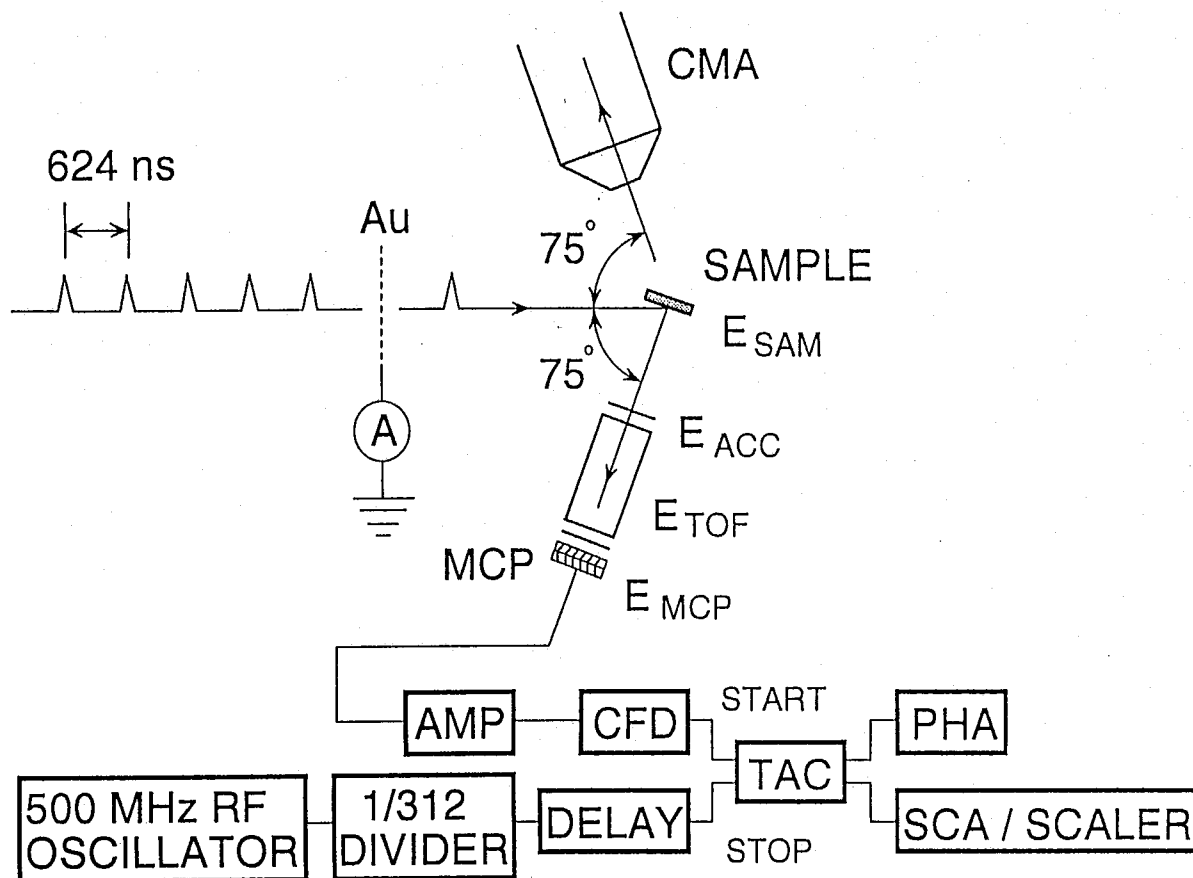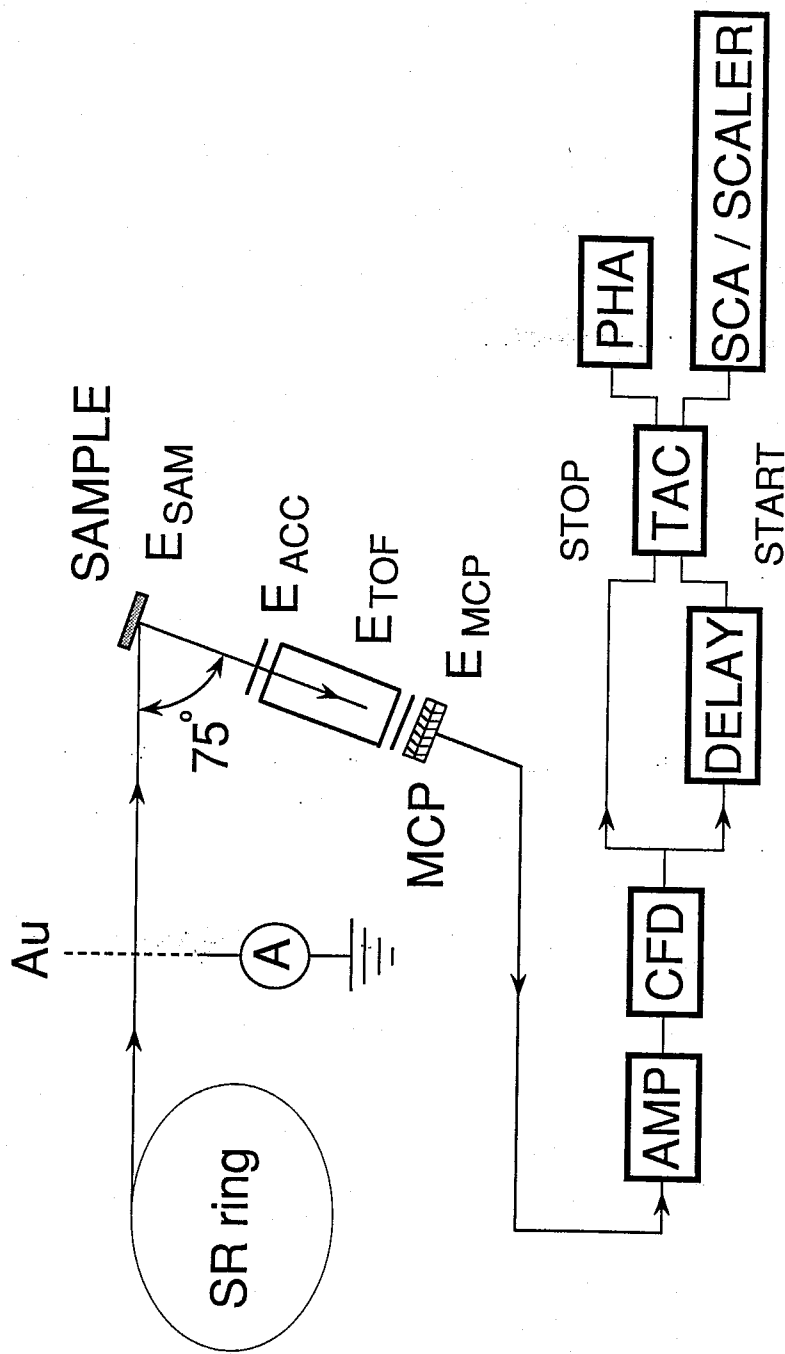
Figure 2-5   Schematic diagram of experimental arrangement for PIPICO measurements. The abbreviations used are as follows: Au, gold-coated tungsten grid; A, amperemeter; AMP, amplifier; CFD, constant-fraction discriminator; DELAY, delay circuit. See text for other abbreviations.

2.4 Measurement and data treatment of the relative photon stimulated ion desorption (PSID) yield spectra

A relative photon stimulated ion desorption (PSID) yield spectrum was obtained by acquiring the output signals of the TAC within a particular single-channel analyzer (SCA) window corresponding to the ion to be analyzed as a function of the photon energy. These measurements were made in the 515-610 eV energy range, which covers O K-shell excitation. To normalize all spectra for the incident photon flux (I_0), a gold-coated tungsten grid was used as an I_0 detector. The characteristic dips caused by the absorption of a chromium on the optics (Cr $2p_{1/2}$ 584.9 eV, $2p_{3/2}$ 576.5 eV)[2] were observed in the I_0 spectrum and were used for an absolute energy calibration. PSID yield spectra were obtained by averaging 5 independent measurements in which the data point, the energy step and the accumulation time were 256, 0.353 eV and 70 sec, respectively. A slit width of 30 μm for both entrance and exit slits and a 1200 lines/mm grating were used, giving an energy resolving power of ca. 2 eV at 500 eV.

As shown in Figure 2-6 (a), the H^+ ion was observed even below the O K-edge and has the substantial background constituents in the ion yield above the K-edge. This is mainly caused by L-shell excitation of the substrate Si atoms, which disturbs determination of the amount of the H^+ desorption from the surface OH species only by the O $1s$ excitation. To eliminate the background constituents, the photoabsorption spectrum of the pure Si [Figure 2-6 (b)][3] was subtracted from the observed H^+ yield spectrum [Figure 2-6 (a)] after normalization, so as to make the subtracted H^+ yield spectrum [Figure 2-6 (c)] show zero at 515 eV, just below the O K-edge.
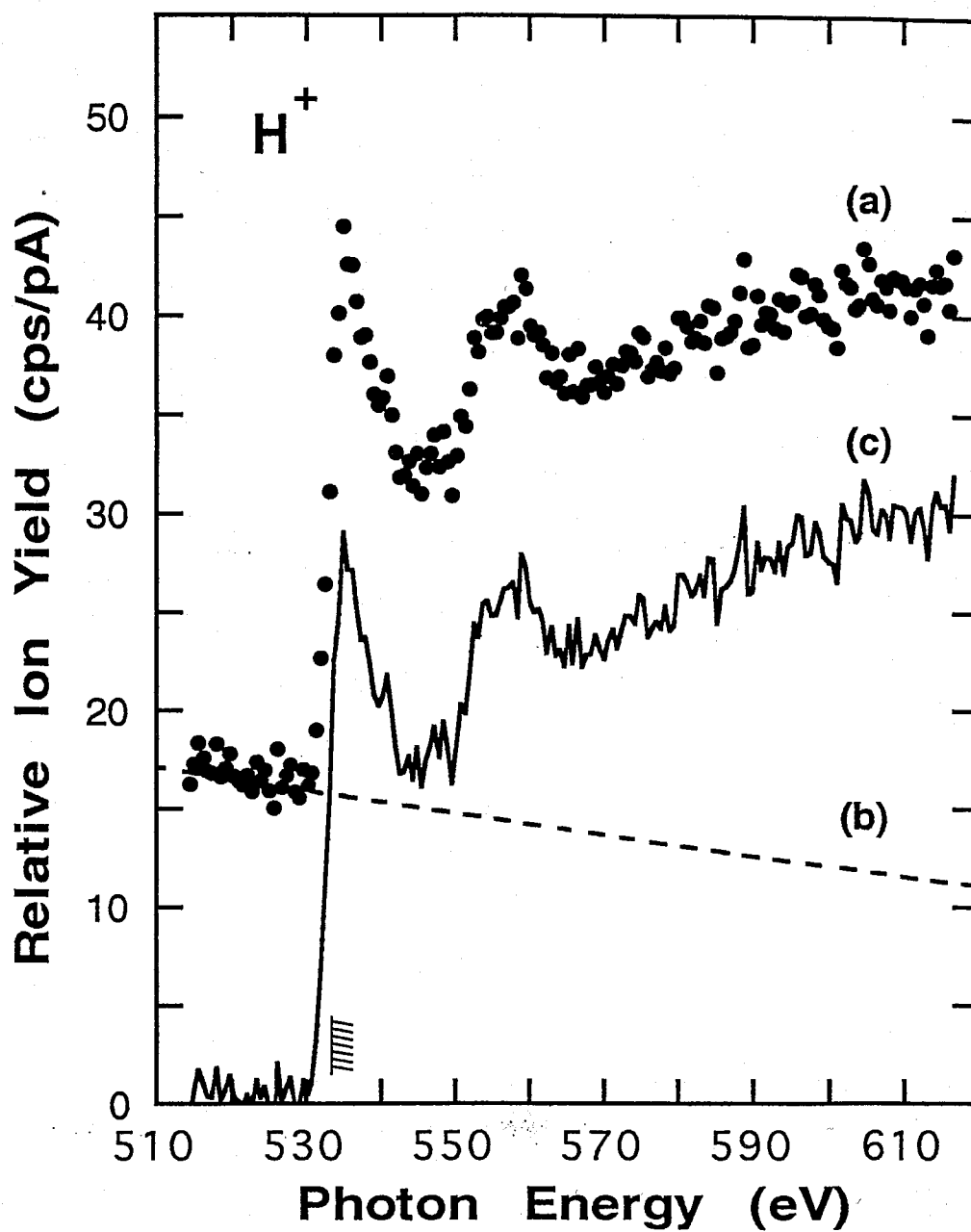
Figure 2-6 (a) PSID yield spectrum of H+ from H2O/Si(100); (b) The component of Si L-shell excitation. (c) The subtracted H+ yield spectrum (a-b). The O 1s binding energy [Ref. 41] relative to the Fermi level is indicated by slant line.

2.5 Measurement and data treatment of the Auger electron yield (AEY) spectrum

To obtain the photoabsorption cross section of the adsorbate OH in this experimental system, an AEY spectrum, which corresponds to the absorption spectrum, was measured in the 515-600 eV energy range by monitoring the intensity of the angle-integrated oxygen KVV Auger electron (503 eV) of the adsorbate, where the Auger decay electron spectra of this system did not change at any excitation energies and the maximum was 503 eV. The electron analyzer was calibrated by using the Si 2p3/2 peak (E_b^F = 99.2 eV)[4] of the clean Si. The AEY spectrum was normalized using the photon flux in the same way as was described in the ion yield spectra.

A typical AEY spectrum obtained by monitoring the electrons with the kinetic energy of 503 eV is shown in Figure 2-7 (a). Besides Auger electron signals obtained above 530 eV, background arising from valence level and Si $2p$ photoelectrons and inelastically scattered electrons are seen above ca. 500 and 600 eV, respectively. To determine the contribution of these photoelectrons, the blank (background) spectrum was measured by monitoring the electrons having kinetic energy other than 503 eV, which do not include the Auger electrons. Figure 2-7 (b) shows a blank spectrum obtained by monitoring 530 eV electrons. Because the excitation photon energy is much higher than the binding energy of these valence electrons, the photoionization cross section of these valence electrons is considered to be almost constant in these two spectra. Thus, the blank spectrum in Figure 2-7 (b) can be used for the background contribution in the observed AEY spectrum. The net AEY spectrum is obtained by subtracting the blank spectrum [Figure 2-7 (b)] from the observed

AEY spectrum [Figure 2-7 (a)] after aligning the position of the Si 2p peak and normalizing the intensity just below the O K-edge and is shown in Figure 3-2 (a).
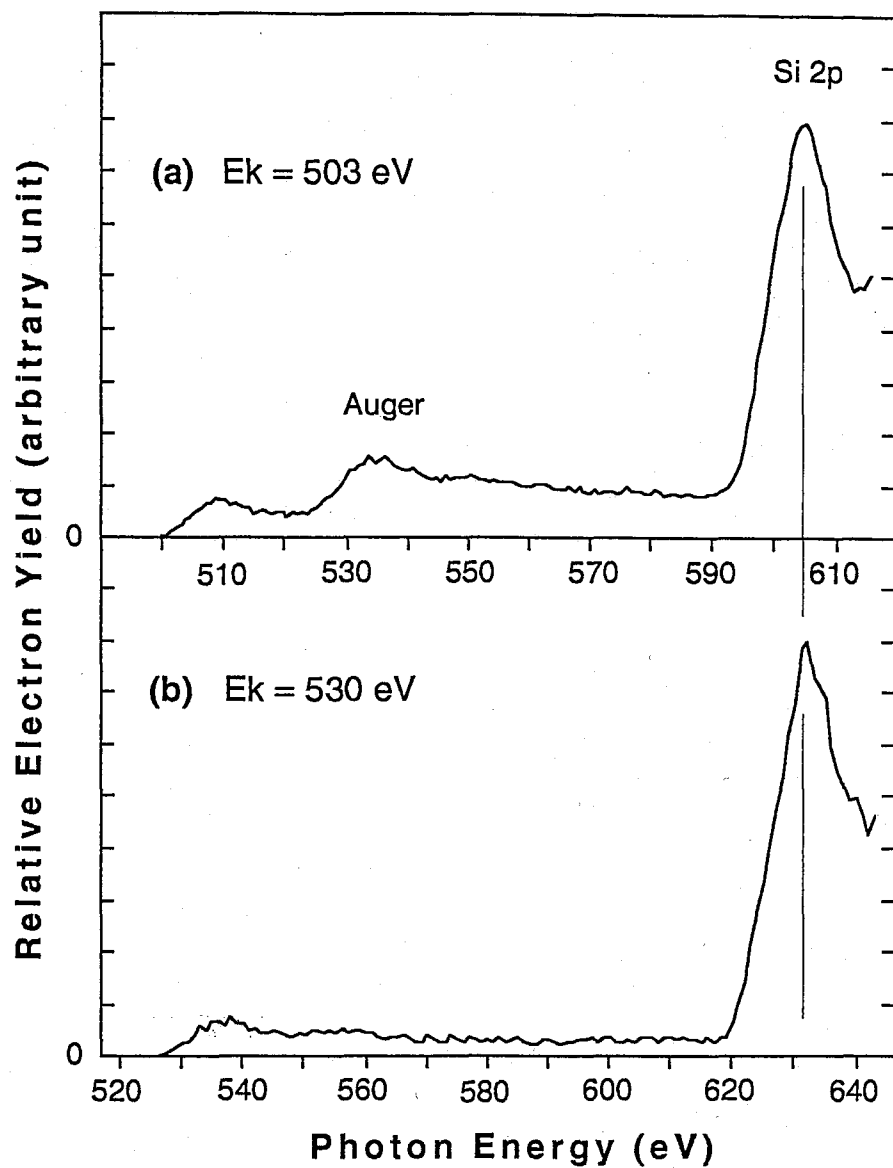
Figure 2-7   Partial electron yield spectrum at the kinetic energy of (a)

503 eV and (b) 530 eV.

2.6 Sample preparation

The author used a Si(100) wafer (n-type, P-doped, >1000 Ωcm) having a rectangular shape ($15 \times 13 \times 0.8$ mm^3) as a sample substrate. It was first degreased and dipped in buffered hydrogen fluoride solution to remove surface contaminants and native oxide. Subsequently it was immersed in an acidic-H_2O_2, and rinsed with pure water to grow a new oxide layer which protects the clean surface from carbon contamination[5]. After chemical cleaning, it was transferred in air to the manipulator in the UHV chamber. A Si(100)-(2x1) surface was cleaned by a cycles of annealing (1200 K, 10 min.), Ar$^+$ ion bombardment (750 K, 900 eV, 20 min.) and annealing (1200 K, 10 min.), and then was slowly cooled down to room temperature.

After each cycle, elimination of the oxide protection layer was verified by the Si 2p XPS spectrum. Figure 2-8 shows Si 2p XPS spectra before and after cleaning a sample crystal, which was obtained with the photon energy of 260 eV. Two peaks in the observed XPS spectra are easily assigned; the peaks observed at $E_b^F = 104.2$ eV and $E_b^F = 107.2$ eV correspond to bulk silicon (Si^0) and oxide silicon (Si^{4+}), respectively[6-9]. The carbon impurity level was checked by observing the C (KLL) peak in an Auger electron spectrum. Figure 2-9 shows the Auger electron spectrum obtained with 2 keV electron beam before and after cleaning sample. As shown in Figure 2-9, intensities of C(KLL) and O(KLL) peaks become negligibly small relative to that of Si(LVV) peak after cleaning sample. These procedures were repeated until the surface became clean. The surface cleanness was also verified by the absence of the F$^+$ desorption peak upon 700 eV excitation. No surface order was checked.

Commercially available H_2O (Junsei Chemical Co.) was used as an adsorbate gas. H_2O in a stainless-steel bottle was degassed by several freeze-pump-thaw cycles in a vacuum system. After degassing, the bottle was attached to the experimental apparatus via a variable-leak valve. The sample substrate was exposed to 10L (1×10^{-7} Torr. $\times$ 100 sec.) H_2O at room temperature, resulting in saturation coverage. The adsorption of H_2O on the Si(100)-(2x1) surface at room temperature results in dissociative adsorption (SiH + SiOH), as described above.
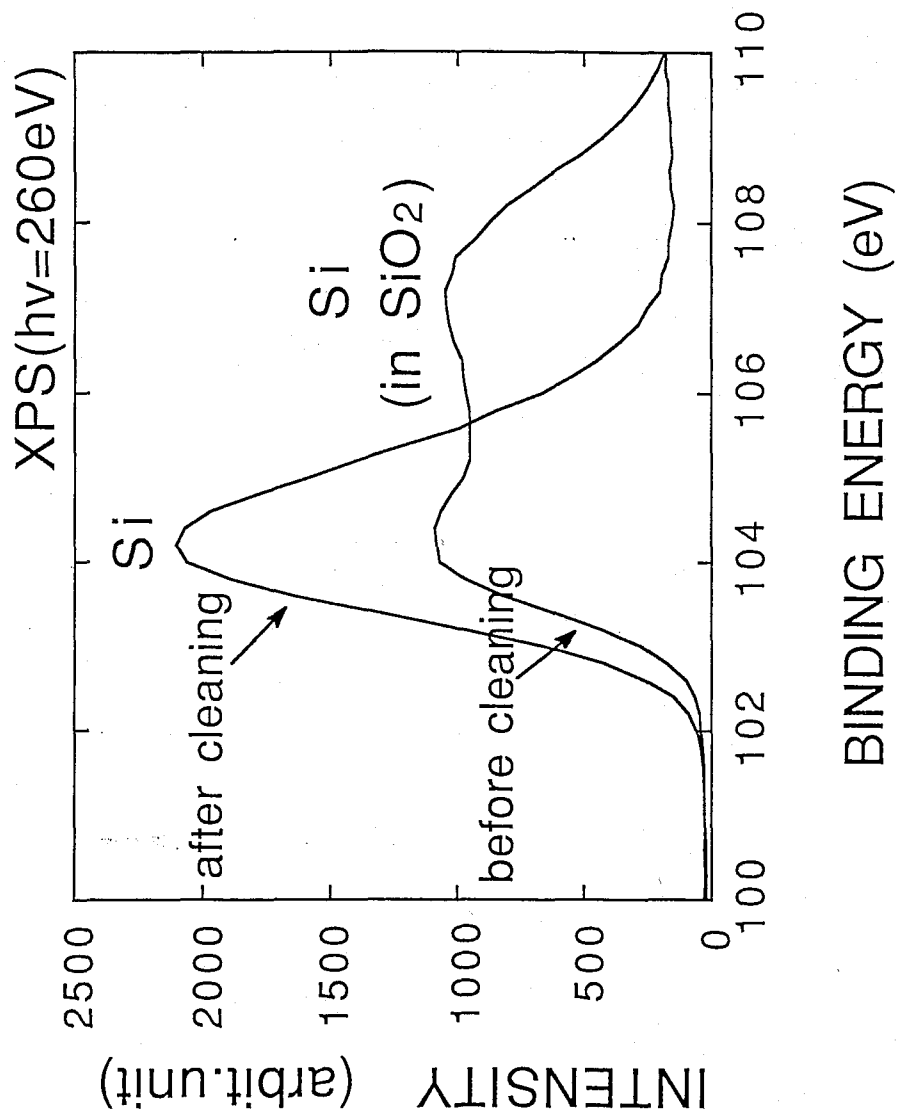
Figure 2-8   Si 2*p* XPS spectra of Si(100) before and after cleaning sample.

(a) before cleaning
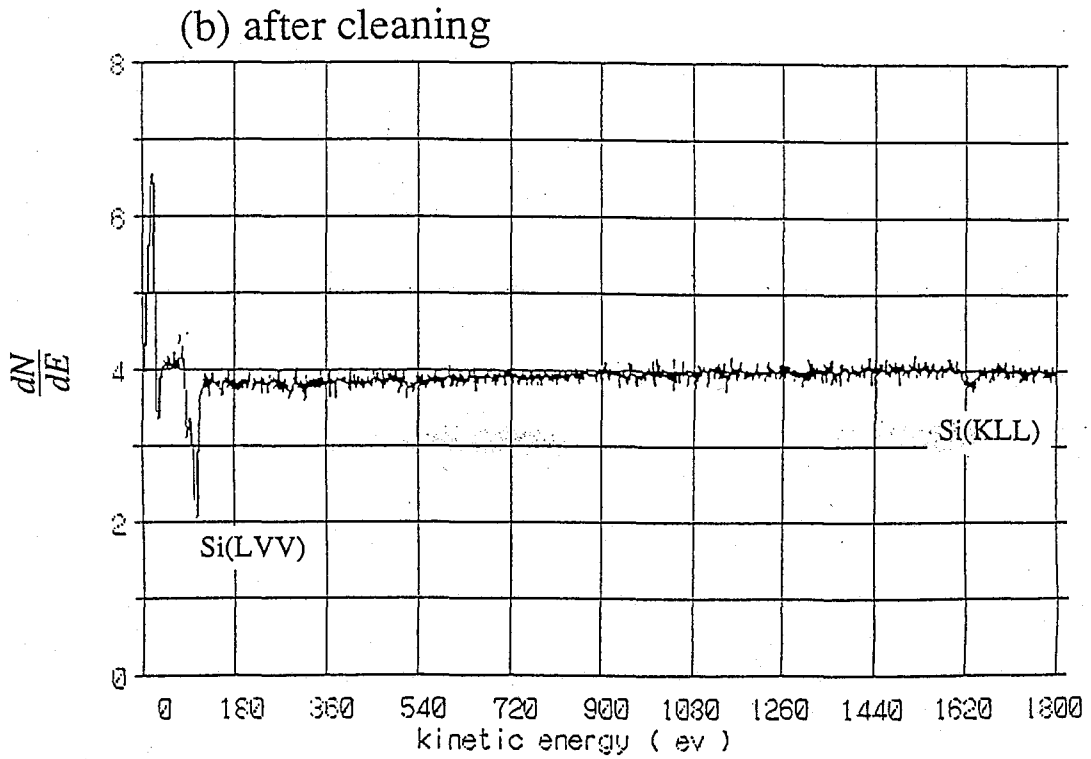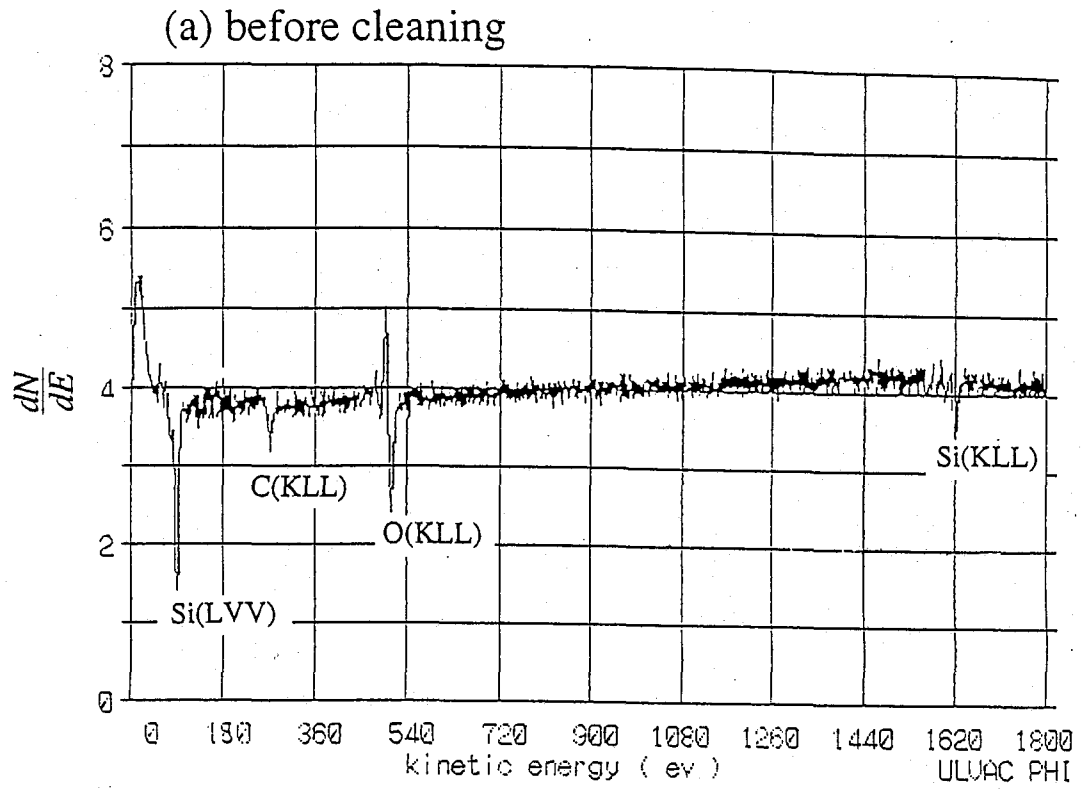
(b) after cleaning

Figure 2-9   Auger electron spectra of Si(100) obtained with 2-keV

electron beam energy (a) before and (b) after cleaning sample.

2.7 Experimental apparatus for gas phase photodissociation

A TOF-MS and experimental chamber[10] used for the gas phase photofragment measurements is schematically shown in Figure 2-10. It consists of an ionization section of variable length (typically 14 mm), an accelerating plate, a field-free drift tube of 44 cm length, and MCP for the fragment ion detection. These are assembled in a vacuum chamber with 500 l/s turbomolecular pump. The photon beam is focused on the center of the ionization section for the TOF-MS. Sample gas is introduced to the ionization section as an effusive beam through a nozzle with a diameter of 0.8 mm so that the molecular beam crosses the photon beam at the right angle.

MCP

Drift tube

Deflector

Gas nozzle

MCP

510ℓ/sec
Turbo molecular pump
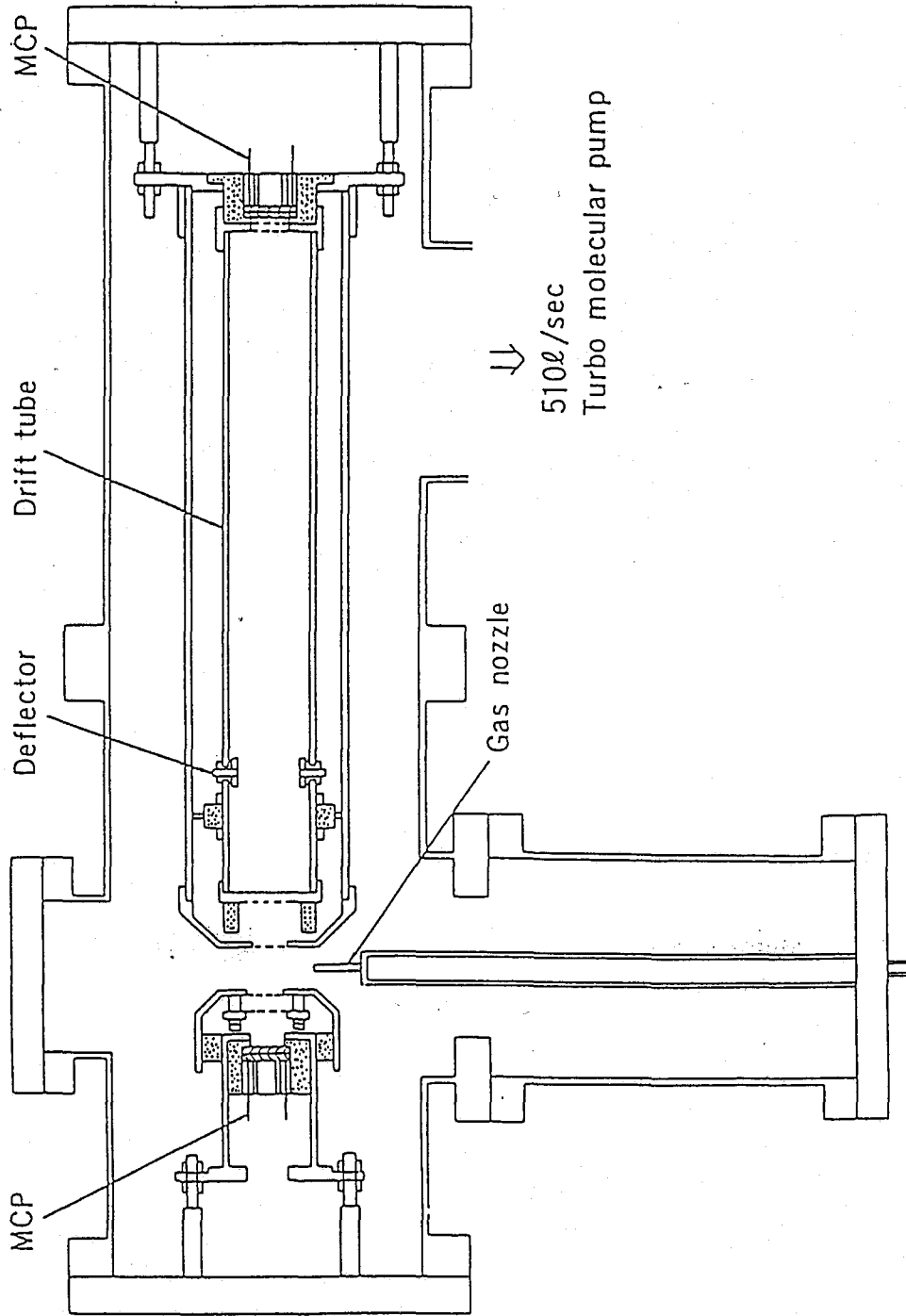
Figure 2-10   Schematic view of time-of-flight mass spectrometer.

53

2.8 Measurement and analysis of ion kinetic energy released distributions

Kinetic energy released distributions (KERDs) of ions were calculated from time-of-flight (TOF) spectra which were measured with high time resolution. To resolve the TOF spectra as well as possible, a shorter TAC range was used, by which a peak of interest was expanded to wider time scale: the TAC was used in 50 or 500 ns range for ion KERD measurement, instead of 1000 ns range for ion yield spectra measurement. In addition, ions were flied as longer time as possible by lowering potentials of the TOF-MS analyzer, by which the time resolution, i.e., $t/\Delta t$, was increased[11,12]. The time of flight, t, (from the sample surface into the MCP detector) is given as a function of initial kinetic energy (E_k) of ions[12-14],

$$t = \sqrt{\frac{2\,m}{e}} \sum_{i=1}^{5} \frac{L_{i,i+1}}{\sqrt{E_k + E_i - E_1} + \sqrt{E_k + E_{i+1} - E_1}}, \qquad \text{Equation (2-1)}$$

where $L_{i,i+1}$ means spacing between grid i and $i+1$; E_i, potential of i-th grid in the TOF-MS detector; m, mass of ion in a.m.u.; and e, the elementary charge. This equation is derived from conservation law of momentum. The grids consist of the sample substrate, the accelerating plate (P_{acc}), the entrance plate of the TOF drift tube (DT), the exit plate of the TOF drift tube, the focusing plate, the plate on the MCP detector. These grids are depicted in Figure 2-2. Typical values of the E_i were described in Section 2.2. The spacings are given as $L_{12}(30)$, $L_{23}(9)$, $L_{34}(85)$, $L_{45}(5)$, and $L_{56}(13mm)$. The relation between
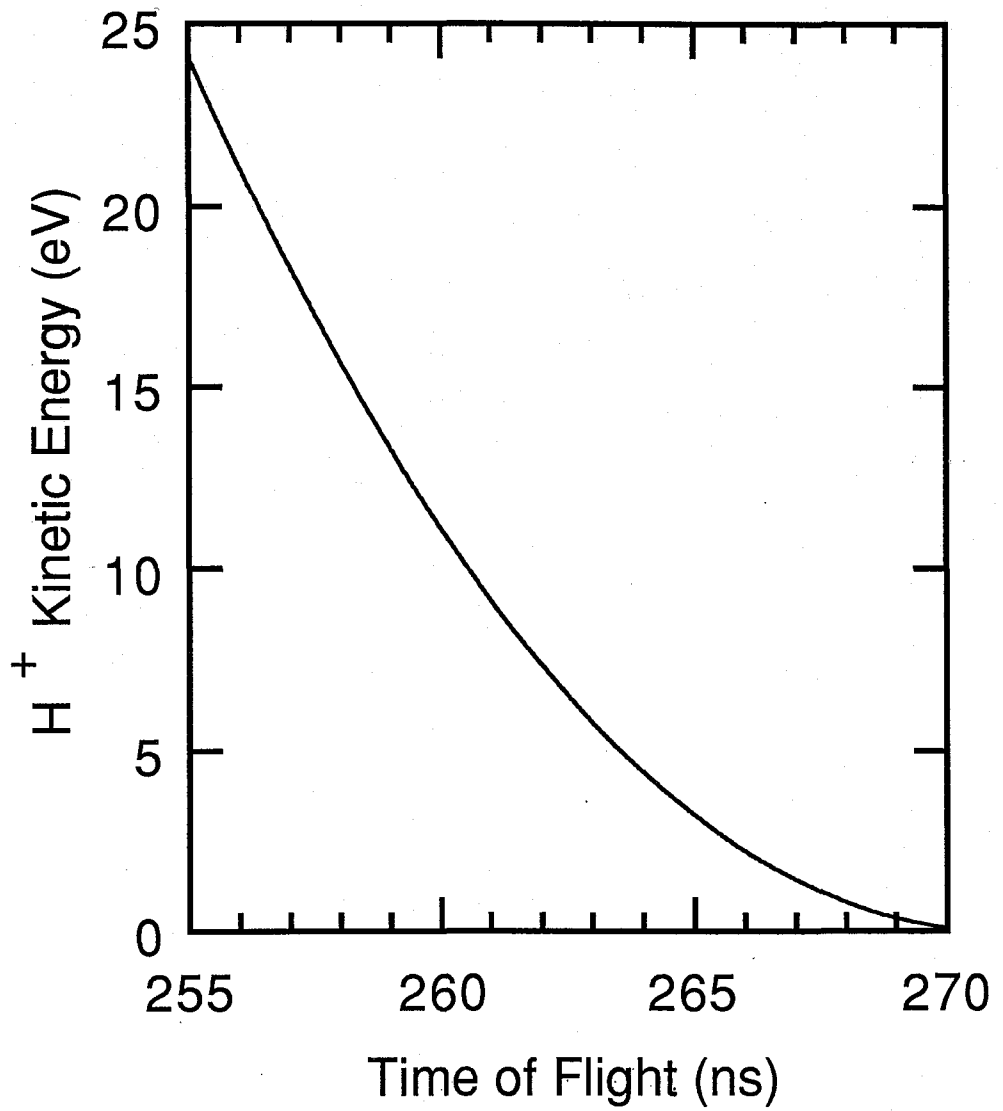
Figure 2-11　　　　Relation between time-of-flights of desorbed ions and their initial ion kinetic energies.

E_k and TOF calculated from Equation (2-1) was shown in Figure 2-11. The TOF spectra were converted to translational energy distribution using the relation. The calculated kinetic energy tends to be large, compared with those of literature. Absolute kinetic energy scale was obtained by calibrating it using reference's values[15-17]. In a typical TOF measurement, the electric field applied between the sample substrate and the accelerating plate was about 800 V/cm. This achieves about 4 eV kinetic energy resolution. The same sample as that for ion yield spectra was used in measurement of the ion KERD, which was a 10L H_2O/Si(100) adsorption system. The ion KERDs were measured with low resolution of the excitation energy with the 200μm of entrance and exit slits of the grasshopper monochromator. The resolution of photon energy (ΔE) in the experimental conditions was about 6 eV as measured on the line broadening in an AEY spectrum. (The H+ and O+ desorption ion yield spectra were measured with 30μm entrance and exit slits which correspond to ΔE = ca. 2 eV at 500 eV.)

2.9 References

[1] M. Yanagihara, H. Maezawa, T. Sasaki, Y. Suzuki, and Y. Iguchi, KEK report 84-17 (1984).

[2] D.R. Chopra, T.K. Hatwar, and L. Smothermon, Surf. Sci., **169**, L311 (1986); N.K. Del Grande, Physica Scripta, **41**, 110 (1990).

[3] B.L. Henke, P. Lee, T.J. Tanaka, R.L. Shimabukuro, and B.K. Fujikawa, Atomic Data and Nuclear Data Tables, **27**, 1 (1982).

[4] M. Cardona and L. Ley, *"Photoemission in Solids I: General Principles"* (Springer-Verlag, Berlin, 1978).

[5] R.C. Henderson, J. Electrochem. Soc., **119**, 772 (1972).

[6] F.J. Himpsel, F.R. McFeely, A. Taleb-Ibrahimi, J.A. Yarmoff, and G. Hollinger, Phys. Rev., **B38**, 6084 (1988).

[7] F.J. Grunthaner and P.J. Grunthaner, Mater. Sci. Rep., **1**, 65 (1986).

[8] M. Niwano, H. Katakura, Y. Takakuwa, and N. Miyamoto, Appl. Phys. Lett., **56**, 1125 (1990); N. Niwano, Y. Takeda, Y. Takakuwa, and N. Miyamoto, Surf. Sci., **261**, 349 (1992).

[9] I. Ochiai, T. Ogawa, Y. Takakuwa, and K. Mochiji, Surf. Sci., **287**, 175 (1993).

[10] K. Ueda, E. Shigemasa, Y. Sato, A. Yagishita, T. Sasaki, and T. Hayaishi, Rev. Sci. Instr., 60, 2193 (1989); E. Shigemasa, Master thesis (1988).

[11] K. Ueda and A. Takano, *"Desorption Induced by Electronic Transitions, DIET IV"*, edited by R.H. Stulen and M.L. Knotek (Springer, Heidelberg, 1988), p. 385.

[12] K. Ueda and A. Takano, Technol. Rep. Osaka Univ., **38**, 217 (1988).

[13] W.C. Willey and I.H. McLaren, Rev. Sci. Inst., **26**, 1150 (1955).

[14] N. Itabashi, I. Ochiai, S. Yamamoto, T. Ono, K. Mochiji, Appl. Surf. Sci., **79/80**, 67 (1994).

[15] S.L. Bennett and E.M Williams, DIET IV, p. 218.

[16] K. Sakamoto, H. Daimon, and S. Suga, unpublished results.

[17] K. Sakamoto, K. Nakatsuji, H. Daimon, T. Yonezawa, and S. Suga, Surf. Sci., **306**, 93 (1994).

Chapter 3

RESULTS AND DISCUSSION

3.1   PSID species from $H_2O/Si(100)$

In a typical TOF spectrum obtained in the 10L $H_2O/Si(100)$ adsorption system at an excitation energy of 700 eV, H^+ and O^+ were dominant ions as already shown in Figure 2-4. The intensity of O^{2+} ions was much weak. The relative intensity of $H^+ : O^+ : O^{2+}$ was about 1 : 0.25 : 0.0025 at 700 eV excitation. In condensed H_2O on a Ru(001) surface[1], only H^+ was observed as dominant ions, whereas O^+, H_2O^+, and OH^+ were barely detected by less than a factor of 1/500 at 600 eV excitation. The considerably small ratios compared to our results are of interest, because the different surface system plays different role in the surface dynamics. In particular, reneutralization plays an important role in determining the desorbing ion yield as discussed below.

No OH^+ ion could be detected under our experimental conditions; this ionic species was observed in the SiO_2 system upon excitation with unmonochromatic light[2,3]. Despite the exposure of only H_2O, F^+ ion desorption was often observed. After careful Ar^+ sputter cleaning, F^+ desorption became negligible. Thus, the F^+ ions were thought to come from the acid which was used for the chemical cleaning.

3.2 Relative PSID yield spectra and AEY spectrum

Figure 3-1 shows that the relative PSID yield spectra for the H^+, D^+, O^+, and F^+ together with a total electron yield (TEY) from the same sample for an extended energy range. The relative ion yields were obtained by acquiring the individual signal (cps) and dividing by the photoelectric current I_0 (pA) of the beam flux monitor. A slit width of 200μm and 1200 lines/mm grating of the monochromator were used in this measurement which resulted in a resolution of ca. 13 eV at 500 eV and 1.2 eV at 150 eV. The actual intensities of H^+, D^+, O^+, and F^+ ions, total electrons, and Io current obtained are typically 60, 40, 20, 9, 9×10^5 cps, and 15 pA, respectively, at 700 eV. In 100-200 eV region, the profile of PSID yield of H^+, D^+, and F^+ resembles that of TEY, which increases rapidly at ca. 100 eV(Si L-edge) and has a broad maximum at ca. 150 eV. Thus, it can be assumed that the core excitation of Si L level results in these ion desorption. It should be added that O^+ yield is exceptionally small in this region.

Figures 3-2 (b) and (c) show the relative PSID yield spectra for H^+ and O^+ obtained in the 510-620 eV energy region, respectively, where the contribution of L-shell excitation was already removed, as stated in the experimental section. These spectra show some salient features; 1) the H^+ ion yield is dominant in all of the energy region investigated, 2) the H^+ spectrum exhibits two broad peaks (peak a at 535 eV and peak b at 558 eV) near the O K-edge (E_b^F = 532.6 eV)[4], and 3) O^+ exhibits a delayed threshold by about 35 eV higher than the O K-edge. The sharp rise in the H^+ spectrum near the O K-edge clearly indicates that the H^+ ions mainly result from surface OH species.
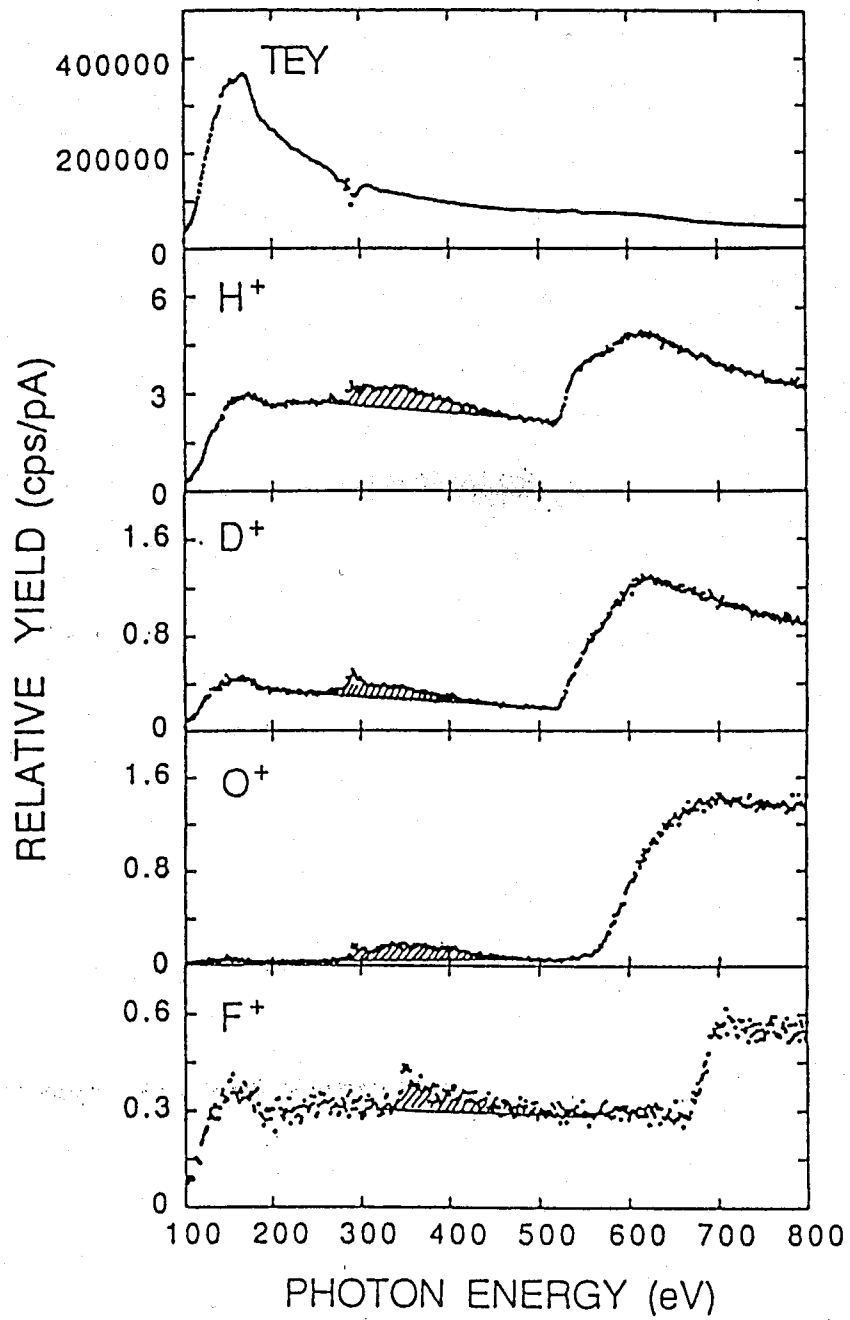
Figure 3-1   Relative PSID yield spectra of H^+, D^+, O^+, and F^+ and total

electron yields of $D_2O/Si(100)$ system for an extended region.
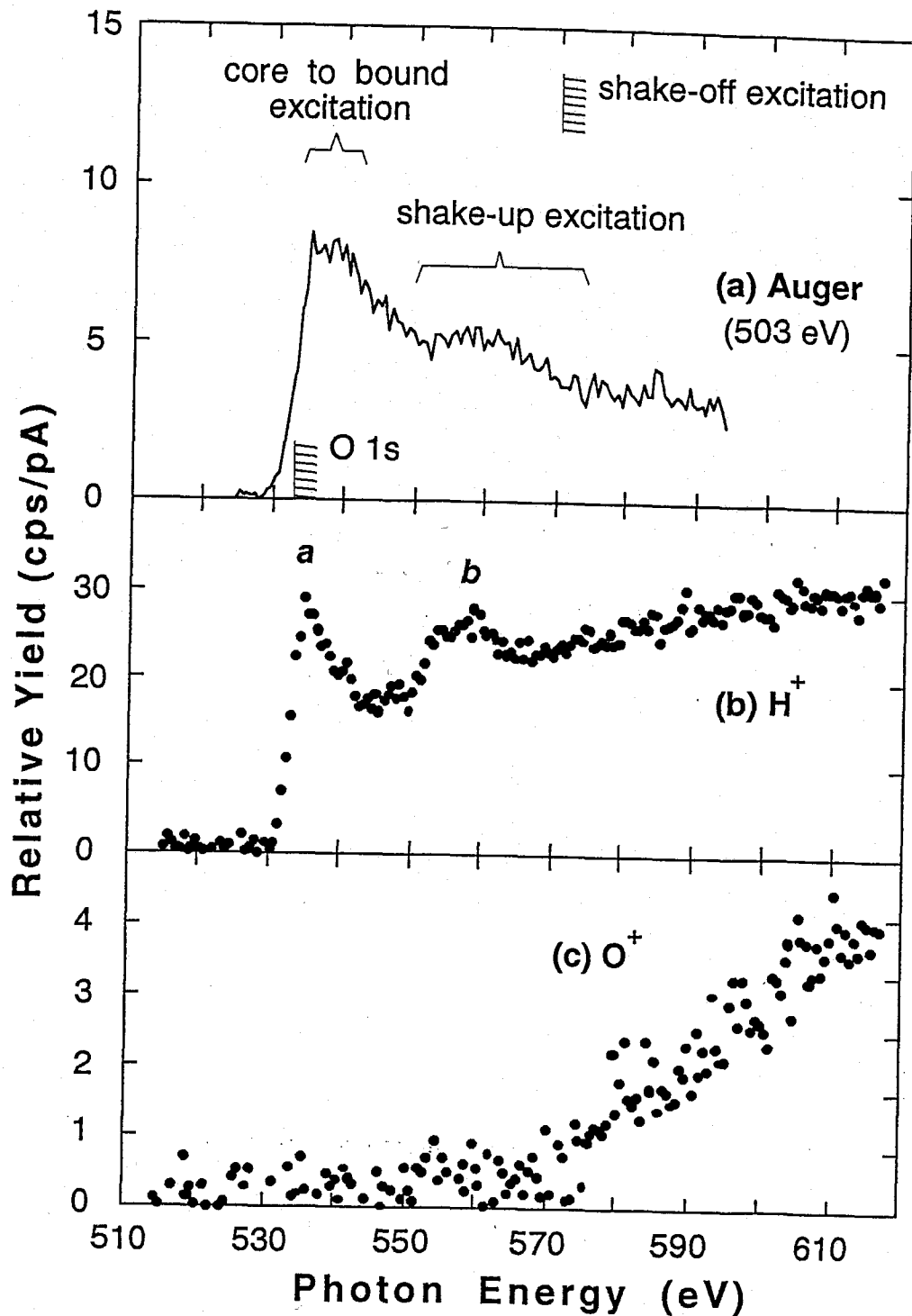
Figure 3-2   (a) O (*KVV*) Auger electron yield spectrum of H₂O/Si(100)

obtained by subtracting the spectrum in figure 2-7 (b) from that

in figure 2-7 (a). Slant lines show the O 1s binding energy

relative to the Fermi level and the threshold of the shake-off

ionization. (b) PSID yield spectrum of H⁺ in H₂O/Si(100). The

contribution of L-shell excitation is removed. (c) PSID yield

spectrum of O⁺ in H₂O/Si(100).

It is interesting to compare the PSID spectra with the previous results in the $D_2O/Si(111)$[5], $H_2O/Ru(001)$, and $D_2O/Ru(001)$[1] systems, where water adsorbs dissociatively on the Si(111) surface and molecularly on the Ru(001) surface. The H^+ PSID yield spectra previously reported exhibit a relatively narrow peak at 533.6 eV and a broad peak at approximately 560 eV, which are in good agreement with our results within the experimental error, although the width of the former peak is slightly different to each other. On the other hand, the behavior of O^+ was not mentioned in either of the previous studies, because attention was mainly paid to near O K-edge region (520-580 eV).

The PSID yield spectra were compared with the O (KVV) AEY spectrum corresponding to the K-shell absorption spectrum. The PSID yield may simply follow the absorption cross section, if only simple valence 2-holes cause desorption. On the other hand, if some excitation results in a highly repulsive or localized final state, it may enhance the ion yield over the absorption cross section. The AEY spectrum obtained with the same sample is shown in Figure 3-2 (a), in which the valence photoelectrons and the inelastically scattered electrons contributions have been already removed. The AEY spectrum is in good agreement with the O K-edge NEXAFS spectrum in the $H_2O/Si(111)$ adsorption system, which was recently reported by Lindsay *et al.*[6]. Several important features are found in the AEY spectrum; the Auger yield exhibits a sharp rise at 530 eV, a large broad peak at 535 eV and a broad shoulder peak at ca. 558 eV, which coincide in position with those of the H^+ PSID yield.

Before comparing the PSID and AEY spectra, the author assigns the AEY spectrum to examine the role of the primary excitation in the PSID. Photofragmentation experiments of the gas phase H_2O were carried out; H^+ ,

OH+ , H$_2$O+ , O+ , O^{2+} , and O^{3+} ions were observed in the 525-615 eV photon energy region. Relative ion yield spectra for O+, O^{2+}, and O^{3+} obtained with an energy resolution of ca. 1 eV are shown in Figure 3-3. Several peaks near the K-edge are well resolved in the O$^+$ ion yield spectrum. The overall structure of this ion yield spectrum resembles those of the electron energy-loss spectroscopy (EELS) spectrum[7] of H$_2$O and the AEY spectrum, as shown in Figure 3-4 and 3-2 (a), respectively, although the resolution of this measurement is different from each other. On the other hand, O^{3+} is observed [Figure 3-3 (c)] and its yield spectrum shows almost no structure near the O K-edge and starts to increase at ca. 570 eV. Near the edge, fine structures were interpreted in terms of Rydberg excitations from O 1s into 3sa$_1$, 3pb$_2$, 3pa$_1$, 4s, 4p Rydberg[7,8] and/or unoccupied molecular orbitals. The two lowest peaks were recently identified as being transitions into the mixed Rydberg-valence states, 3sa$_1$/4a$_1$ (534 eV) and 3pb$_2$/2b$_2$ (536 eV) based on photodissociation[9] and photoabsorption studies[10]. Table 3-I lists *ab-initio* SCF-CI MO calculations of isolated H$_2$O in the O 1s excitation region[12], which were performed by Kosugi of I.M.S. with the GSCF3 program. Figure 3-5 shows the AEY spectrum from Figure 3-2 together with transition energies listed in Table 3-I. From the Table 3-I, the excited states from the O 1s core into the two lowest unoccupied molecular orbitals of H$_2$O lie at 534.6 eV($1a_1^{-1}4a_1$) and 536.5 eV($1a_1^{-1}2b_2$). The doubly excitation or shake-up ionization occur from 550.2 to 575.3 eV. Therefore, the feature around 555 eV is thought to correspond to a shake-up ionization (or doubly excitation) in which the main characteristic involves $O_{1s},3a_1 \rightarrow c,4a_1$ (c stands for continuum)[11]. Indeed, a small broad peak was observed in both O$^+$ yield [555 eV, Figure 3-3 (a)] and AEY [558 eV, Figure 3-2 (a)]. In addition, a shake-off ionization in which the main characteristic involves $O_{1s},1b_1 \rightarrow c,c'$ or $O_{1s},3a_1 \rightarrow c,c'$ has been theoretically predicted to have a threshold energy
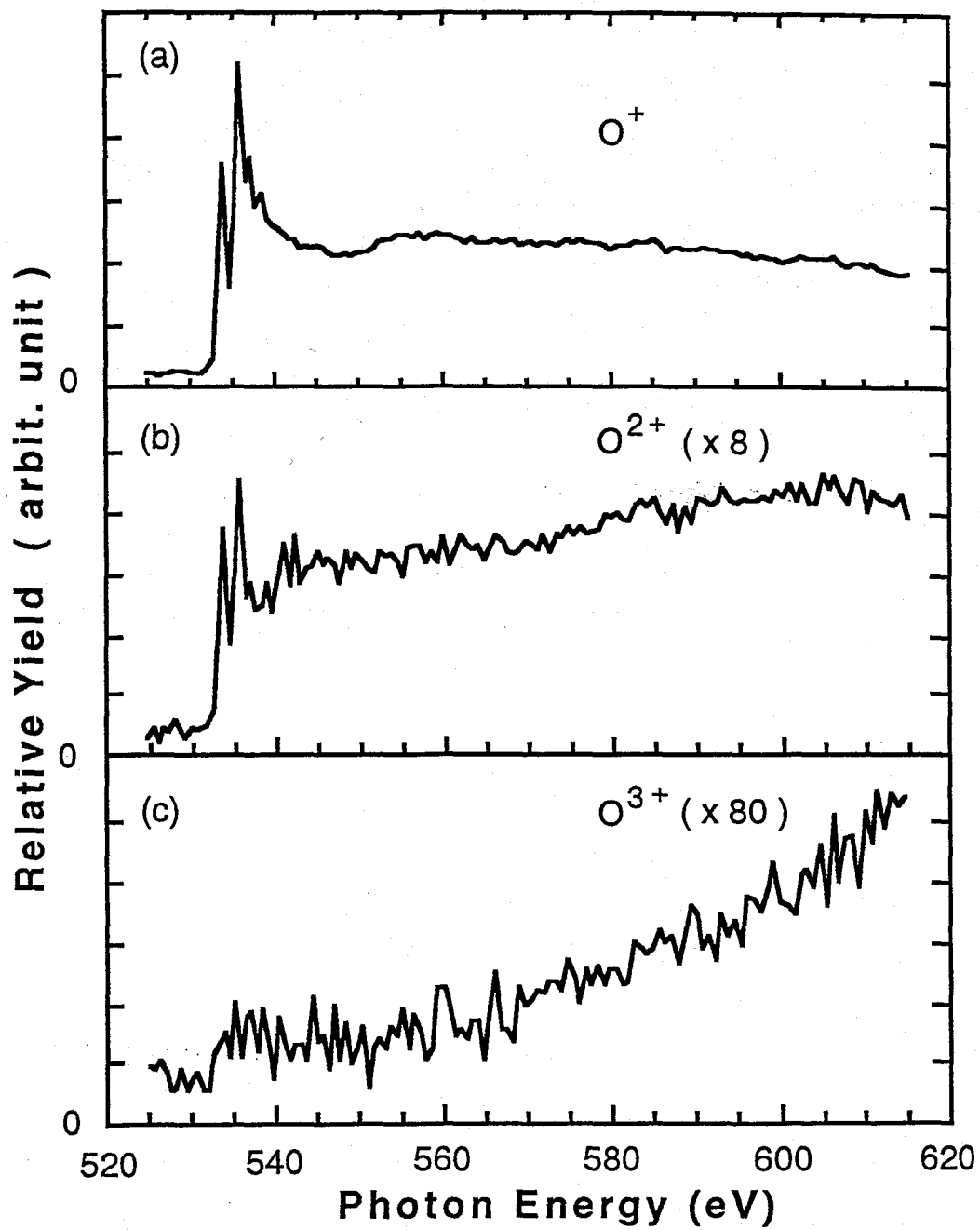
Figure 3-3   Fragment ion yield spectra of gas phase water near O 1s
excitation; (a) O+, (b) O2+ and (c) O3+.
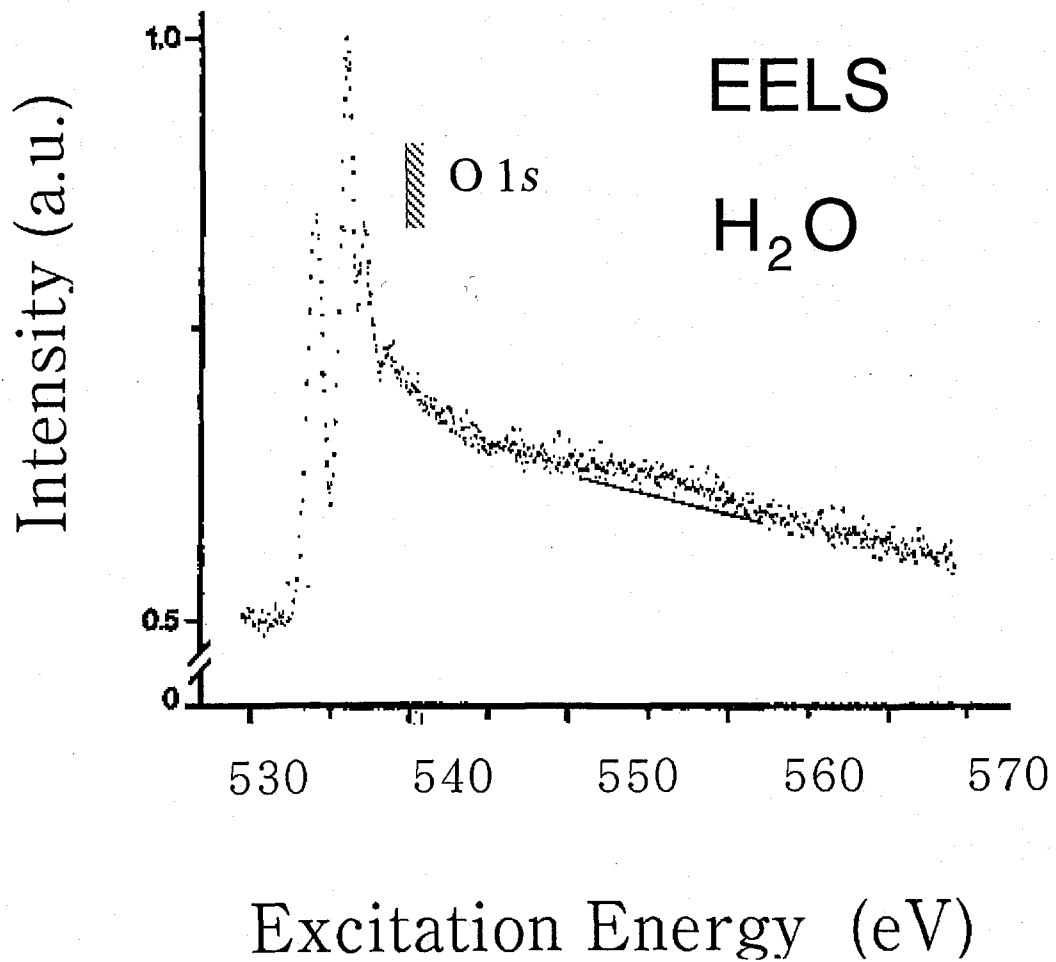
Figure 3-4   Electron energy loss spectrum (EELS) of gas phase H_2O in the O 1s excitation region. This figure was reproduced from Ref. 7.

Table 3-I *ab-initio* SCF-CI MO calculations for isolated H_2O in the singly and multiply excitation regions relating O $1s$ core ionization [Ref. 12]. The calculations were performed by Prof. Kosugi of I.M.S. with the GSCF3 program.

	Electronic configuration							Energy
H_2O :	1a1	2a1	1b2	3a1	1b1	4a1	2b2	(eV)
Excitation	1	2	2	2	2	1		534.6
	1	2	2	2	2		1	536.5
Ionization limit	1	2	2	2	2			539.7
Doubly excitation	1	2	2	1	2	2		550.2
	1	2	1	2	2	1	1	554.2
	1	2	2	1	2		2	556.0
	1	2	2	1	2	1	1	549.4
	1	2	1	2	2	2		553.3
	1	2	1	2	2		2	558.5
	1	1	2	2	2	(20/02/11)		~570
shake up	1	2	2	1	2	1		556.3
	1	2	1	2	2		1	562.2
	1	1	2	2	2	1		575.3
shake off	1	2	2	1	2			571.7
	1	1	2	2	2			~590
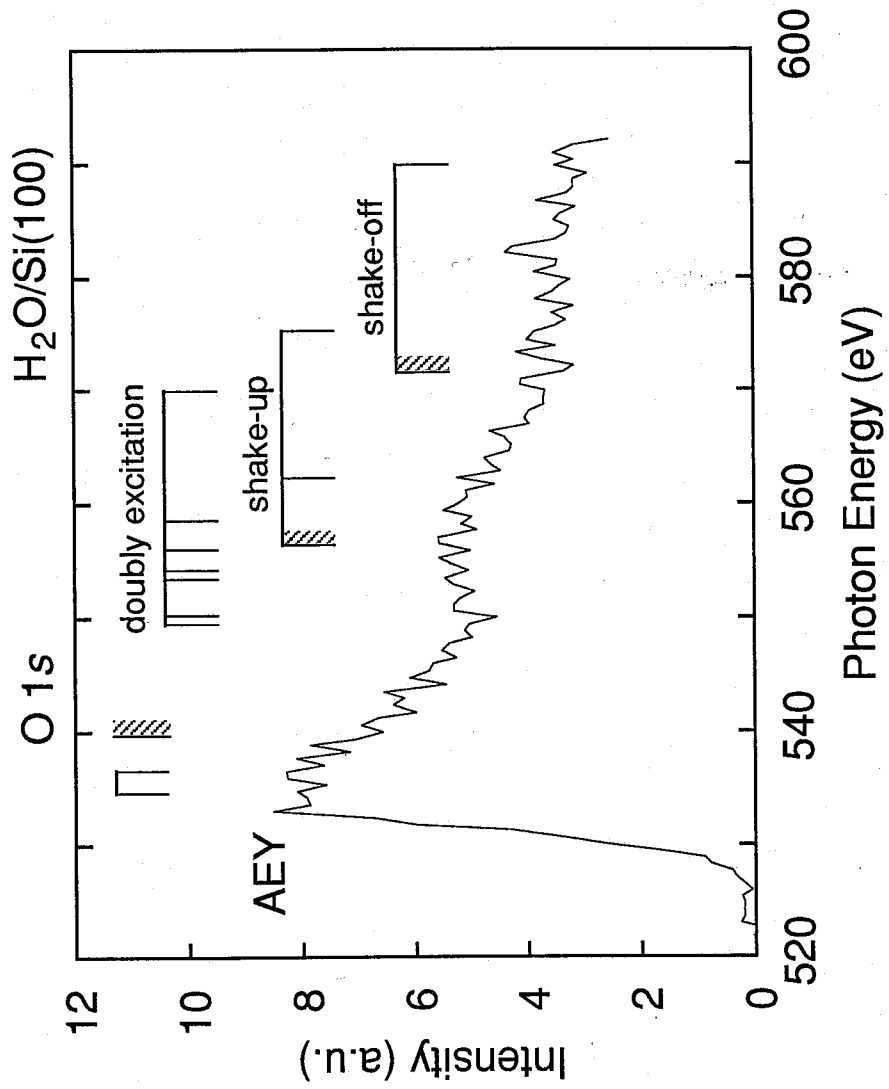
Figure 3-5   The AEY spectrum of the 10L H2O/Si(100) system together with transition energies from ground state into core excited states of isolated H2O; calculation were performed by Kosugi [Ref.12].

around 570 eV[12,13]; among them, the $O_{1s}, 3a_1 \rightarrow c, c'$ is more possible because $3a_1$ and $1b_1$ orbitals have bonding and nonbonding character, respectively. The surface OH molecule has at least two unoccupied $4\sigma^*$ and $2\pi^*$ molecular orbitals[14]. By a comparison of the AEY spectrum [Figure 3-2 (a)] with the O^+ ion yield spectrum from gaseous H_2O [Figure 3-3 (a)], the near edge peak (535 eV) of the AEY spectrum can be assigned to core-to-bound state (possibly $4\sigma^*$) excitation, and the shoulder peak (558 eV) to shake-up ionization.

Several salient features are found by a comparison of the PSID spectra [Figures 3-2 (b) and (c)] with the AEY spectrum [Figure 3-2 (a)]; for example, although the H^+ ion yield and the AEY spectra show two peaks approximately at the same excitation energy (peak *a* , 535 eV and peak *b* , 558 eV), relative peak intensities are different. In addition, the O^+ ion yield spectrum evidently deviates from the AEY spectrum. Above 570 eV, the PSID spectra of not only O^+ but also H^+ show marked deviation from the AEY spectrum. Since the AEY spectrum is considered to correspond to the K-shell absorption spectrum, the disagreement between the ion yield and AEY spectra indicates that core hole creation does not necessarily result in ion desorption near the O K-edge. Further, the smooth increase in both H^+ and O^+ yields above 570 eV suggests that the increase in excess energy of the core-hole state plays an important role in the PSID.

3.3 Mechanism of ion desorption

A question is raised as to whether adsorbates are desorbed by direct or indirect excitation caused by outgoing Auger electrons, secondary electrons, or photoelectrons. The indirect mechanism is called as the X-ray excited electron stimulated desorption (XESD) mechanism[15,16]. Ramaker et al. , however, pointed out that XESD was not dominant in the NH_3/Ni system, and discussed the contribution of XESD in various cases[17]. They concluded that when the direct core level Auger-stimulated desorption (ASD) process was active, the indirect XESD contribution was generally of the order of 35% or less, and that the XESD contribution apparently dominated the total yield only when the direct ASD contribution was suppressed. Recently, Rosenberg et al.[5] studied PSID from $H_2O/Si(111)$ near the Si L-shell excitation with high resolution; they concluded that XESD was not a major part in H^+ ion desorption due to an apparent discrepancy between the total electron yield and H^+ ion yield spectra. In the energy range of our experiments, although the O $1s$ photoabsorption coefficient[18] is considerably large, the number of electrons arising from monolayer of the adsorbate is very small compared to those from the Si substrate. As shown in Figure 2-6 (a), the H^+ yield shows a sharp and considerable large rise near the O K-edge. Consequently, the structures observed in PSID yield spectra reflect true PSD events, and the XESD mechanism is considered to play a minor part in the ion-desorption yield in the $H_2O/Si(100)$ system.

The author now considers the PSID process in terms of the primary excitations, where (1) resonant excitation (peak a at 535 eV), (2) shake-up ionization (peak b at 558 eV), and (3) shake-off ionization (≥ 570 eV) take

place. First, the author discusses the role of the spectator-electron in the desorption process near the K-edge excitation. When a strong antibonding orbital (σ^* is more effective than π^*) is occupied in the core-excitation, a neutral core-excited state partly transfers to a 2h-1e state through the spectator Auger process and induces desorption if the antibonding electron survives without delocalization through coupling to the surface[19,20]. In addition, ultra-fast dissociation is expected to occur when a light particle, such as H, desorbs through resonant excitation within the core lifetime[1,21,22]. Besides these dissociation processes, fast electronic relaxation process can occur during the core decay, through which an antibonding orbital electron (surface exciton like) transfers into the bulk, i.e., delocalization of the $4\sigma^*$ electron. Such fast electronic relaxation induces the lifetime-shortening of the core-excited states. This results in the broadening of the resonant peak in the inner-shell photoabsorption spectra. Thus, the broadening (FWHM $\approx$ 10 eV) of the AEY spectrum [Figure 3-2 (a)] as compared with the O+ yield spectrum [Figure 3-3 (a), FWHM $\approx$ 1.5 eV] and the EELS spectrum [Figure 3-4] for gas phase H_2O may be due to the electronic relaxation effect. The relaxation may be caused by the $4\sigma^*$ electron transfer into the substrate conduction band during the time scale of the core decay. On the basis of the relation between the transition energy of $O_{1s} \rightarrow 4\sigma^*$ (535 eV) and O $1s$ binding energy relative to Fermi level (532.6 eV)[4], the energy level of $4\sigma^*$ is concluded to overlap to the substrate conduction band[23] within the independent particle model. Thus, the author insists here that the resonant excitation $(O_{1s} \rightarrow 4\sigma^*)$ mainly produces a 2-hole final state via normal-Auger decay instead of a 2h-1e final state via spectator Auger decay. The author measured the Auger decay spectra in H_2O/Si(100) adsorption system, however, the change in the decay spectra could not be observed between on-resonant and off-resonant excitations. This can be explained as follows; the interaction between the adsorbate OH and the substrate

71

atom is greatly strong, so that, most of the $4\sigma^*$ electron does not stay on O-H site before or during the core decay.

Difference in the core decay spectra on- and off-resonant excitation could not be observed. For the resonant excitation at the peak **a**, the H^+ ion yield, however, was weekly but substantially enhanced as compared with the AEY spectrum (Figure 3-2). In addition, the ion kinetic energy released distributions indicate that a highest kinetic energy component is enhanced at the resonant excitation. Therefore, the author should assume some repulsive states as a result of resonant excitation; the $O_{1s}^{-1} 4\sigma^*$ repulsive core excited state or 2h-1e repulsive final states occupying $4\sigma^*$ electron which are generally assumed to be effective for the ion desorption than the 2h state[19,24,25]. For the resonant excitation, above mentioned discrepancy can be interpreted as a following sequence of processes: (1) the primary excitation of the core electron to a $4\sigma^*$ antibonding orbital; (2) fast elongation of the O-H bond in the core excited states by the antibonding electron which competes with fast transfer of the $4\sigma^*$ electron into the substrate conduction band; (3) most of core holes decay through so-called normal Auger process to form 2h final states; (4) among the core excited states on the resonant excitation, substantial amount of the 2h1e states produce, only which effectively would survive surface quenching and induce H^+ ion desorption. The role of the $4\sigma^*$ antibonding electron at the core-resonant excitation is discussed below (in Section 3.5) in detail on the basis of the observed KERDs of H^+ ions. In contrast to our results, a predominant sharp peak (FWHM $\approx$ 1.5 eV) at 533.6 eV was observed in the H^+ desorption from condensed water[1], which is considered to be due to the absence of an electron transfer channel to Si surface and the effective enhancement by the $4\sigma^*$ antibonding electron.

Identification of primary excitation for the peak **b** [Figure 3-2 (b); 558

72

eV] is more complicated, since it may involve either doubly-excitation and/or shake-up ionization[11]. These primary excited states decay to 3h-ne (n=0,1,2) final states via the Auger process. Due to the high repulsiveness and highly localized property, these 3h-ne states are considered to be highly effective for ion desorption[26]. This is the reason why H+ is enhanced at this energy, although the net probability of each shake-up ionization [Figure 3-2 (a); 558 eV] is relatively small.

To examine the role of primary excitation, the probability of ion desorption is obtained by dividing the PSID yields by AEY (Y_{ion}/Y_{Auger}) and plotted as a function of the photon energy for the H+ and O+ ions in Figure 3-6. For H+ ions, the relative value of Y_{ion}/Y_{Auger} at the peak *b* is larger than that at the peak *a*, indicating that H+ desorption is enhanced at the peak *b*. In the high energy region than the peak *b*, the probability for H+ desertion increases smoothly with increase in photon energy. The probability for O+ also increases with photon energy above 570 eV. These smooth increases cannot be explained by the KF model and suggest that another type of enhancement plays an important role above 570 eV. Since OH is bound with the O-atom pointing to the surface, the neutralization probability of oxygen atom cations is considered to be much higher than that of H+. Therefore, even if O+, O^{2+}, and possibly O^{3+} are formed by primary excitation, they may be immediately neutralized and desorbed as a neutral O-atom or may be recaptured to the surface. Figure 3-7 schematically shows the mechanism to explain the PSID process in the $H_2O/Si(100)$ system. The excitation below 570 eV results in 2 or 3-hole surface species. Thus, these multi-hole species would decompose and produce a surface precursor, i.e., (O+ + H+) or (O^{2+} + H+). The top-most and light hydrogen atom can considerably survive neutralization[27] and desorb as H+ ions, while surface O+, O^{2+}, and possibly
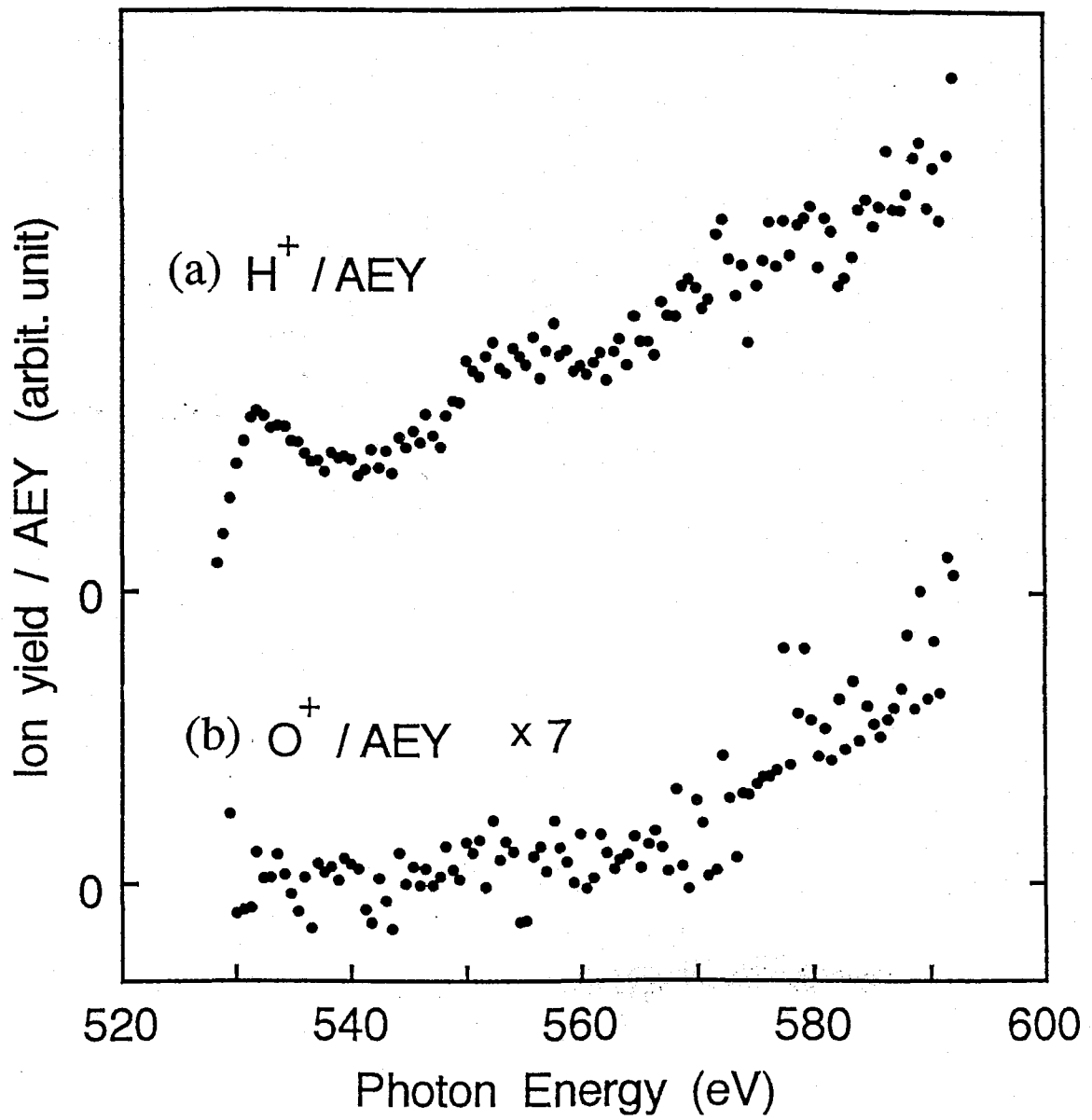
Figure 3-6   Ratio of the ion yield and O (KVV) Auger yield in
$H_2O/Si(100)$; (a) H+ and (b) O+.
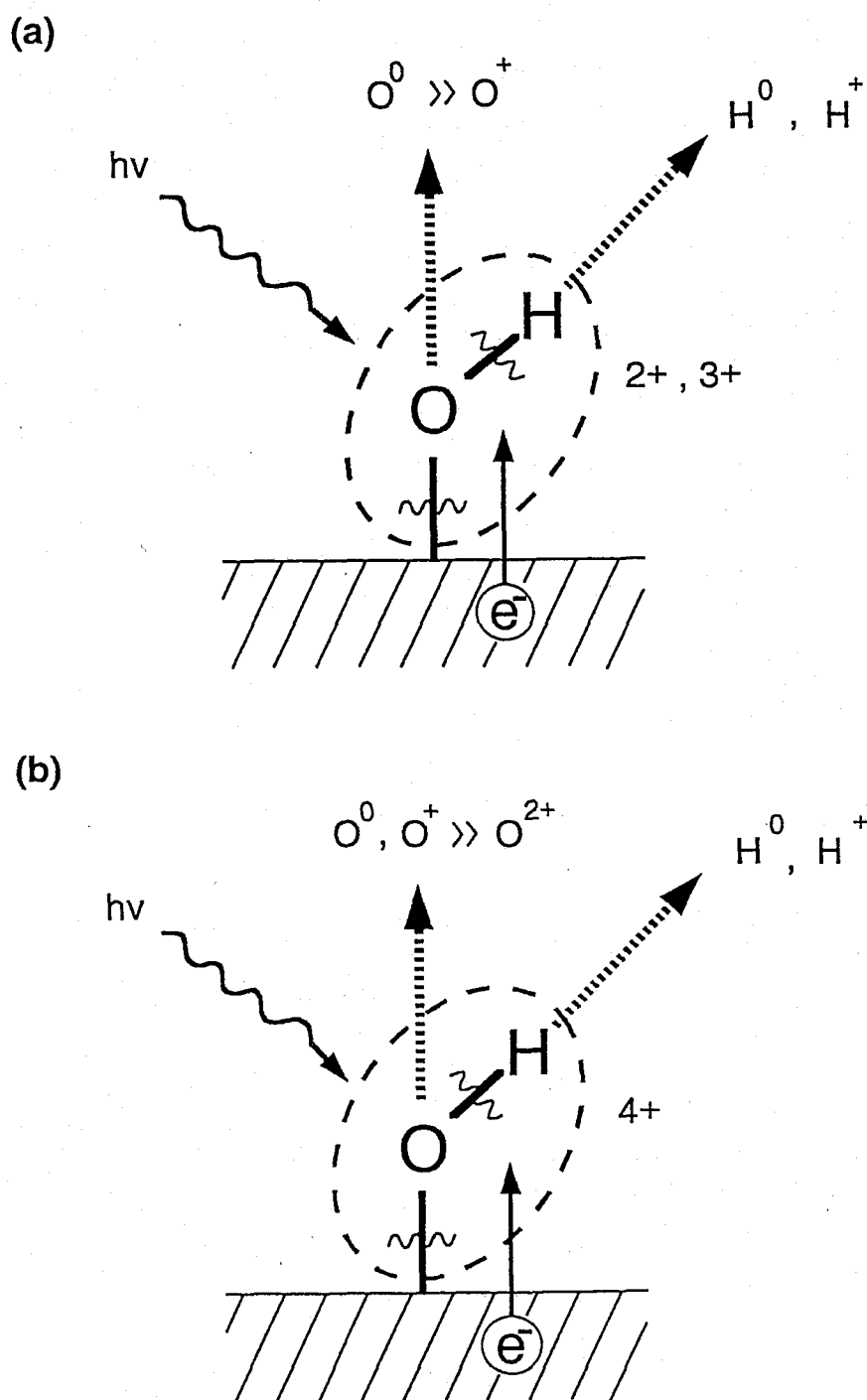
Figure 3-7   Schematic PSID mechanism in $H_2O/Si(100)$ at the excitation
(a) below 570 eV and (b) above 570 eV.

O^{3+} are effectively quenched with an extremely high neutralization probability of them. The shake-up ionization at the peak b (558 eV) considerably generates 3-hole final states, however, the O^+ PSID yield is negligible at the shake-up energy. This confirms that the surface O^{2+} (formed through 3h states) are effectively quenched.

The shake-off ionization occurs above 570 eV and yields $(OH)^{n+}$ $(n \geq 3)$ final states, where mainly n=3 through normal-Auger decay and n=4 through double-Auger decay with ~6%[28]. As described above, the 3-hole precursor does not contribute to the O^+ PSID. Thus the author concludes that, most probably, the 4-hole precursor states produced by shake-off ionization followed by the double-Auger process contribute to O^+ desorption. The probability of the shake-off process relative to the normal core ionization is available from Ref. 13, that is $\leq 2\%$, and the probability of the following double-Auger process relative to the normal-Auger process is also available from reference [Ref. 28], i.e., ~6%. The net probability of a series of sequential two events should be the product of two processes. Thus, the probability is estimated to be $\leq 0.1\%$. In spite of such a very small probability of 4-hole production, the 4-hole precursor state is expected most probably to survive neutralization due to its extremely high localization effect[25,29,30] or shrinkage effect[31]. Therefore, as shown in Figure 3-7 (b), a simple explanation is given as that the surface precursor $(OH)^{4+}$, which is extremely unstable, decomposes into $(O^{3+} + H^+)$ and starts to desorb. For the OH-bonded oxygen end down to the surface, the initial trajectory of O^{3+} in Coulomb explosion of $(OH)^{4+}$ would be into the bulk. Thus, O^{3+} ions cannot escape as it is, but escapes as O^+ ions after incomplete neutralization. The enhancement of H^+ by this shake-off ionization [≥ 570 eV in Figure 3-6] can also be explained in terms of an increase in the Coulomb repulsive energy of the $(O^{3+} + H^+)$ precursor.

The PSID mechanism proposed in Figure 3-7 successfully explains our results in terms of multiply ionized species. Furthermore, the presence of trace amounts of O^{2+} ions seen in the TOF spectrum obtained at 700 eV (Figure 2-4) is considered to be one evidence for this mechanism. According to the mechanism shown in Figure 3-7, one can predict that multiply charged ions, such as O^{3+}, are first produced above 570 eV, which are assumed to be the surface precursor for the PSID. To confirm the production of such multiply charged ions, photodissociation experiments in the gas phase were performed. As already shown in Figure 3-3 (c), O^{3+} fragment ions were surely observed, and their yield spectrum was in good agreement with the O^+ PSID yield spectrum given in Figure 3-2 (c); both spectra show the same threshold at 570 eV and a similar energy dependence. The similarity between these spectra suggests that the mechanism of O^+ PSID is closely related to that of O^{3+} production.

As mentioned in the Section 3.2, the shake-off ionization in which the main characteristic involves $O_{1s}, 1b_1 \rightarrow c, c'$ or $O_{1s}, 3a_1 \rightarrow c, c'$ is theoretically predicted to have a threshold at around 570 eV[12,13]. Since the O^{3+} ion yield from gaseous H_2O is small by two orders of magnitude relative to the O^+ yield, and its appearance energy coincides with the shake-off threshold, thus O^{3+} is assumed to be formed from multiply charged precursor ions, such as H_2O^{3+} or H_2O^{4+}, produced by shake-off ionization. The author speculates that O^{3+} above 570 eV is enhanced mainly by H_2O^{4+}, on the basis of following regions: shake-off ionization results in three hole (H_2O^{3+}) or four hole (H_2O^{4+}) final states and hardly results in two hole state; thus, O^+ ion yield in Figure 3-3 (a) does not show onset at 570 eV while O^{2+} and O^{3+} ion yields show the onset; therefore, the author presumes that the enhancement of O^{2+} and O^{3+} above 570 eV are, respectively, due to decomposition of H_2O^{3+} and H_2O^{4+} into

(O^{2+} + H^+ + H) and (O^{3+} + H^+ + H). The H_2O^{4+} precursor ions are considered to be produced by shake-off ionization and the following double-Auger process.

The author here notes the difference between the O^+ PSID and O^{3+} fragment yield from gaseous H_2O in the 540-570 eV excitation region. For O^{2+} and O^{3+} yields, a monotonically decreasing component substantially comprises above the K-shell ionization threshold ($\geq$ ca. 540 eV). The author speculates that O^{2+} in this region forms from H_2O^{3+} intermediates which can be produced by normal K-shell ionization and following double Auger processes. Although H_2O^{2+} and H_2O^{3+} are possible intermediate for O^{2+} production, the author assumes that H_2O^{2+} hardly leads to O^{2+} + H + H as compared with O^+ + H^+ + H and H^+ + H^+ + O processes. By analogy with the O^{2+}, the O^{3+} in this region is assumed to be produced largely from H_2O^{4+} which can be produced by normal K-shell ionization and following triple-Auger processes.

Figure 3-8 shows multiple photoionization of gaseous Ne in the K-shell ionization region[28]. The author (of the present thesis) discusses the multiply charged states of H_2O by comparing with the isoelectronic Ne. As shown in Figure 3-8, ion yield spectra of Ne^{2+}, Ne^{3+}, and Ne^{4+} present similar energy dependence with, respectively, O^+, O^{2+}, and O^{3+} from the gas phase H_2O (Figure 3-3(a-c)). In particular, the enhancement of Ne^{3+} and Ne^{4+} yields above shake-off threshold (i.e., ca. 920 eV) is surely observed. The enhancement of Ne^{4+} yield above 920 eV is clearly due to the shake-off ionization and following double Auger process. Because O^+ PSID yield shows a similar energy dependence not only to that of O^{3+} yield from gaseous H_2O but also to that of Ne^{4+} yield, the O^+ PSID can be explained by the four hole (OH^{4+}) mechanism which has been described above in this section.
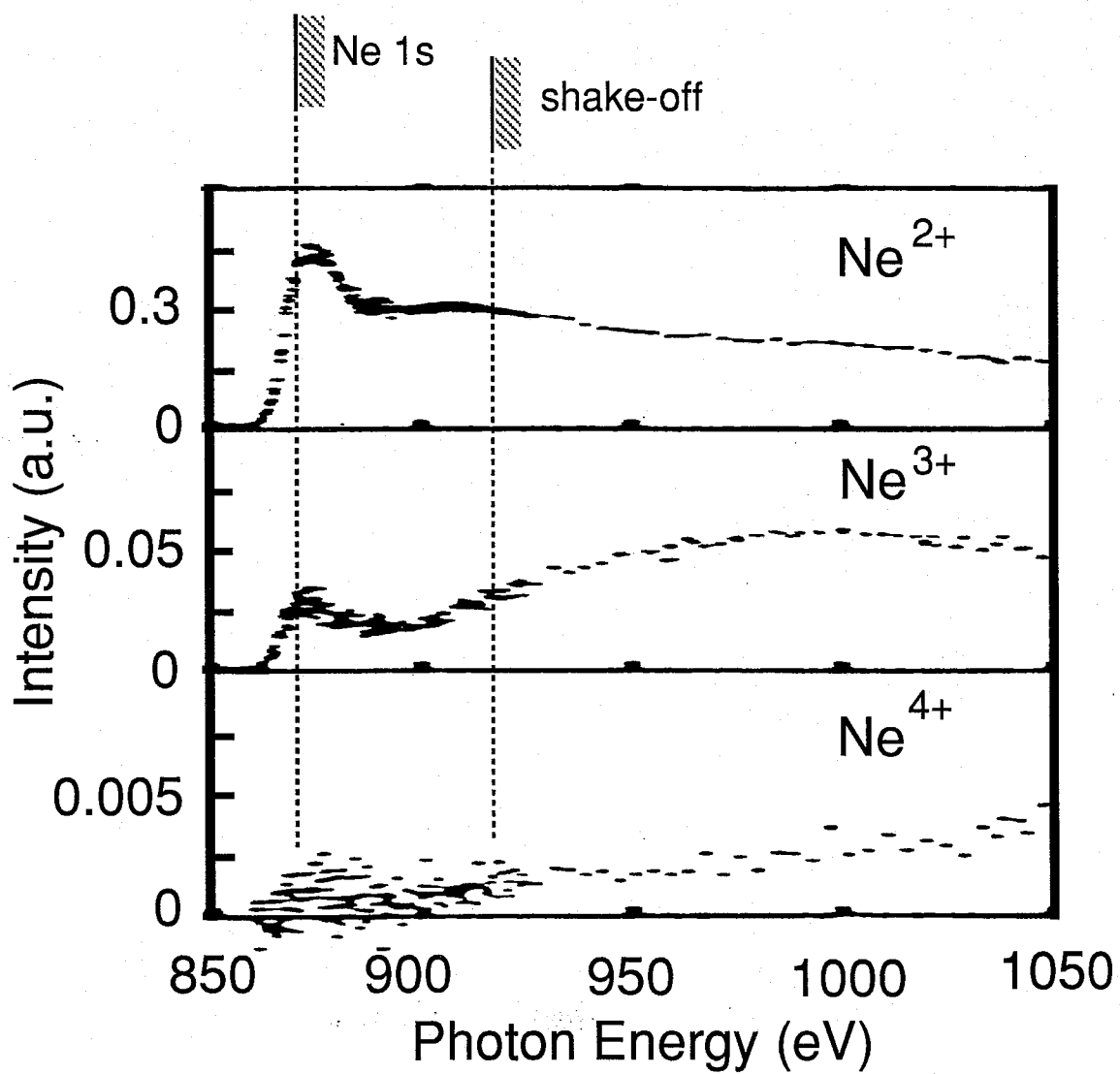
Figure 3-8   Multiple photoionization spectra of gas phase Ne in the Ne 1s

excitation region, which were taken from Ref. 28.

An alternative pathway to form OH^{4+} can be the triple-ionization process which is core ionization associated with two-electron ejection ($O_{1s},v,v' \rightarrow c,c',c''$), followed by the normal-Auger process. According to the Equivalent Core Approximation[32], the threshold of the triple-ionization is obtained to be about 620 eV using 80.3 eV as the double-ionization energy of F^+[33]. This threshold is considerably higher than the threshold energy of 570 eV for O^{3+} formation. The author thus concludes that the triple-ionization process can be negligible for excitation energies below 620 eV, but may become possible above 620 eV.

The results on gaseous water are all consistent with our O^+ PSID mechanism (Figure 3-7) in which multiply charged ions are assumed to be produced by the shake-off ionization followed by the double-Auger process. Although multiply charged ions strongly interact with surface, incompletely neutralized ions escape as singly charged ions. A similar relation between gaseous and adsorbed molecules has already been studied on CO molecules. Treichler et al.[26,34] observed the delayed threshold (~560 eV) for higher fragment, e.g., C^+, O^+, and O^{2+} ions from CO/Ru(001) in O K-shell excitation and interpreted this as being due to the polarization-independent shake-off ionization. Hitchcock et al.[35] studied the ionic fragmentation of gaseous CO and found that the O^{2+} and C^{2+} partial yield spectra were identical to the absorption spectrum of CO below excitation energy of 560 eV but deviated upward above this energy. As this energy was the same with the threshold energy for C^+, O^+ and O^{2+} PSID from CO/Ru(001) observed by Treichler et al., the enhancement of O^{2+} and C^{2+} ion yields above 560 eV was concluded to result from the shake-off ionization. In addition, they suggested that O^{2+} and C^+ ions were desorbed through the shake-off ionization followed by ionic dissociation of (C^+ + O^{2+}) and (C^{2+} + O^+) multiple charged ions

which were dissociative surface-precursors.

3.4 PIPICO spectra

It is particularly interesting to know whether H^+ and O^+ ions are produced simultaneously from surface OH molecules or not. Thus, PIPICO[36] measurements were made. The PIPICO spectrum obtained at a photon energy of 750 eV is shown in Figure 3-9. The PIPICO signals (O^+ + H^+) were obviously obtained at the time-of-flight difference (792 ns) between O^+ (1056 ns) and H^+ (264 ns); this observation is definite evidence for the simultaneous desorption of O^+ and H^+ from surface OH molecules. The PIPICO yield spectrum was obtained by acquiring the PIPICO signals as a function of the photon energy and is shown in Figure 3-10 together with the PSID yield spectrum of O^+. From Figure 3-10, the PIPICO yield is found qualitatively to follow the PSID yield of O^+. The PIPICO results support the mechanism in which H^+ and O^+ are simultaneously formed from surface OH^{4+}. Under our experimental conditions, the total ion count rate and the PIPICO (O^+ + H^+) signal rate were ca. 2000 and ca. 0.1 cps, respectively, at photon energy of 700 eV. Therefore, the number of true coincidence events per measured ion event is ca. 5×10^{-5}, which is extremely small compared with the values of several tenth for the photodissociation of small free molecules at core excitation[35]. This is considered to be a surface-specific effect, which is mainly caused by neutralization. This experiment demonstrates that PIPICO can be successfully applied to study PSID from the surface at the first time and reveals the

simultaneous formation of H^+ and O^+ ions in the adsorbed H_2O system. This technique will be a very useful tool to reveal PSID mechanism in complicated systems where several kinds of ions are formed.
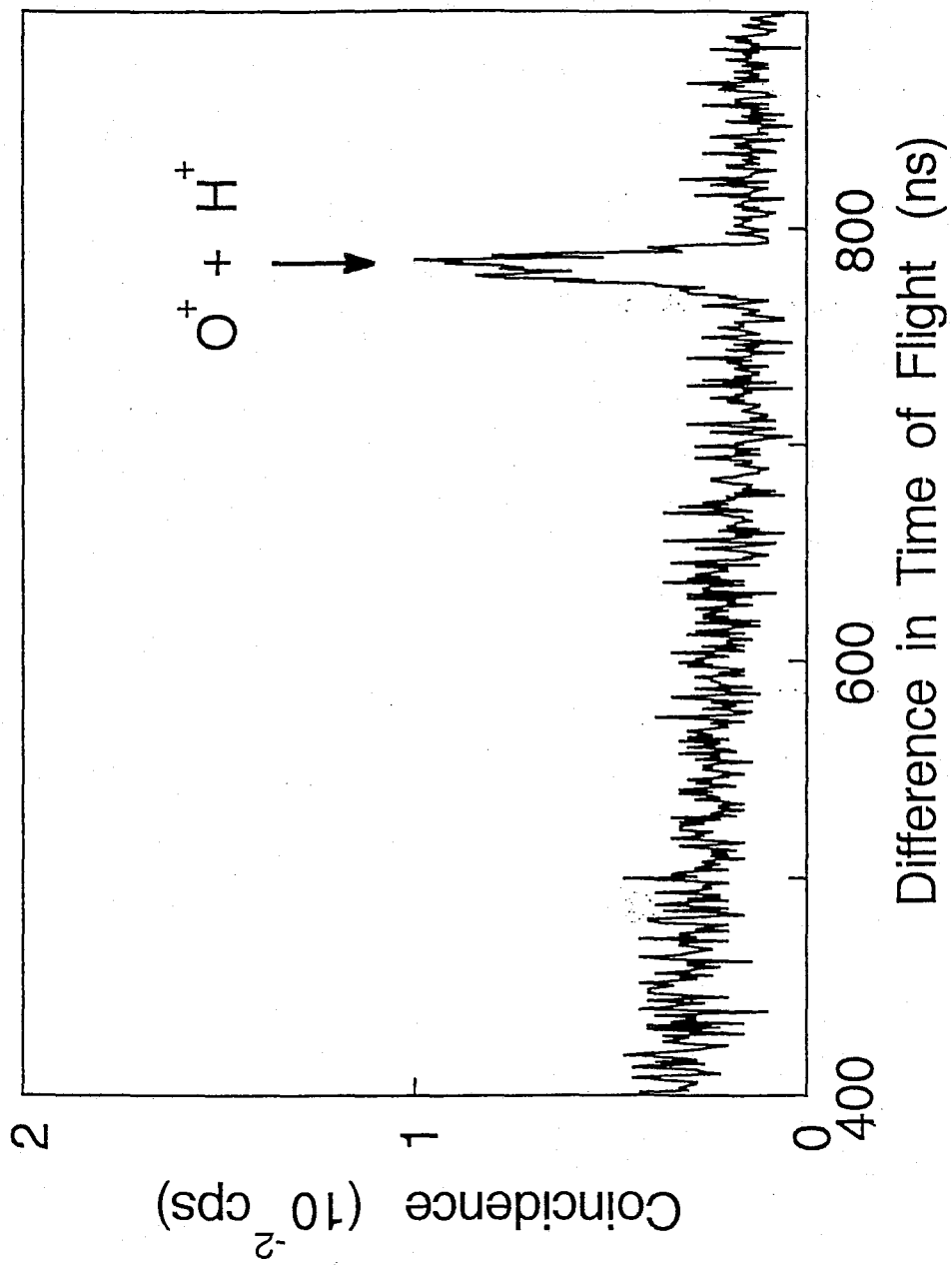
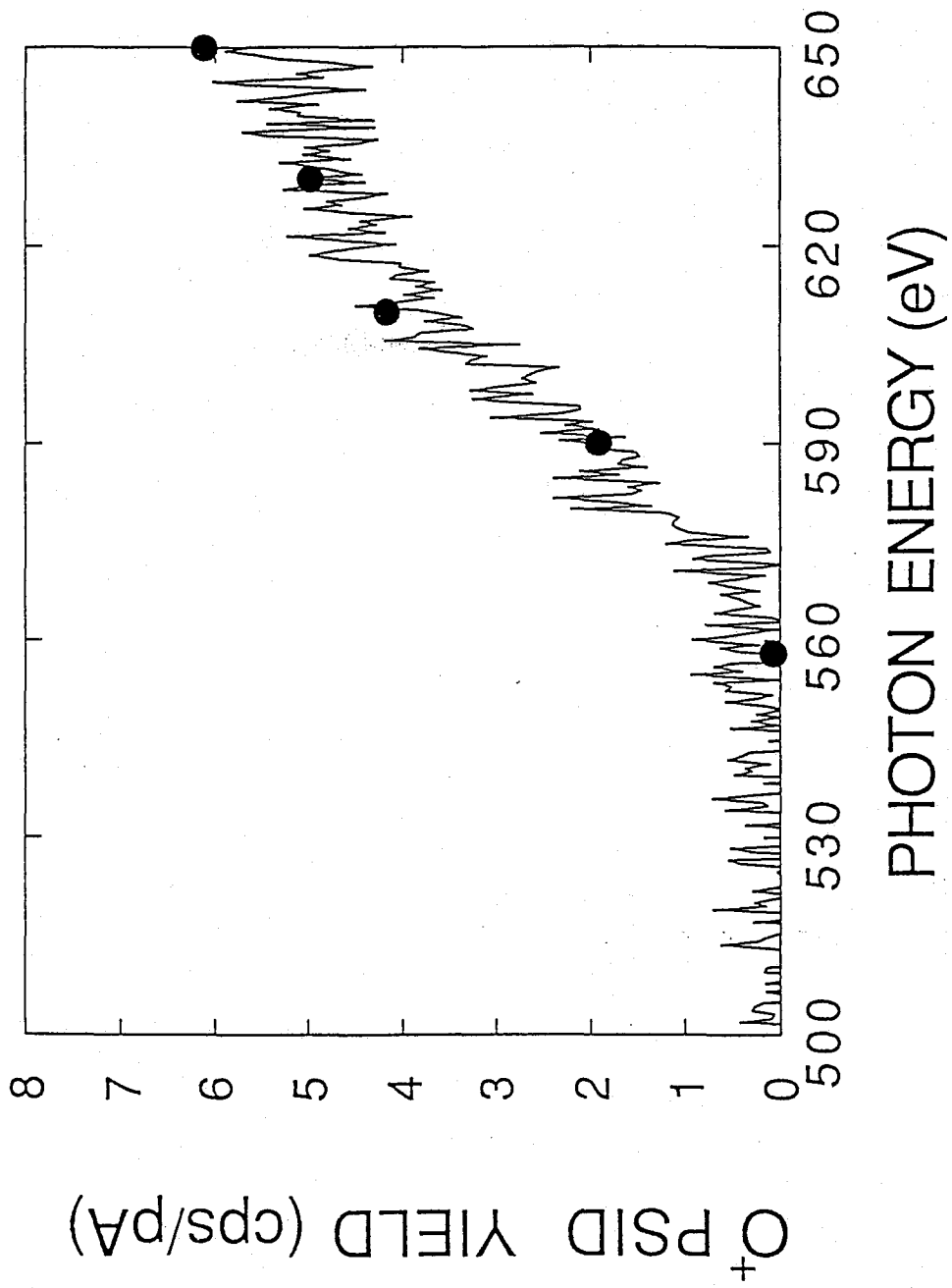Figure 3-9   Typical PIPICO spectrum in H_2O/Si(100) obtained at photon energy of 750 eV.

Figure 3-10   PIPICO yield spectrum (●) together with the PSID yield
spectrum of O^+ in $H_2O/Si(100)$.

3.5 Kinetic energy released distributions of H+ ions

As described above, the H^+ and O^+ ions are desorbed from the H_2O-covered Si(100) surface in the O $1s$ excitation region. The TOF profiles of H^+ ion obtained at the photon energies of 500, 535, 570, and 700 eV, are shown in Figure 3-11. The peak of the TOF profiles substantially changes between 500 and 535 eV and depends on the excitation energy. This is induced by the variance of ion kinetic energy released distribution (KERD). The ion KERDs calculated from the TOF profiles of H^+ ion obtained with excitation energies from 500 to 700 eV are shown in Figure 3-12. As shown in Figure 3-12, the KERDs of the H^+ ions substantially change with changing excitation energy, suggesting that the maximum is shifted to a higher kinetic energy side in higher energy excitation. Figure 3-13 represents the dependence of average kinetic energy upon the excitation energy. This figure shows that the average kinetic energy depends on the excitation energy and suggests that it increases both at the O K-edge (537 eV) and shake-off ionization (ca. 570 eV) thresholds.

In order to explain the changes in the KERD against the excitation energy, the author assumes that the KERD is formed as a linear combination of three components of any functions. For curve-fitting analysis, the author tentatively adapted an asymmetrically broadened Gaussian function which has four independent parameters: position, width, height, and an asymmetric parameter. Clinton et $al.$[37] originally proposed that the KERD in ESD was approximately expressed by a Gaussian distribution under some assumptions in the MGR model: these assumption are harmonic oscillation of the adsorbed atom, a constant gradient of the repulsive potential curve near equilibrium position and a low neutralization probability for the desorbed ions.

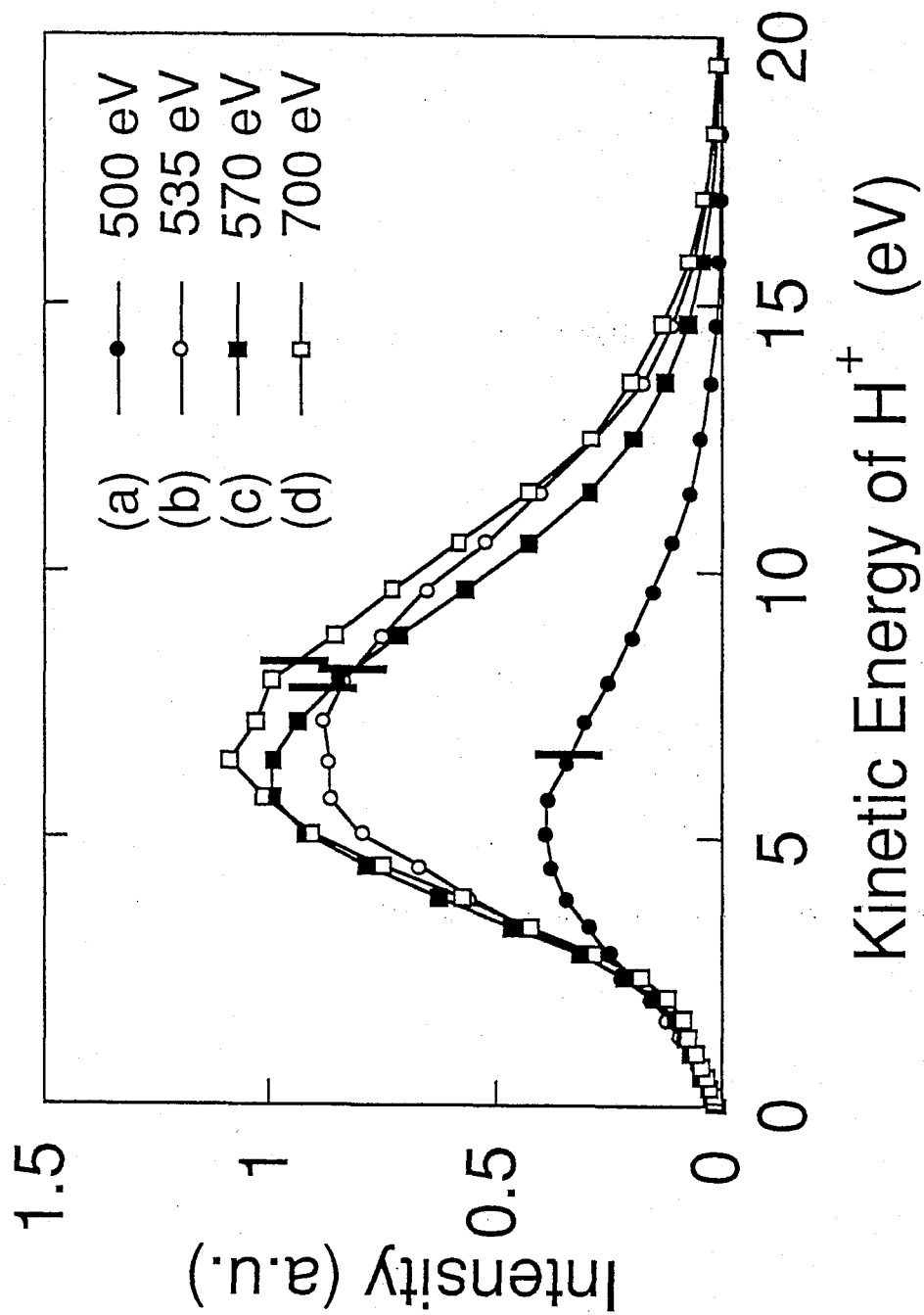Figure 3-11 Dependence of H+ ion flight time on the incident photon energy. The photon energies are (a) 500, (b) 535, (c) 570, and (d) 700 eV.
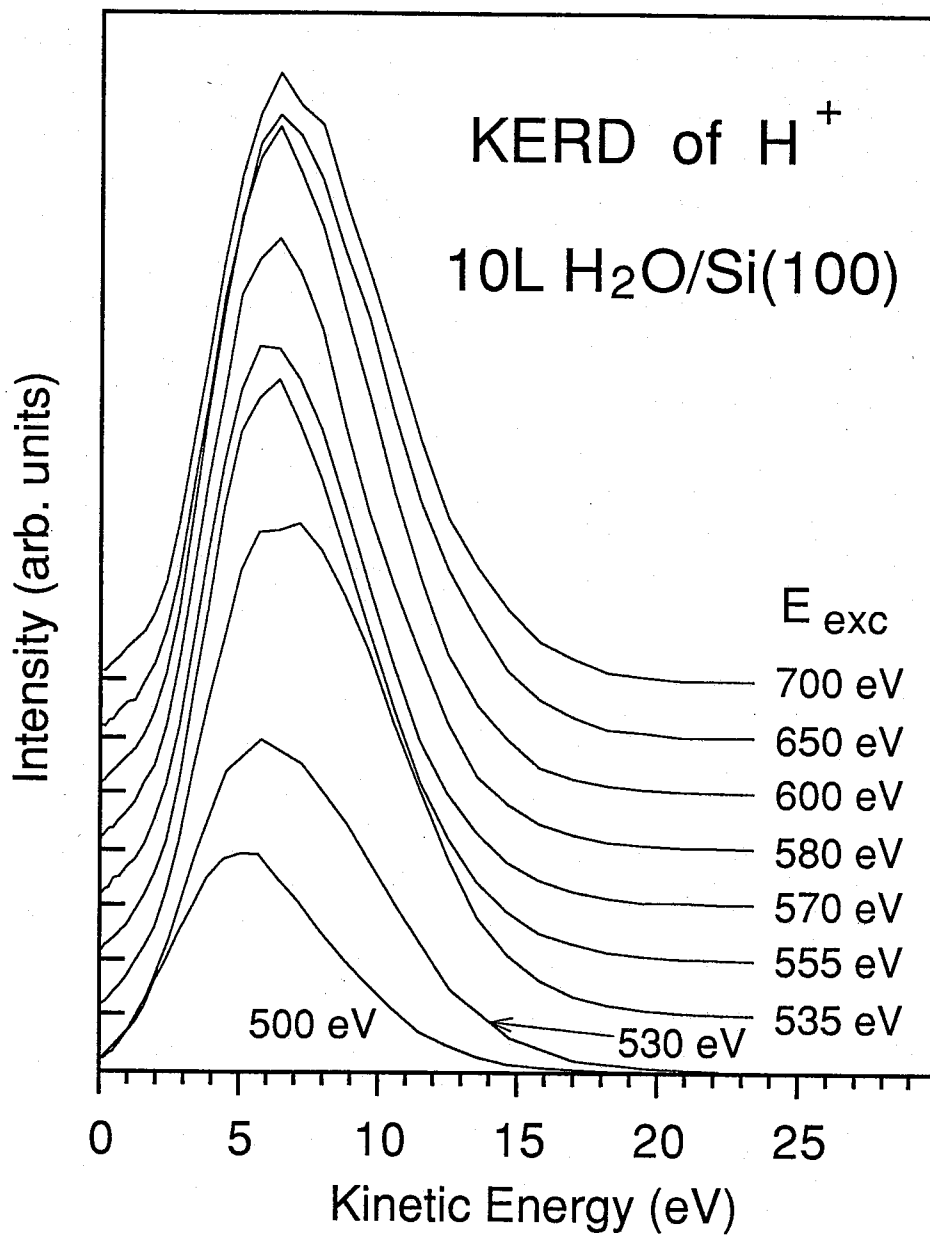
Figure 3-12   The kinetic energy released distributions of the H+ ions obtained with excitation energies from 500 to 700 eV.
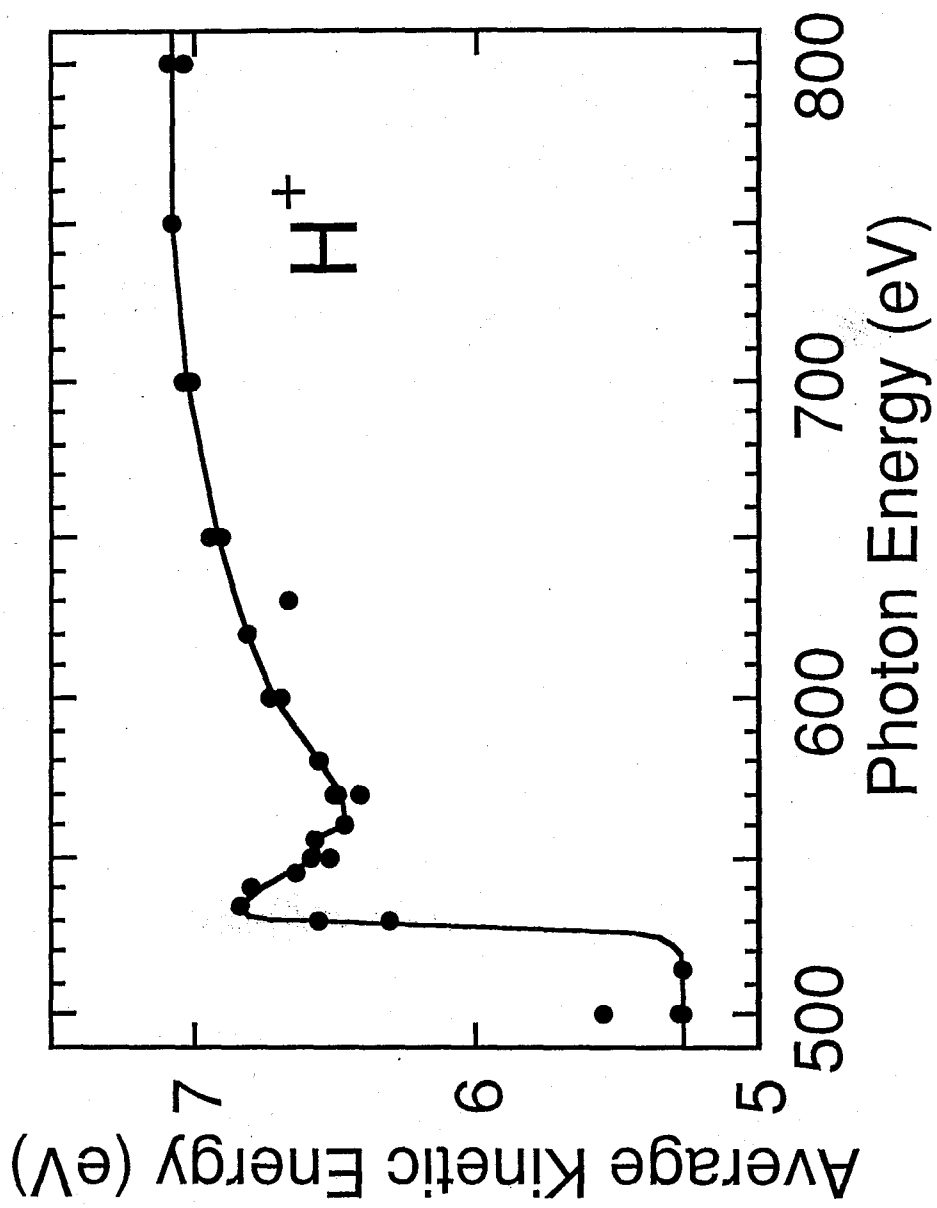
Figure 3-13   The dependence of average kinetic energy versus the excitation energy, which is obtained with the photon energies ranged from 500 to 800 eV.

Here, three distributions are used to decompose the observed KERDs. The parameters were determined by a nonlinear least-squares fitting routine. The three components of the optimized distributions, which are shown in Figure 3-14, were determined as follows: the distribution observed below the K-shell ionization threshold energy (537 eV) is assumed by an α component. The distribution observed with the energy between 550 and 570 eV is assumed by a linear combination of the α and an additive β components. The distribution observed above the second threshold energy (570 eV) is simulated by a linear combination of three (α, β, and an additive γ) components. The peak energies and widths of each distribution are summarized in Table 3-II together with the mechanisms proposed below. What type of function we should use it for the curve-fitting is not essential in the present study. The author has confirmed that the deviation of the parameters within $\pm$ 5 percents from the optimized values does not affect the results described below. The asymmetric shape of the distribution for the three deconvoluted components will be theoretically clarified in the future studies.

Figure 3-15 shows that the integrated intensities of all the components markedly depend on the excitation energy and exhibit some characteristic thresholds or peaks indicated as **1** to **4** depicted at the top of Figure 3-15. This is due to different desorption mechanisms for each component. To our knowledge, the higher core-excited states (i.e., shake-up and -off) of the OH adsorbate have not been reported. Thus, the author discusses the desorption mechanism with the aid of the unambiguous assignments for the higher core-excited states of H_2O[11,13]. The excitation energies and possible assignments corresponding to the thresholds and peaks observed are summarized in Table 3-III.

KERD of H$^+$

E$_{exc}$ = 700 eV
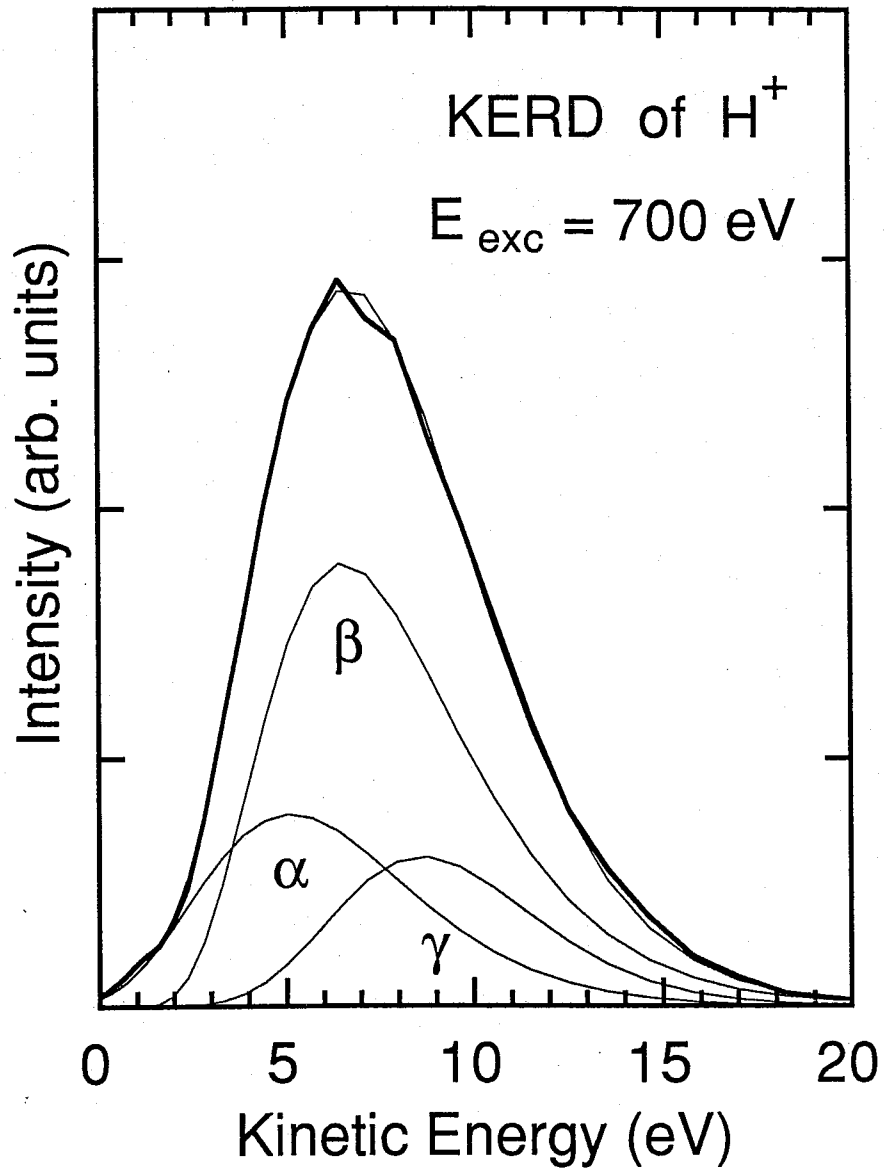
Figure 3-14   Decomposition of the kinetic energy distributions into three
components which are expressed by asymmetrically broadened
Gaussian distribution: α, β, γ, and the function optimized for the
observed KERD with 700 eV.

Table 3-II   Peak energies, widths, and possible desorption
mechanisms for the three kinetic energy components.

	Peak (eV)	Width (eV)	Mechanisms		
α	5.1	6.6	Si $2p \rightarrow \infty$	and	Si $2s \rightarrow \infty$
β	6.5	6.3	O $1s \rightarrow \infty$	and	O $1s$, $3a_1 \rightarrow 4a_1, \infty$
γ	8.6	6.2	O $1s \rightarrow 4a_1/\sigma^*(O-H)$	and	O $1s$, $3a_1 \rightarrow \infty, \infty$
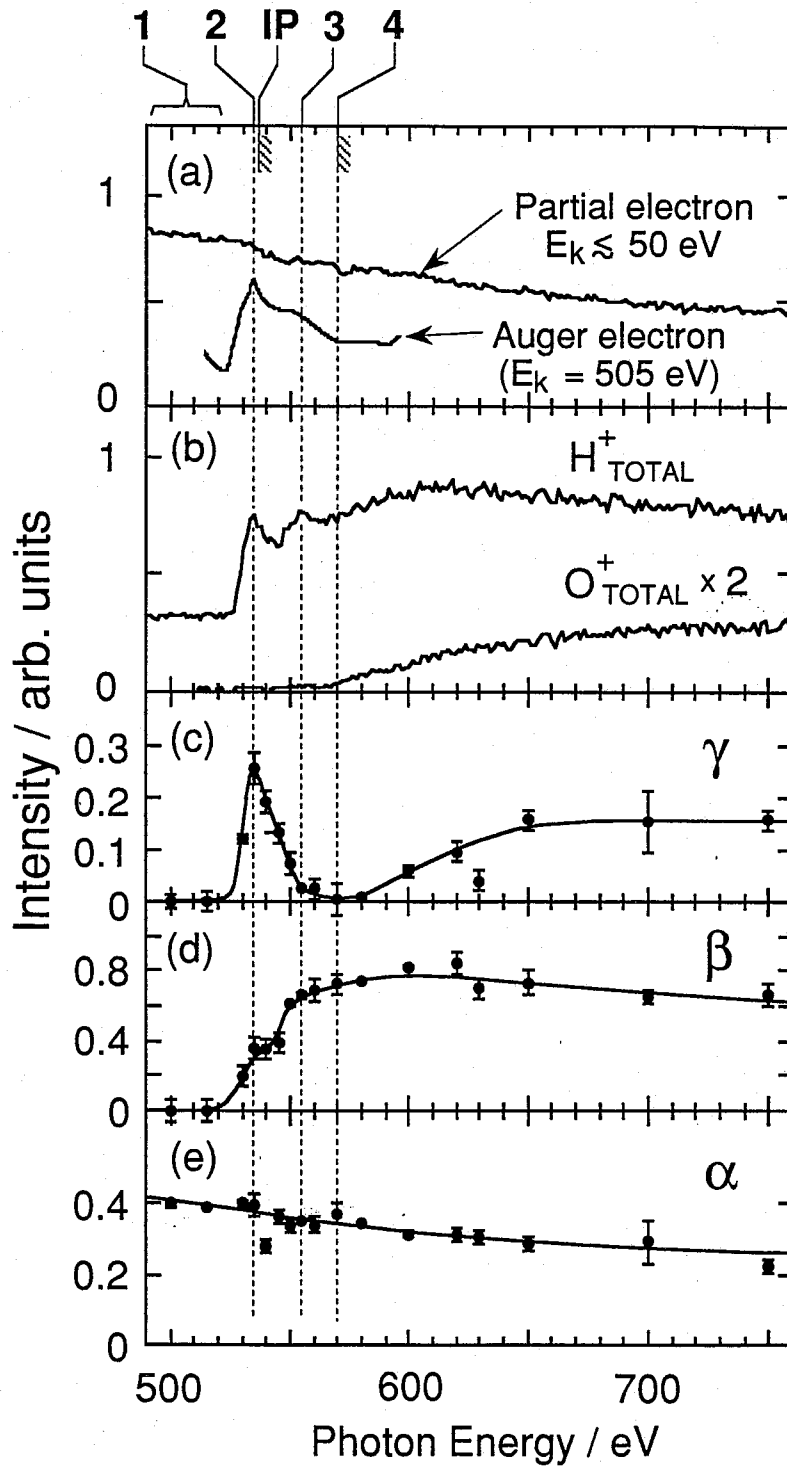
Figure 3-15   (a) Partial electron yields (PEY) and O(KVV) AEY, (b) H$^+$

total yield and O$^+$ total yield, and the integrated intensities for

(c) γ, (d) β, (e) α components as a function of photon energies

ranged from 500 to 750 eV.

Table 3-III   The energies of threshold (E_{th}), peaks (E_p) seen in
the ion yield spectra in the $H_2O/Si(100)$ adsorption
system, and their possible assignments.

Feature	E_{th} (eV)	E_p (eV)	Excitation
1	99	$\cdots$	Si $2p \rightarrow \infty$
1	150	$\cdots$	Si $2s \rightarrow \infty$
2	$\cdots$	535	O $1s \rightarrow 4a_1/\sigma^*(O\text{--}H)$
Ip	537	$\cdots$	O $1s \rightarrow \infty$
3	$\cdots$	556	O $1s, 3a_1 \rightarrow 4a_1, \infty$
4	570	$\cdots$	O $1s, 3a_1 \rightarrow \infty, \infty$

The desorption mechanisms discussed below are summarized in Table 3-II. The α component, peaked at 5.1 eV, has a minor contribution as a whole. Although the O K-shell ionization threshold lies at about 537 eV, the α component [Figure 3-15(e)] monotonically decreases with increasing excitation energy. This is consistent with both the partial electron yield (PEY) spectrum (electron kinetic energy, E_k < 50 eV) [Figure 3-15(a)] that represents an Si L-shell photoabsorption cross section of Si substrate and the theoretical Si L-shell photoabsorption cross section of atomic silicon reported by Henke *et al.*[18]. This fact indicates that the α component is not induced by the creation of an oxygen core hole but induced by the Si L-shell photoionization. The β component [Figure 3-15(d)], peaked at 6.5 eV, has a dominant contribution. It does not appear below O K-edge threshold and substantially exhibits two onsets at about 537 eV (**IP**) and about 555 eV (**3**), which correspond to the O K-shell ionization and the lowest shake-up ionization (O $1s, 3a_1 \rightarrow 4a_1, \infty$)[11], respectively (see Table 3-III). This indicates that these two desorption channels open above 537 and 555 eV.

The highest kinetic energy component (γ), peaked at 8.6 eV, shows an interesting behavior in the excitation spectrum. This component is characterized by two types of desorption mechanisms. It shows intense peak (**2**) at about 535 eV and an onset (**4**) at about 570 eV, which correspond to the resonant excitation and the shake-off ionization, respectively (See Table 3-III). This resonant feature can also seen both in the O(KVV) Auger electron yield (AEY) spectrum [Figure 3-15(a)] corresponding to the O K-shell photoabsorption cross section of the OH adsorbate and in the H^+ total yield spectrum [Figure 3-15(b)], both of which show the features at the same energies. It can be said, therefore, that the resonant component is successfully separated from the H^+ total yields. The resonant feature of the γ component

can not be explained by the desorption mechanisms shown in Figure 3-7. As described above, the feature at **2** can be characterized to the excitation involving the strongly antibonding- and valence-MO localized on an O-H bond (the so-called σ^*(O–H) MO) because the highest kinetic energy component shows the high yield at the feature **2**; occupation to antibonding orbital such as σ^* would weaken an O-H bond. Therefore, it is thought that the feature **2** at 535 eV is closely correlated with the core-excitation into the $4a_1$ in the H_2O molecule, for which the repulsive property was appeared both in the gas and solid phases[1,10]. For the feature **2**, the Rydberg states are ruled out because of their less-repulsiveness[38].

The most probable energy for the γ component is about 8.6 eV. For the resonant excitation of the feature **2**, the author explains this value in terms of the 2h1e (1e = σ^*(O–H)) ionic intermediates through the spectator Auger processes. In the study of the electron stimulated desorption (ESD) of H^+ ions from ice water on Ni(111), bimodal kinetic energy distributions were observed. By 28-45 eV excitations, high (7-8 eV) energetic H^+ ions were appeared and concluded to be responsible for the shake-up ionization that results in the 2h1e (1e = $4a_1$) states, most of which are repulsive on the basis of a RHF-CI calculations of H_2O[39]. The most probable energy (8.6 eV) for the γ component is consistent with the kinetic energy (7-8 eV) through the 2h1e states. Auger final states such localized two holes on bonding and one electron on antibonding MO along the O-H bond have the strong repulsive-property[24,39,40]. These states are effective in bond breaking, survive the neutralization with the substrate, and efficiently bring about ion desorption. For the resonant excitation of 535 eV, the author concludes that the enhancement in the H^+ total yield and in the γ component are due to the 2h1e (1e = σ^*(O–H)) ionic intermediates through the spectator Auger processes.

The excess energy would convert to translational energy and high energetic H^+ ions would be desorbed.

For initial process in PSID, the so-called ultra-fast dissociation[1,21,22], reported by Coulman et al., may occur and enhance the γ component at 535 eV. The author summarizes it as follows: after the core to σ^* excitation, an electron on antibonding σ^* orbital rapidly contributes to movement of a light particle such as hydrogen atom and to weakening of a chemical bond in the core excited state. In the present study, according to this mechanism, the neutral hydrogen atom accumulates the kinetic energy in the core excited state which has extremely steep potential curve along O-H axis. This is possible because the repulsive property of this state of H_2O appears both in the gas and solid phases[1,10]. Thus, the author speculates as follows: during the rapid elongation of O-H in core lifetime, the H particle stores a few electron volts; after that, Auger processes occur; among various final states, only 2h-1e through Spectator Auger process would lead to H^+ ion desorption with 8-10 eV kinetic energy.

The γ component shows a delayed onset at about 570 eV and an increase up to a steady level at about 700 eV, the onset, which corresponds to the shake-off ionization. It should be noted that this onset is also seen both in the H^+ total yields and O^+ total yields, as shown in Figure 3-15(b); the H^+ yields increases above 570 eV and the O^+ yields starts to desorb at this energy. This was previously explained using the mechanisms illustrated in Figure 3-7. According to this mechanism, ion desorption are promoted by the shake-off ionization followed by the double Auger process. This excitation leads to the formation of the multiple-hole states (OH^{3+} or OH^{4+}). For the H^+ desorption, rapture of O-H bond by intense hole-hole repulsion results in effective desorption. The O^+ desorption can be explained by decomposition of OH^{4+}

into O^{3+} + H^+, after which the O^{3+} can survive surface deexcitation and/or neutralization and desorb as O^+ ions[41]. This mechanism can consistently explain also the results of the observed KERDs of H^+ ions: the multiple-hole states would have the steep repulsive-potential curves along the R_{Si-O} as well as the R_{O-H} coordinates[42]. Then the desorbing H^+ particle would store large kinetic energy during escape from ionic oxygen atom. It enhances the highest kinetic energy component (γ) through the shake-off ionization. Therefore, the author concludes that the onset seen in the γ component intensively supports the proposed mechanism shown in Figure 3-7.

The author briefly summarizes the KERD results. The KERDs of H^+ ions desorbed from $H_2O/Si(100)$ surface were successfully decomposed to the three components, all of which can be assigned on the basis of thresholds or peaks seen in their excitation spectra. In particular, the highest kinetic energy (γ) component shows the intense peak at 535 eV corresponding to the $O_{1s} \rightarrow \sigma^*(O-H)$ resonance, which is closely correlated with the excitation into $4a_1$ antibonding orbital of the H_2O molecule. The author notes that this is the first demonstration on the state-specific ion-desorption by kinetic energy analysis, in which the strongly antibonding $(4a_1 / \sigma^*(O-H))$ MO plays an important role. The KERD measurements provide the information on the core resonant excitation in ion desorption, which can not given from the ion yield spectra. The analysis of the KERD will be applied to a variety of adsorbate systems as a powerful technique for investigating the desorption mechanism.

3.6 References

[1] D. Coulman, A. Puschmann, W. Wurth, H.-P. Steinrück, and D. Menzel, Chem. Phys. Lett., **148**, 371 (1988); D. Coulman, A. Puschmann, U. Höfer, H.-P. Steinrück, W. Wurth, P. Feulner, and D. Menzel, J. Chem. Phys., **93**, 58 (1990).

[2] M. Niwano, Y. Takakuwa, H. Katakura, N. Miyamoto, J. Vac. Sci. Technol., **A9**, 212 (1991).

[3] T. Ogawa, I. Ochiai, K. Mochiji, and A. Hiraiwa, Appl. Phys. Lett., **59**, 794 (1991).

[4] J.A. Schaefer, J. Anderson, and G.L. Lapeyre, J. Vac. Sci. Technol., **A3**, 1443 (1985).

[5] R.A. Rosenberg, P.J. Love, V. Rehn, I. Owen, G. Thornton, J. Vac. Sci. Technol., **A4**, 1451 (1986); R.A. Rosenberg, C.R-. Wen, and D.C. Mancini, in *"Desorption Induced by Electronic Transition, DIET III"*, edited by R.H. Stulen and M.L. Knotek, (Springer, Berlin, 1987), p.220.

[6] R. Lindsay, P.L. Wincott, C.A. Muryn, G. Thornton, S.P. Frigo, J.K. Simons, and R.A. Rosenberg, Jpn. J. Appl. Phys., **32, Suppl. 32-2**, 347 (1992).

[7] G.R. Wight and C.E. Brion, J. Elect. Spect. Relate. Phenom., **4**, 25 (1974).

[8] A. Schmitt and J. Schirmer, Chem. Phys., **164**, 1 (1992).

[9] D.Y. Kim, K. Lee, C.I. Ma, M. Mahalingam, D.M. Hanson, and S.L. Hulbert, J. Chem. Phys., **97**, 5915 (1992).

[10] J. Schirmer, A.B. Trofimov, K.J. Randall, J. Feldhaus, A.M. Bradshaw, Y. Ma, C.T. Chen, and F. Sette, Phys. Rev., **A47**, 1136 (1993).

[11] J.S. Tse and G. Loubriel, J. Chem. Phys., **74**, 5190 (1981); D.K. Creber, J.S. Tse, and G.M. Bancroft, J. Chem. Phys., **72**, 4291 (1980); R. Arneberg, J. Müller, and R. Manne, Chem. Phys., **64**, 249 (1982).

[12] N. Kosugi, private communication.

[13] S. Svensson, H. Ågren, and U.I. Wahlgren, Chem. Phys. Lett., **38**, 1 (1976); H. Ågren and V. Carravetta, J. Chem. Phys., **87**, 370 (1987).

[14] A.B. Anderson, Surf. Sci., **105**, 159 (1981).

[15] R. Jaeger, R. Treichler, and J. Stöhr, Surf. Sci., **117**, 533 (1982).

[16] R. Jaeger and J. Stöhr, Surf. Sci., **134**, 547 (1983); R. Jaeger, J. Stöhr, T. Kendelewicz, Phys. Rev., **B28**, 1145 (1983).

[17] D.E. Ramaker, T.E. Madey, R.L. Kurtz, and H. Sambe, in DIET III, p.182; D.E. Ramaker, T.E. Madey, R.L. Kurtz, and H. Sambe, Phys. Rev., **B38**, 2099 (1988).

[18] B.L. Henke, P. Lee, T.J. Tanaka, R.L. Shimabukuro, and B.K. Fujikawa, Atomic Data and Nuclear Data Tables, **27**, 1 (1982).

[19] T.E. Madey, D.E. Ramaker, R. Stockbauer, Ann. Rev. Phys. Chem., **35**, 215 (1984).

[20] W. Wurth, C. Schneider, R. Treichler, E. Umbach, and D. Menzel, Phys. Rev., **B35**, 7741 (1987); W. Wurth, P. Feulner, and D. Menzel, Physica Scripta, **T41**, 213 (1992).

[21] D. Menzel, G. Rocker, H.-P. Steinrück, D. Coulman, P.A. Heimann, W. Huber, P. Zebisch, and D.R. Lloyd, J. Chem. Phys., **96**, 1724 (1992); D. Menzel, G. Rocker, D. Coulman, P. Feulner, and W. Wurth, Physica Scripta, **41**, 588 (1990); D. Menzel, AIP Conference Proceedings No.258, *"Synchrotron Radiation and Dynamic Phenomena"*, edited by A. Beswick (Amer. Inst. Phys., 1992).

[22] P. Morin and I. Nenner, Phys. Rev. Lett., **56**, 1913 (1986).

[23] J. Chelikowsky, D.J. Chadi, and M.L. Cohen, Phys. Rev., **B8**, 2786 (1973).

[24] D. E. Ramaker, Chem. Phys., **80**, 183 (1983); J. Chem. Phys., **78**, 2998 (1983).

[25] D.E. Ramaker, C.T. White, and J.S. Murday, Phys. Lett., **89A**, 211 (1982); D.E. Ramaker, J. Vac. Sci. Technol., **A1**, 1137 (1983). D.E. Ramaker, Phys. Rev. **B21**, 4608 (1980); B.I. Dunlap, F.L. Hutson, and D.E. Ramaker, J. Vac. Sci. Technol., **18**, 556 (1981).

[26] R. Treichler, W. Riedl, P. Feulner, and D. Menzel, Surf. Sci., **243**, 239 (1991); R. Treichler, W. Wurth, W. Riedl, P. Feulner, and D. Menzel, Chem. Phys., **153**, 259 (1991).

[27] R.D. Ramsier and J.T. Yates, Jr., Surf. Sci. Rep., **12**, 243 (1991).

[28] N. Saito and I.H. Suzuki, Physica Scripta, **45**, 253 (1992).

[29] M. Cini, Phys. Rev., **B32**, 1945 (1985).

[30] H.H. Madden, D.R. Jennison, M.M. Traum, G. Margaritondo, and N.G. Stoffel, Phys. Rev., **B26**, 896 (1982).

[31] P.J. Feibelman, Surf, Sci., **102**, L51 (1981).

[32] G. R. Wight and C. E. Brion, Chem. Phys. Lett., **26**, 607 (1974).

[33] C.E. Moore, in "*Ionization Potential and Ionization Limits Derived from the Analyses of Optical Spectra*", NSRDS-NBS 34, National Bureau of Standards, Washington, D.C. (1970).

[34] R. Treichler, W. Riedl, W. Wurth, P. Feulner, and D. Menzel, Phys. Rev. Lett., **54**, 462 (1985); in "*Desorption Induced by Electronic Transition, DIET II*", edited by W.Brenig and D.Menzel, (Springer, Berlin, 1984), p. 68.

[35] A.P. Hitchcock, P. Lablanquie, P. Morin, E. Lizon A Lugrin, M. Simon, P. Thirty and I. Nenner, Phys. Rev., **A37**, 2448 (1988).

[36] G. Dujardin, S. Leach, O. Dutuit, P-.M. Guyon, and M. Richard-Viard, Chem. Phys., **88**, 339 (1984).

[37] W.L. Clinton, S. Pal, and R.E. Jutila, Phys. Rev., **B36**, 4123 (1987).

[38] J.A. Kelber, R.R. Daniels, M. Turowski, G. Margaritondo, N.H. Tolk, and J.S. Kraus, Phys. Rev., **B30**, 4748(1984).

[39] J.O. Noell, C.F. Melius, and R.H. Stulen, Surf. Sci., **157**, 119(1985).

[40] J.C. Leclerc, J.A. Horsely, and J.C. Lorquet, Chem. Phys., **4**, 337(1974).

[41] T. Sekiguchi, H. Ikeura, K. Tanaka, K. Obi, N. Ueno, and K. Honma, J. Chem. Phys., **102**, 1422(1995); K. Tanaka, H. Ikeura, N. Ueno, Y. Kobayashi, K. Obi, T. Sekiguchi, and K. Honma, AIP Conference Proceedings No. 258, "*Synchrotron Radiation and Dynamic Phenomena*", edited by A. Beswick (Amer. Inst. Phys., 1992); H. Ikeura, T. Sekiguchi, K. Tanaka, K. Obi, N. Ueno, and K. Honma, Jpn. J. Appl. Phys., **32, Suppl. 32-2**, 246 (1993).

[42] T.G. Heil, S. Green, A. Dalgarno, Phys. Rev., **A26**, 3293(1982).

Chapter 4

SUMMARY

In this thesis, the photon stimulated ion desorption (PSID) of H^+ and O^+ from monolayer H_2O adsorbed on $Si(100)$ in the 510-800 eV photon energy range has been presented. The comparison of the PSID yields of H^+ and O^+ with the Auger electron yield, i.e., photoabsorption cross section, shows that the ion desorption yields strongly depend on the primary excitation and are greatly enhanced with higher excitation. The author found that multiple excitation, such as shake-up or shake-off ionization, was effective in PSID. The author concluded that, most probably, the surface OH^{4+} precursor produced by shake-off ionizations followed by the double-Auger processes plays an important role in O^+ desorption above 570 eV. The delayed threshold of the O^+ PSID can be explained by a mechanism in which the multiply charged precursor ions (e.g., O^{3+}) are desorbed as O^+ ions through incomplete neutralization.

For photodissociation experiments of free H_2O, the appearance of O^{3+} above 570 eV can be explained due to decomposition of the H_2O^{4+} precursor produced by shake-off followed by the double-Auger process. The proposed mechanism is supported by a similarity between the O^+ PSID from $H_2O/Si(100)$ and O^{3+} from free H_2O. The PIPICO measurements also support this mechanism in which simultaneous desorption of O^+ and H^+ is included. Ion kinetic energy released distributions (KERDs) of H^+ ions confirm the formation of the multiply charged precursor (OH^{3+} or OH^{4+}) by the shake-off ionization above 570 eV. In addition, the KERDs provided the picture that the

strongly antibonding molecular orbitals such as a $4a_1/\sigma^*(O-H)$ played an important role in an ion desorption. The author notes that this is the first demonstration on the state-specific ion-desorption by means of kinetic energy analysis. The KERD measurements provided the information on the core resonant excitation in ion desorption, which can not be given from the ion yield spectra. The analysis of the KERD will be applied to a variety of adsorbate systems as a powerful technique for investigating the desorption mechanism.